NASA TECHNICAL NOTE

NASA TN D-7314

NASA TN D-7314

AN EXPERIMENTAL INVESTIGATION OF A HIGHLY UNDEREXPANDED SONIC JET EJECTING FROM A FLAT PLATE INTO A SUBSONIC CROSSFLOW

by

Craig S. Shaw

Langley Directorate, U.S. Army Air Mobility R&D Laboratory
Hampton, Va. 23665

and

Richard J. Margason

Langley Research Center
Hampton, Va. 23665

NATIONAL AERONAUTICS AND SPACE ADMINISTRATION • WASHINGTON, D. C. • DECEMBER 1973

1 Report No.	2 Government Accession No	3. Recipient's Catalog No
NASA TN D-7314		

4 Title and Subtitle	5. Report Date
AN EXPERIMENTAL INVESTIGATION OF A HIGHLY UNDER-EXPANDED SONIC JET EJECTING FROM A FLAT PLATE INTO A SUBSONIC CROSSFLOW	December 1973
	6 Performing Organization Code

7 Author(s)	8. Performing Organization Report No
Craig S. Shaw (Langley Directorate, U.S. Army Air Mobility R&D Laboratory) and Richard J Margason (Langley Research Center)	L-8863
	10 Work Unit No. 760-61-02-03

9. Performing Organization Name and Address	11. Contract or Grant No
NASA Langley Research Center Hampton, Va. 23665	
	13. Type of Report and Period Covered: Technical Note

12 Sponsoring Agency Name and Address	14. Sponsoring Agency Code
National Aeronautics and Space Administration Washington, D.C. 20546	

15. Supplementary Notes

16. Abstract

The induced static pressures due to a highly underexpanded sonic jet ejecting normally from a flat plate into a subsonic crosswind have been investigated. These pressure data have been recorded on the flat plate for a range of nominal jet-to-free-stream dynamic-pressure ratios from 0 to 1000 at free-stream Mach numbers of 0.1, 0.2, 0.4, and 0.6. The static-pressure data measured on the flat plate are presented and correlated based upon the Riemann shock geometry in the jet plume. This data correlation improves with increasing free-stream Mach number.

17. Key Words (Suggested by Author(s))	18. Distribution Statement
Underexpanded sonic jet Riemann shock Subsonic crossflow Control jet Jet plume	Unclassified – Unlimited

19. Security Classif. (of this report)	20. Security Classif. (of this page)	21. No. of Pages	22. Price*
Unclassified	Unclassified	88	Domestic, $3.75 Foreign, $6.25

*For sale by the National Technical Information Service, Springfield, Virginia 22151

AN EXPERIMENTAL INVESTIGATION OF A HIGHLY UNDEREXPANDED SONIC JET EJECTING FROM A FLAT PLATE INTO A SUBSONIC CROSSFLOW

By Craig S. Shaw
Langley Directorate, U.S. Army Air Mobility R&D Laboratory

and Richard J. Margason
Langley Research Center

SUMMARY

The induced static pressures due to a highly underexpanded sonic jet ejecting normally from a flat plate into a subsonic crosswind have been investigated. These pressures were measured on the flat plate for a range of nominal jet-to-free-stream dynamic-pressure ratios from 0 to 1000 at free-stream Mach numbers of 0.1, 0.2, 0.4, and 0.6. The results of this investigation indicate that for a given free-stream Mach number, as the jet-to-free-stream dynamic-pressure ratio increases, there is a greater variation of static-pressure data on the flat plate. In addition, increasing the free-stream Mach number for a constant jet-to-free-stream dynamic-pressure ratio causes an increased positive pressure upstream of the jet (blockage region), while to the side and downstream of the jet there is a larger negative pressure area (entrainment region). These results indicate that the jet-free-stream interaction causes a loss in jet-reaction force and a moment on the flat plate. Subsequently, the results are used to demonstrate a satisfactory method of correlating the static pressure induced by the jet interference on the flat plate. This static-pressure correlation was accomplished by nondimensionalizing the radial distance from the jet exit to a point on the flat plate by the plume length to the Riemann shock of the underexpanded sonic jet. The best data correlation was achieved using analytically determined plume lengths. This correlation improved with increasing free-stream Mach number.

INTRODUCTION

Reaction jets have found increased usage in missile control systems in recent years. The complex flow field caused by the interaction of the flow from the reaction jets with the free-stream flow produces an aerodynamic interference on the vehicle which the designer

must be able to understand and predict. Satisfactory tools for accurate prediction of this aerodynamic interference have not yet been developed, and the designer must spend a large amount of time selecting the best configuration from the results of extensive wind-tunnel tests. References 1 and 2 present qualitative descriptions of the reaction-jet flow field as well as comparisons of several related experimental and analytical investigations. The experimental investigation reported in reference 3 presents data showing the influence of the transonic airstream upon the control effectiveness of a nose-mounted supersonic-control jet exhausting radially from an ogive-cylinder body.

In order to obtain further information on the magnitude and extent of this jet-induced aerodynamic interference at high jet-pressure ratios, an experimental investigation of a highly underexpanded sonic jet exhausting from a flat plate into a subsonic crosswind was conducted jointly by the U.S. Army Missile Command and the NASA Langley Research Center. The static pressures on the flat plate were measured and presented in plotted form to illustrate the nature of the pressure fields on the plate. Tabulated data from this investigation are presented in reference 4 as a data report without analysis. The present report contains some analysis and correlation of the results obtained by a method similar to that of references 1 and 2.

This investigation was conducted in the Langley high-speed 7- by 10-foot tunnel at free-stream Mach numbers of 0.1, 0.2, 0.4, and 0.6. The nominal jet-to-free-stream dynamic-pressure ratios covered in the tests ranged from 0 to 1000. Corresponding ratios of jet total pressure to free-stream static pressure as high as 93 were recorded for the underexpanded sonic jet in the subsonic crossflow. Schlieren photographs of the underexpanded sonic jet exhausting to ambient conditions were taken to document Riemann shock geometries for comparison with previous experiments (refs. 5 and 6). Correlations of static-pressure data on the flat plate were made by use of a curve fit based upon photographed Riemann shock geometries and by use of an analytical equation (eq. A-7) developed in reference 1.

SYMBOLS

The units used for the physical quantities defined in this paper are given in the International system of Units (SI) and parenthetically in the U.S. Customary Units. Conversion factors for the SI system are presented in reference 7.

C_p static-pressure coefficient, $\frac{p - p_\infty}{q_\infty}$

d reaction-jet moment arm about center of mass, cm (in.)

D	jet diameter, 0.84 cm (0.33 in.)
F	static thrust produced by reaction jet, N (lbf)
ΔL	incremental lift force induced on a vehicle by reaction jet, N (lbf)
l	plume length; distance along jet axis from nozzle exit to Riemann shock wave (see fig. 23), cm (in.)
ΔM	pitching-moment increment induced on a vehicle by reaction jet, N-m (ft-lbf)
M_∞	free-stream Mach number
p	local static pressure, N/m^2 (lb/ft^2)
p_∞	free-stream static pressure, N/m^2 (lb/ft^2)
p_j	static pressure at jet exit, N/m^2 (lb/ft^2)
$p_{t,j}$	total pressure at jet exit, N/m^2 (lb/ft^2)
q_∞	free-stream dynamic pressure, N/m^2 (lb/ft^2)
q_j	jet dynamic pressure at nozzle exit, N/m^2 (lb/ft^2)
Q_{mom}	jet-to-free-stream dynamic-pressure ratio for data measured at a particular test condition, q_j/q_∞
$\bar{Q}_{mom}$	average jet-to-free-stream dynamic-pressure ratio for data measured through a range of test conditions when Q_{mom} is nearly constant
r	radial distance from center of jet exit to a point on flat plate, m (ft)
s	diameter of Riemann shock, m (ft)
V_∞	free-stream velocity, m/sec (ft/sec)
V_{bl}	velocity in boundary layer, m/sec (ft/sec)

y height of boundary-layer probe above flat plate, cm (in.)

θ azimuthal location on flat plate (see fig. 1), deg

Subscripts:

a analytically determined

e experimentally measured

exit nozzle exit

MODEL AND APPARATUS

A three-view drawing and photographs of the experimental apparatus are presented in figures 1 and 2, respectively. The stainless-steel plate measured 166.60 cm (65.59 in.) by 152.40 cm (60.0 in.) and had the front 40 percent of a NACA 65A003 airfoil section for a leading edge. In order to fix boundary-layer transition, a 0.64-cm-wide (0.25-in.) grit strip was affixed to the plate 16.8 cm (6.63 in.) from the leading edge as shown in figure 1.

Located in the approximate center of the plate was a 0.84-cm-diameter (0.33-in.) converging nozzle. As shown in figure 1, there were 426 static pressure ports located in 13 radial directions about the nozzle center. Data were obtained from a few ports along the 60°, 120°, 270°, and 330° rays; they were used for checking flow symmetry over the plate. These data were presented in reference 4 and have not been included in this report. (See ref. 4 for exact pressure-port locations.)

Figure 2 shows the position of the plate in the tunnel. The leading edge of the plate was located 15.24 cm (6.0 in.) and the trailing edge about 19.05 cm (7.5 in.) from the tunnel wall. The difference in leading-edge and trailing-edge locations was set to account for the tunnel wall divergence, in order to keep the plate parallel to the free stream.

The surface-pressure transducers used were rated (0 to 6.9 N/cm^2 (10 psig)) with an accuracy of 0.5-percent full scale.

TEST PROCEDURES

The static-pressure data recorded on the flat plate near the nozzle exit were of primary interest in this investigation. Each data point presented is the average of three test points taken in succession while maintaining constant test conditions. This procedure was

used to reduce the effects of flow irregularities and experimental scatter in these pressure data. The pressure transducers were selected to measure pressures at high Mach number and dynamic-pressure-ratio conditions. For these conditions, the pressure level was high, but at the lowest test parameters ($M_\infty = 0.1$, $Q_{mom} \approx 0.0$) the pressures obtained were less than 0.1 percent of full scale. Since the gage accuracy was approximately 0.5 percent of full scale, the accuracy limit was exceeded. As a result, there was significant data scatter at the lowest Mach number. Samples of these data illustrating the scatter variation with Mach number are presented in reference 8. The effectiveness of this averaging procedure will be demonstrated subsequently by the satisfactory data repeatability obtained for $Q_{mom} \approx 100$.

In attempting to keep the jet-to-free-stream dynamic-pressure ratio constant while varying q_j and q_∞, it was difficult to preset precisely the jet total pressure. This difficulty resulted in variations from nominal values of Q_{mom} of as much as 10 percent. Because of the variations, an average jet-to-free-stream dynamic-pressure ratio $\bar{Q}_{mom}$ is used in the data presentation.

RESULTS

The results of a wind-tunnel investigation of a highly underexpanded sonic jet issuing from a flat plate into a subsonic crosswind are presented. The static pressures induced on the flat plate are given in coefficient form and are plotted as functions of radial location for a given azimuthal direction. The azimuth angles are illustrated in figure 1. A list of figures in which the data are presented follows:

DISCUSSION

Schlieren photographs (fig. 3) of the free-jet flow fields were obtained at jet-total-to-ambient pressure ratios as high as 84.18. These photographs were used to determine the

experimental plume length of the free jet, which is presented as a function of static-pressure ratio p_j/p_∞ in figure 4. Static-pressure ratios at the nozzle exit for the present investigation were calculated from measured free-stream and nozzle flow conditions. Also presented in figure 4 are the plume lengths reported in references 5 and 6. Very close agreement among the data is evident.

Boundary-layer surveys of the free-stream flow over the flat plate were conducted at two streamwise locations 7.6 cm (3.0 in.) to the side of the plate center line without the jet blowing. The first location was at a point 30.48 cm (12.0 in.) forward of the jet center line, while the second location was at the jet center-line station. The boundary-layer profiles are presented in figure 5 to document the free-stream conditions on the flat plate. It can be shown that the data agree closely with the classical 1/7th power velocity-distribution law for turbulent boundary layers, as expected.

Effects of Varying Free-Stream Mach Number

The average jet-to-free-stream dynamic-pressure ratio $\bar{Q}_{mom}$ is constant in each of figures 6 to 18 where the static-pressure data on the plate are presented as functions of free-stream Mach number.

The near jet-off condition (fig. 6) shows very little variation in the static-pressure distribution on the plate, as expected. At an average dynamic-pressure ratio of 10.6 (fig. 7), the pressure is seen to vary significantly within several diameters of the nozzle. Upstream and slightly to the side of the jet exit (at 0° and 30° rays as shown in fig. 1), the positive pressure represents a deceleration of the flow caused by the blockage of the jet efflux. To the side and downstream of the jet, substantial negative pressure coefficients are caused as the entrained flow is accelerated by the jet plume. The remainder of the data presented in this section (figs. 8 to 18) illustrate that there is a greater variation of static-pressure coefficient as both the dynamic-pressure ratio and the free-stream Mach number increase.

The data in figure 11 along the 30° azimuth show an interesting Mach number effect. For a Mach number of 0.2 there is flow being accelerated into the jet, while at 0.6 the positive pressure indicates some degree of blockage. The data obtained at the intermediate Mach number 0.4 show very little deviation from free-stream static pressure, which fact indicates a balance between entrainment and blockage effects.

In figure 11, the behavior of the flow along the 180° ray is also very different at each Mach number tested; for example, at a Mach number of 0.1, the jet strongly influences the flow for about 2 jet diameters. At the highest Mach number 0.6 the jet influence is felt more than 12 diameters downstream. The relative pressure gradients can be determined from the slope of the data for each Mach number. At a location 3.5 diameters behind

the center of the jet exit in figure 11, there is only a slight pressure gradient at a free-stream Mach number of 0.1. The pressure gradient is slightly greater at a free-stream Mach number of 0.2; thus, the acceleration of flow would be greater. A considerably larger flow acceleration is in evidence for a free-stream Mach number of 0.4, but practically zero acceleration of flow along the plate is inferred 3.5 diameters behind the jet for a free-stream Mach number of 0.6. It is at this point of zero acceleration that the fluid partially separates from the plate and is entrained vertically toward the turbulent mixing region of the jet. For a Mach number of 0.4 this separation point is reached at only 2 diameters behind the jet exit. A more extensive discussion of the flow field in this region is presented in reference 9.

A second set of data for a jet-to-free-stream dynamic-pressure ratio of approximately 100 is presented in figure 12 ($\bar{Q}_{mom} = 104.9$) to show experimental repeatability with data from figure 11. Comparison of these data shows close agreement. Examination of the 170° ray in figures 13, 14, and 15 shows evidence of a localized flow separation for a free-stream Mach number of 0.1.

In general, increasing the Mach number for a given dynamic-pressure ratio increased the magnitude of the positive pressure region upstream of the jet and increased the magnitude of the more extensive negative pressures to the side and in the wake of the jet. At the highest values of dynamic-pressure ratio (figs. 16, 17, and 18 for $\bar{Q}_{mom} = 619.5$, 829.9, and 1052.3, respectively), the entrainment effect had a tendency to dominate the blockage effect as indicated by the increased extent of negative pressure regions. As the dynamic-pressure ratio increases, it approaches the condition of the free jet where the pressure field becomes axisymmetric.

Effects of Varying Q_{mom}

The effects of varying the jet-to-free-stream dynamic-pressure ratio at constant Mach number can be seen in figures 19 to 22 for $M_\infty = 0.1$, 0.2, 0.4, and 0.6, respectively. The original data presented in figures 6 to 18 have been replotted with the free-stream Mach number held constant in each figure. The circular symbols with the flags represent the zero jet-flow condition, since it was found that the data (represented by the plain circular symbols) were obtained with a slight leak in the jet airline. This leak produced ratios of jet total pressure to free-stream static pressure of approximately 1.01. At the lowest test Mach number, 0.1 (fig. 19), an increase in jet dynamic pressure caused increased jet entrainment which in turn increased the magnitude of the negative pressure coefficients when compared with the jet-off condition. There is little variation in pressure coefficient in the wake region further than 3 jet diameters from the jet exit, however. The data presented for Mach numbers of 0.2, 0.4, and 0.6 (figs. 20, 21, and 22) show the expected vari-

ation of pressure coefficient with increasing dynamic-pressure ratio for all azimuths. The increasing jet dynamic pressure causes the jet to become more highly underexpanded and thus forms a larger expansion plume (fig. 3). This plume represents a larger blockage area to the oncoming free stream (more extensive stagnation area) and also produces a larger mixing region for entrainment around the jet exit. The significance of the plume is discussed in the next section.

Correlation of Pressure Data

The history behind the development of the correlation method used is discussed in references 1 and 2. In effect, this technique involves finding a series of factors which, when used to scale the distance from the jet exit to the pressure port location, produce a reduction of the pressure data to a single curve. Correlations based upon theoretical and measured Riemann shock diameters s and distances from nozzle exit to Riemann shock l were attempted in the present investigation.

As the jet-to-free-stream pressure ratio is increased past the critical value (fig. 23(a)), the exiting flow becomes supersonic (fig. 23(b)) and returns to subsonic speed through a normal shock wave (Riemann disk) some distance away from the nozzle exit; this distance is called the plume length l. The supersonic plume has so much more momentum than the free-stream flow that the jet is barely deflected until it passes through the Riemann shock. Beyond this point, the jet effectively behaves as if a subsonic nozzle were exhausting at a distance l from the plate. The greater the pressure ratio is, the greater the distances to this effective nozzle exit are and the larger the effective jet diameter s is. Since it has been shown in figures 20 to 22 that a higher dynamic-pressure ratio produces uniformly larger induced pressures on the flat plate, the correspondingly larger Riemann shock geometries l and s are excellent candidates for scaling the data.

The relationships between the ratio of jet total pressure to free-stream static pressure $p_{t,j}/p_\infty$ and the plume length and shock diameter are illustrated in figure 24. The experimental curves in this figure were found by measuring the distances from the free-jet schlieren photographs in figure 3; these measurements are tabulated in reference 4. The following equations (eqs. (1) and (2)) representing the experimentally determined relationships for s/D and l/D, respectively, have been determined using a generalized quadratic curve-fit technique:

$$\frac{s_e}{D} = 0.0848\,\frac{p_{t,j}}{p_\infty} + 2.6872 - \sqrt{0.0058\left(\frac{p_{t,j}}{p_\infty}\right)^2 - 0.1087\left(\frac{p_{t,j}}{p_\infty}\right) + 8.3440} \qquad (1)$$

$$\frac{l_e}{D} = 0.4293\,\frac{p_{t,j}}{p_\infty} + 3.2837 - \sqrt{0.1540\left(\frac{p_{t,j}}{p_\infty}\right)^2 + 0.2796\left(\frac{p_{t,j}}{p_\infty}\right) + 15.6908} \qquad (2)$$

for

$$\frac{p_{t,j}}{p_\infty} \geqq 1.893$$

The analytical curve of figure 24 was determined in reference 1 and is of the form:

$$\frac{l_a}{D} = 0.755\sqrt{\frac{p_{t,j}}{p_\infty}} \qquad (3)$$

for

$$\frac{p_{t,j}}{p_\infty} \geqq 1.893$$

Initially, a data correlation based upon Riemann shock diameter s was attempted. The data from figure 20 ($M_\infty = 0.2$) are presented in figure 25 where the pressure coefficient is plotted as a function of radial distance r divided by s_e (from eq. (1)). The correlation in figure 25 is poor for the lowest dynamic-pressure ratios. Next, a data correlation based upon plume length was attempted (fig. 26). This time the same (from fig. 20) were scaled by l_e (from eq. (2)). This correlation attempt was s except where the data for average dynamic-pressure ratios of 43.3 and 61.4 devi. om data obtained at other dynamic-pressure ratios.

The best correlation of the data (figs. 27 to 30) was obtained when the radial distance was divided by l_a from the theoretical curve given by equation (3). These correlations demonstrate that moderate success has been achieved for the data obtained at a Mach number of 0.1 (fig. 27). For the Mach numbers 0.2 and 0.4 (figs. 28 and 29) good correlations of the data are obtained. Finally, in figure 30 the data correlation for a Mach number of 0.6 provides the best agreement. The reason for the deficiency of the correlation attempts using equations (1) and (2) can be seen in figure 24. For values of $p_{t,j}/p_\infty$ from the choked condition to approximately 15, the slopes of the two experimentally determined curves are somewhat smaller than the slope determined by equation (3). As can be seen in figure 25, this smaller slope does not cause a sufficient adjustment of the data to the left. The results (using eq. (3)) indicate that the jet-interference effects of a physical

situation similar to that described in this experiment can be estimated quite accurately for the range of conditions tested in the present investigation.

Implications of Investigation Findings

It is emphasized that the present investigation used a jet exiting through a flat plate. The primary purpose of the study was to determine the jet-induced effects caused by a highly underexpanded sonic jet. Previous investigations have been conducted in a subsonic free stream with subsonic jets (ref. 10) and with choked sonic jets (ref. 1). These investigations showed that the jet-induced flow fields on a cylindrical body are similar in character but different in magnitude when compared with similar jet-induced flow fields on a flat plate.

Figure 31 illustrates the overall jet-interference effect for a missile with reaction-control jet located forward of the center of mass. The resultant thrust from the reaction jet is determined by subtracting the lift loss due to aerodynamic interference ΔL from the nominal static jet thrust F. This ΔL usually reduces the resultant thrust since the negative pressure region behind the jet is generally larger than the positive pressure region upstream of the jet. In computing resultant moments, the noseup moment ΔM caused by the induced-pressure regions adds to the moment produced by the reaction-jet thrust. For the control jet located aft of the missile center of mass, ΔM opposes the moment resulting from the reaction-jet thrust. Since the magnitude of the results from the present investigation is not directly applicable to the reaction-jet-induced flow field on a cylindrical missile body, additional experimental investigations would be required for a particular application.

CONCLUSIONS

The results of a wind-tunnel investigation of a highly underexpanded sonic jet ejecting normally from a flat plate into a subsonic free stream indicate the following conclusions:

1. Increasing the free-stream Mach number for a constant jet-to-free-stream dynamic-pressure ratio caused an increased positive pressure area upstream of the jet (blockage) while to the side and downstream of the jet increased entrainment caused the formation of larger negative-pressure regions.

2. Increasing the jet-to-free-stream dynamic-pressure ratio for a given free-stream Mach number increased the magnitude of the negative pressure coefficients on the flat plate.

3. The jet-induced pressure data on a flat plate can be well correlated for a range of dynamic-pressure ratios at constant values of free-stream Mach numbers of 0.1, 0.2, 0.4, and 0.6. This static-pressure data correlation was accomplished by nondimensionalizing the distance from the jet exit to a point on the flat plate by an analytically determined distance from the sonic jet exit to the Riemann shock of the jet plume.

Langley Research Center,
National Aeronautics and Space Administration,
Hampton, Va., September 21, 1973.

REFERENCES

1. Cassel, L. A.; Durando, N. A.; Bullard, C. W.; and Kelso, J. M.: Jet Interaction Control Effectiveness for Subsonic and Supersonic Flight. Rep. No. RD-TR-69-21, U.S. Army, Sept. 1969. (Available from DDC as AD 862 483.)

2. Durando, N. A.; and Cassel, L. A.: Viscous Effects in the Interaction Flowfield Near a Jet in a Subsonic Crossflow. Rep. No. RD-TR-70-31, U.S. Army, Dec. 1970.

3. Lee, Edwin E., Jr.; and Willis, Conrad M.: Interaction Effects of a Control Jet Exhausting Radially From the Nose of an Ogive-Cylinder Body at Transonic Speeds. NASA TN D-3752, 1967.

4. Street, Troy A.: An Experimental Investigation of a Transverse Jet Ejecting From a Flat Plate Into a Subsonic Free Stream. Rep. No. RD-TM-70-5, U.S. Army, May 11, 1970.

5. Love, Eugene S.; Grigsby, Carl E.; Lee, Louise P.; and Woodling, Mildred J.: Experimental and Theoretical Studies of Axisymmetric Free Jets. NASA TR R-6, 1959. (Supersedes NACA RM L54L31 by Love and Grigsby; RM L55J14 by Love; RM L56G18 by Love, Woodling, and Lee; and TN 4195 by Love and Lee.)

6. Vick, Allen R.; Andrews, Earl H., Jr.; Dennard, John S.; and Craidon, Charlotte B.: Comparisons of Experimental Free-Jet Boundaries With Theoretical Results Obtained With the Method of Characteristics. NASA TN D-2327, 1964.

7. Mechtly, E. A.: The International System of Units – Physical Constants and Conversion Factors (Revised). NASA SP-7012, 1969.

8. Street, Troy A.; and Spring, Donald J.: Experimental Reaction Jet Effects at Subsonic Speeds. Analysis of a Jet in a Subsonic Crosswind, NASA SP-218, 1969, pp. 63-83.

9. Mosher, David K.: An Experimental Investigation of a Turbulent Jet in a Cross Flow. Rep. 70-7 (Contract No. DAHC04 68 C 004), School of Aerospace Engineering, Georgia Institute of Technology, Dec. 1970. (Available from DDC as AD 718 798.)

10. Ousterhout, Donald S.: An Experimental Investigation of a Cold Jet Emitting From a Body of Revolution Into a Subsonic Free Stream. NASA CR-2089, 1972.

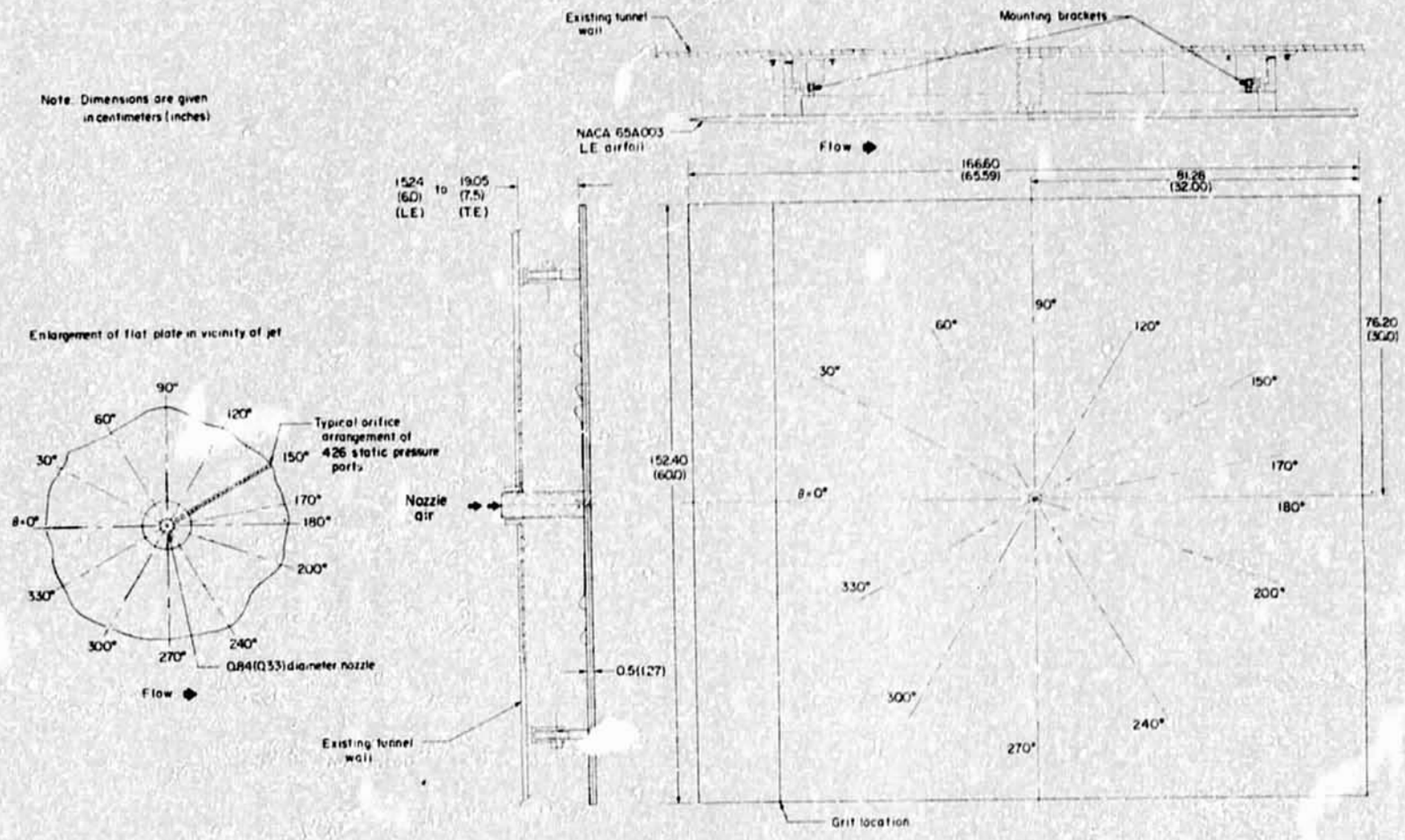

Figure 1.- Three-view drawing of the test model.

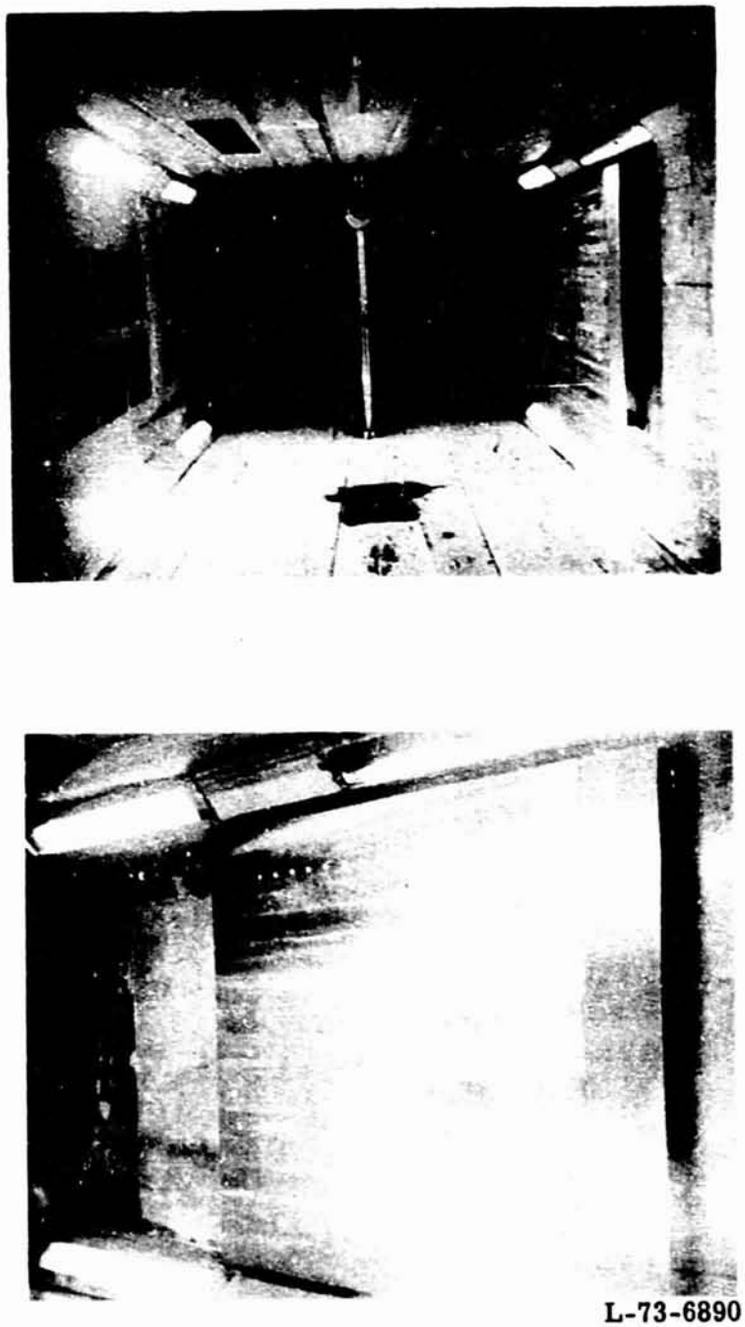

L-73-6890

Figure 2.- Photographs of the experimental setup in the wind tunnel.

(a) $\frac{p_{t,j}}{p_\infty} = 14.61.$

(b) $\frac{p_{t,j}}{p_\infty} = 27.96.$

(c) $\frac{p_{t,j}}{p_\infty} = 41.57.$

(d) $\frac{p_{t,j}}{p_\infty} = 54.91.$

L-73-6891

Figure 3.- Schlieren photographs of the free-jet plume.

(e) $\frac{p_{t,j}}{p_\infty} = 68.93.$

(f) $\frac{p_{t,j}}{p_\infty} = 82.41.$

(g) $\frac{p_{t,j}}{p_\infty} = 84.18.$

L-73-6892

Figure 3.- Concluded.

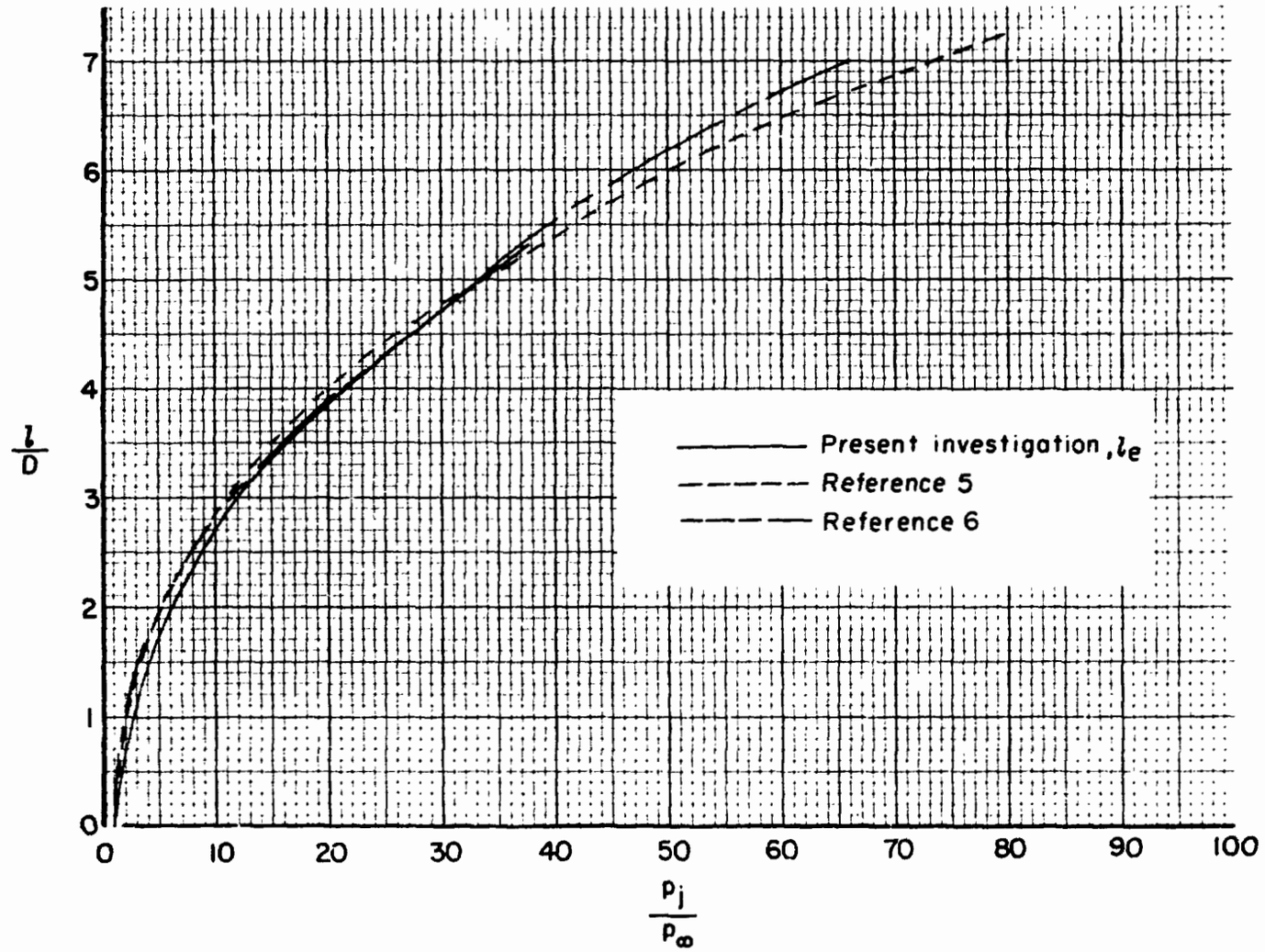

Figure 4.- Comparison of experimentally determined plume lengths of underexpanded sonic free jets.

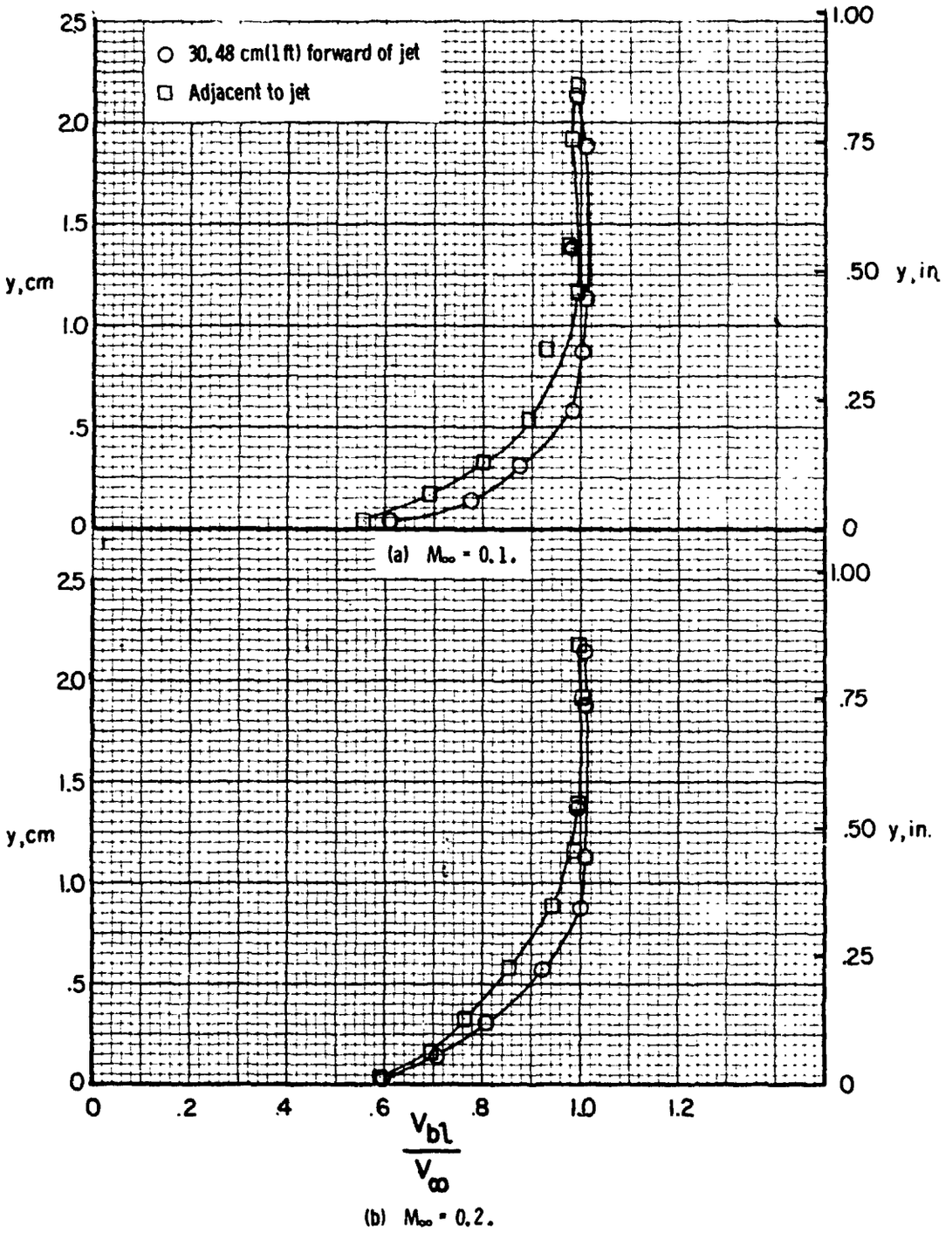

Figure 5.- Boundary-layer profiles measured on the flat plate at two locations 7.6 cm (3.0 in.) to the side of the plate center line.

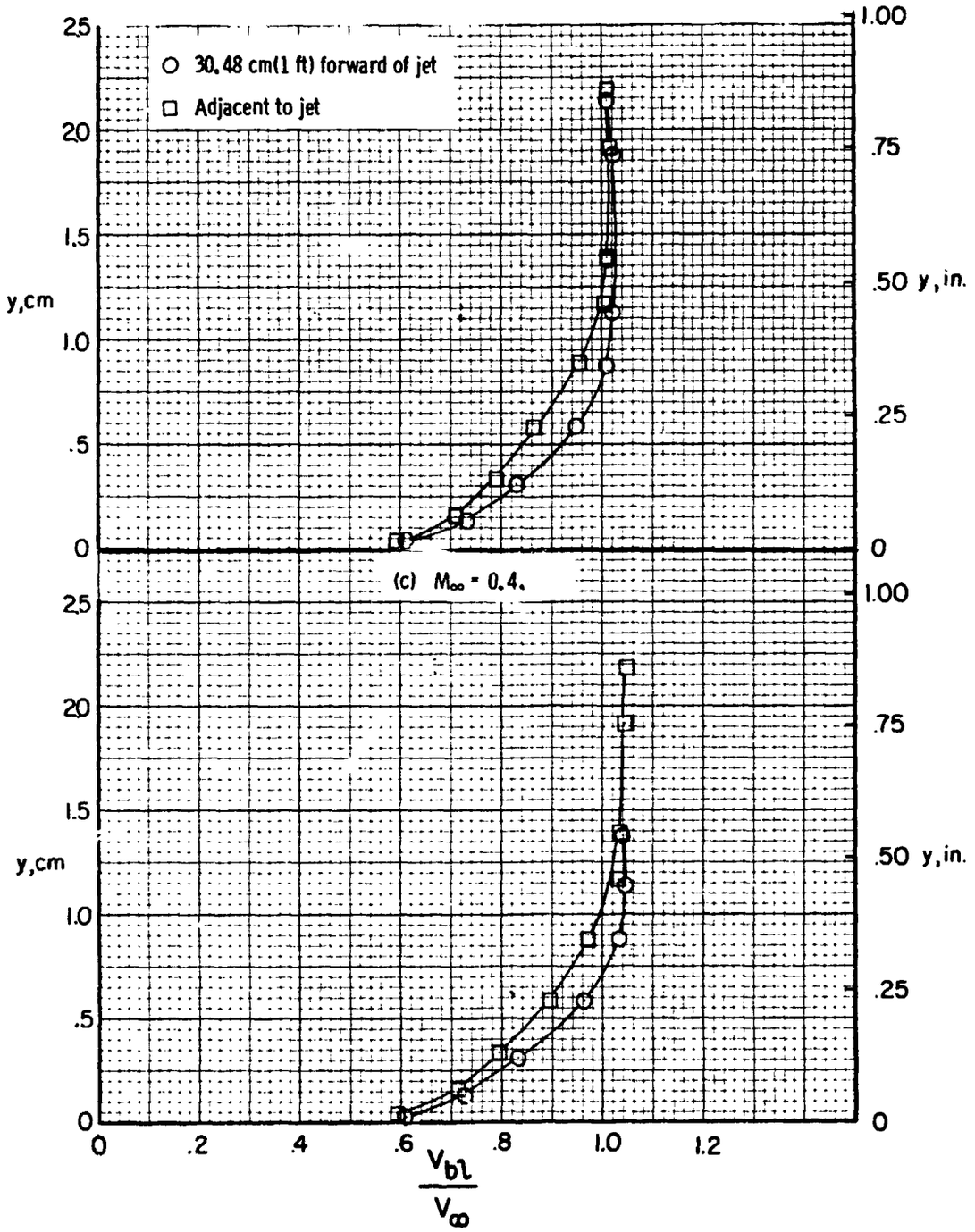

Figure 5.- Concluded.

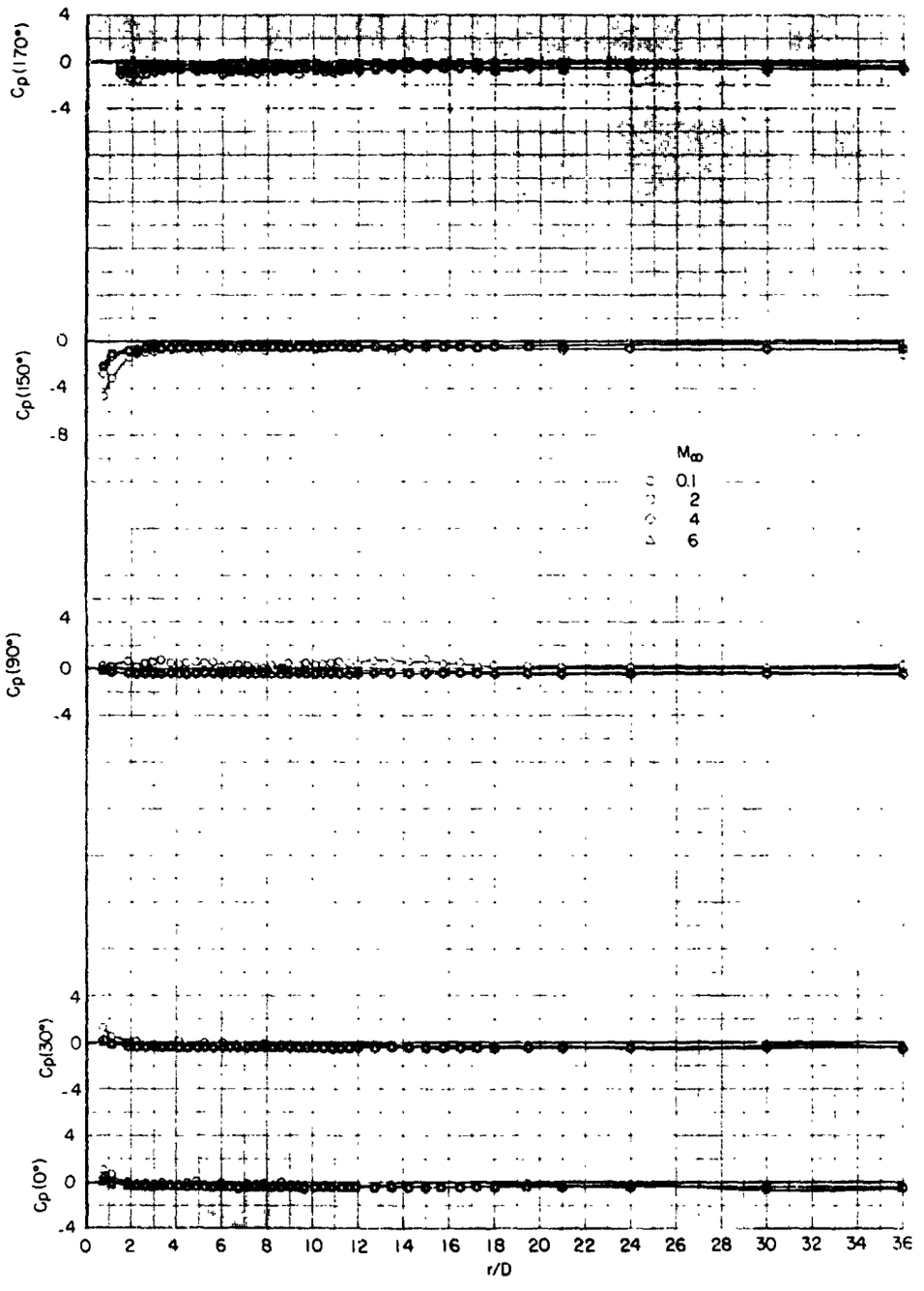

Figure 6.- Induced static-pressure coefficients on the flat plate for $\bar{Q}_{mom} = 0.7$.

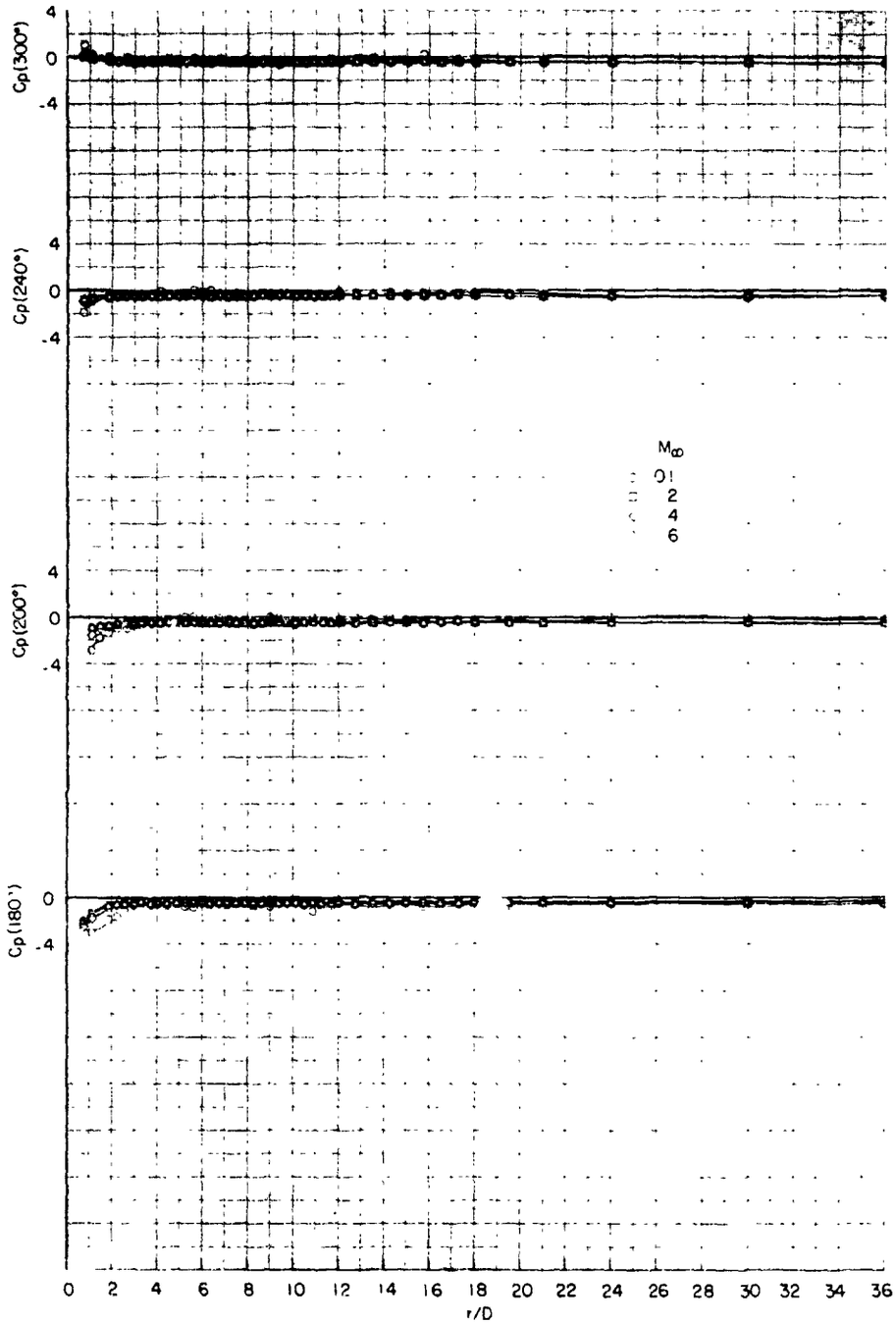

Figure 6.- Concluded.

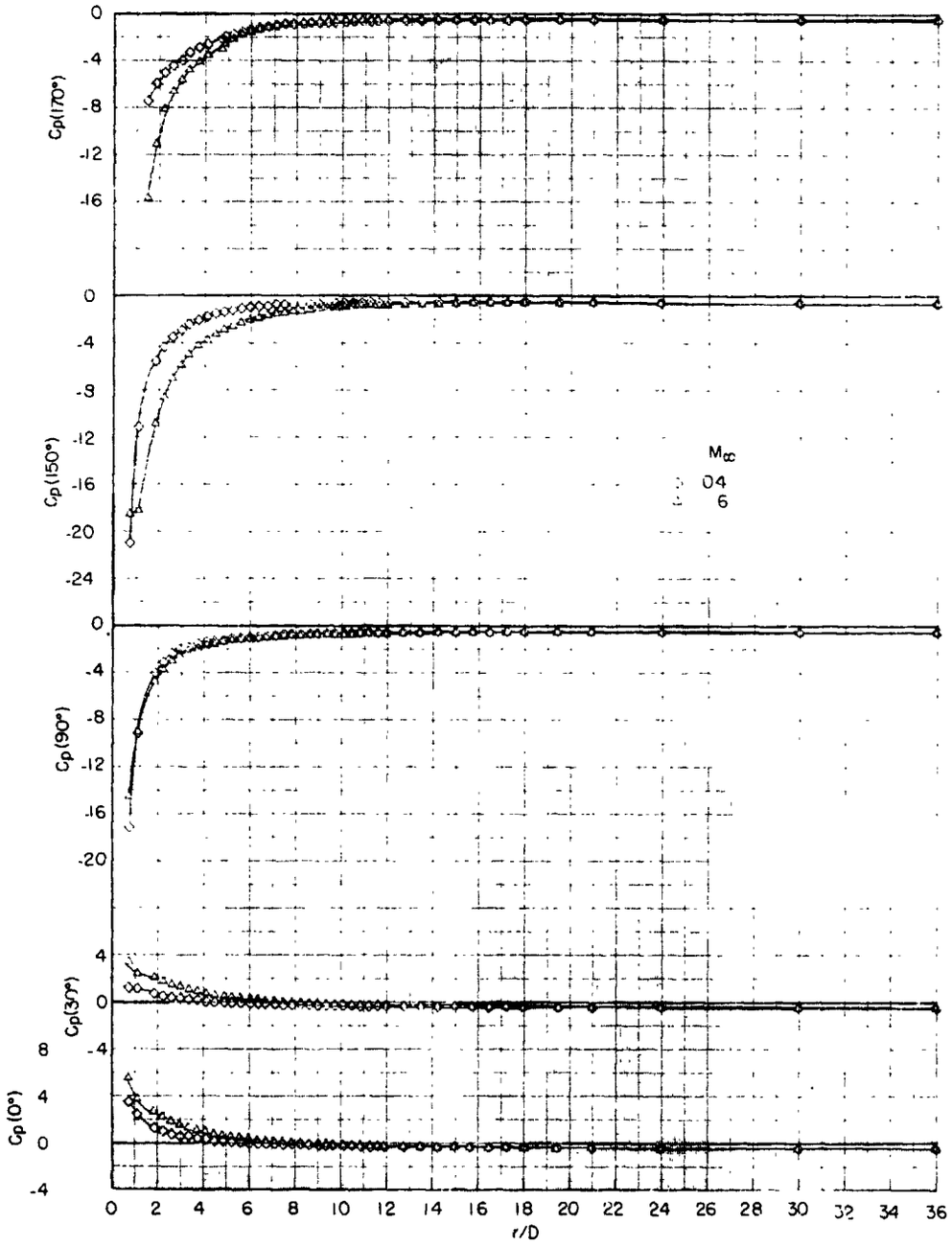

Figure 7.- Induced static-pressure coefficients on the flat plate for $\bar{Q}_{mom} = 10.6$.

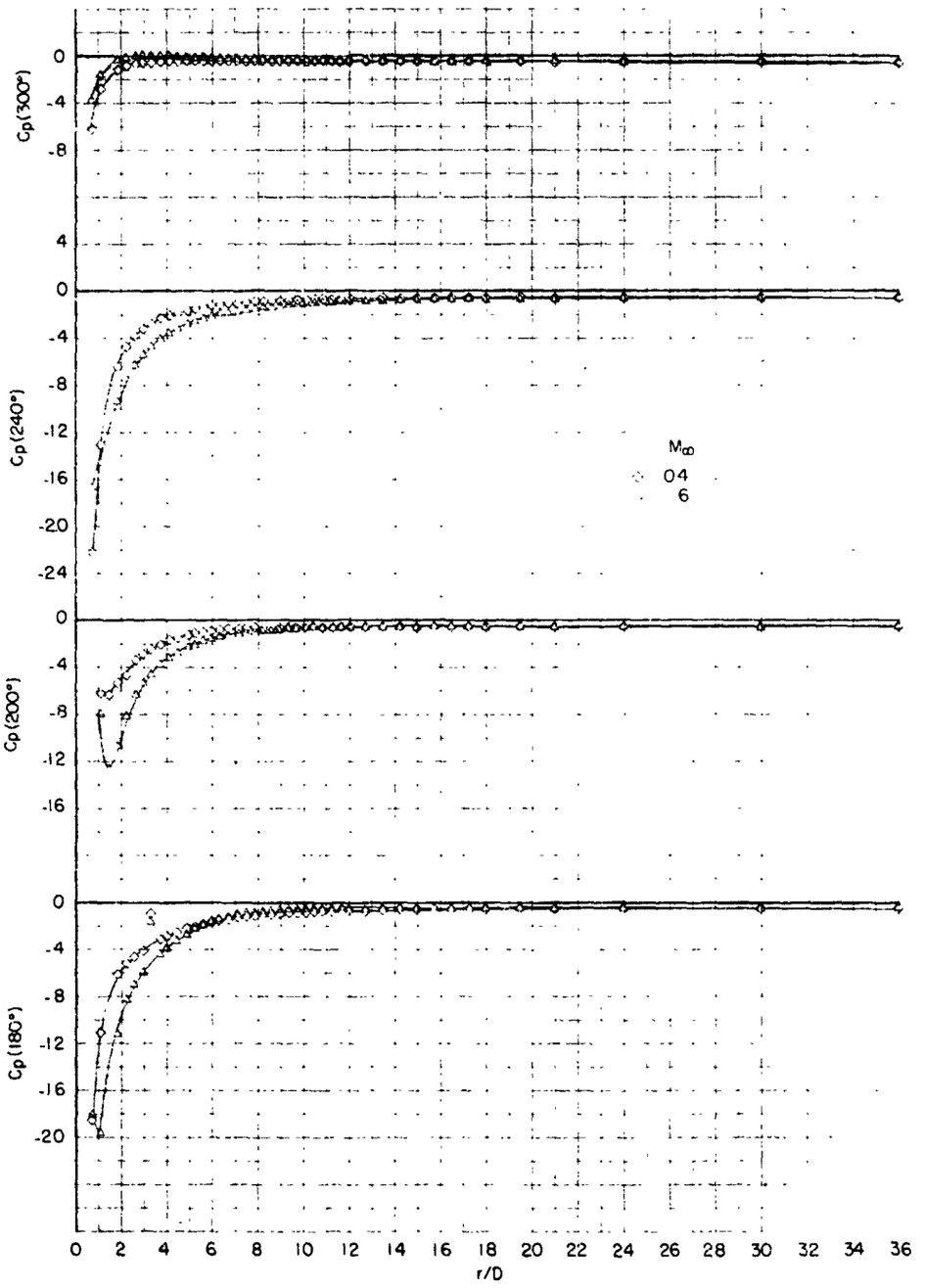

Figure 7.- Concluded.

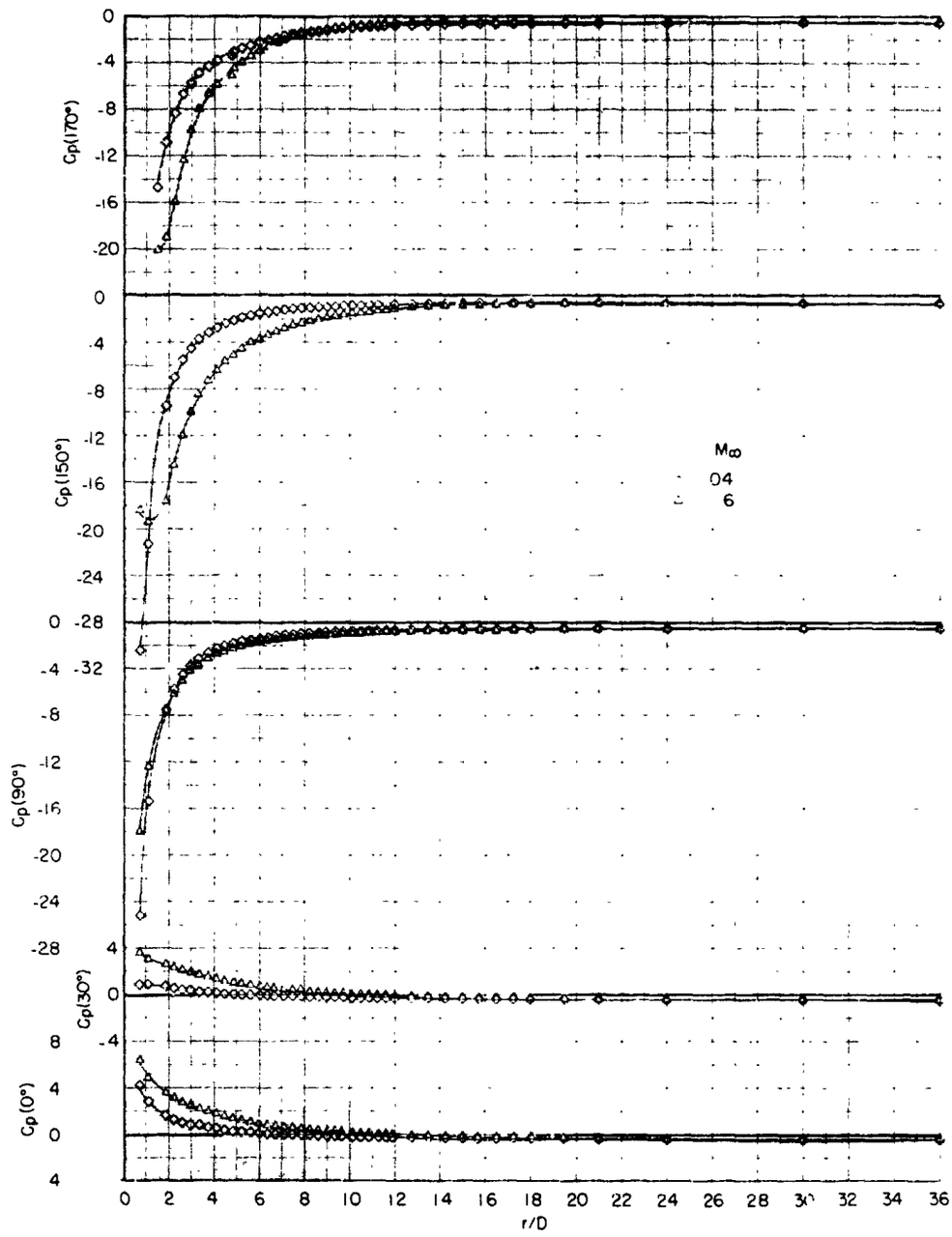

Figure 8.- Induced static-pressure coefficients on the flat plate for $\bar{Q}_{mom} = 20.6$.

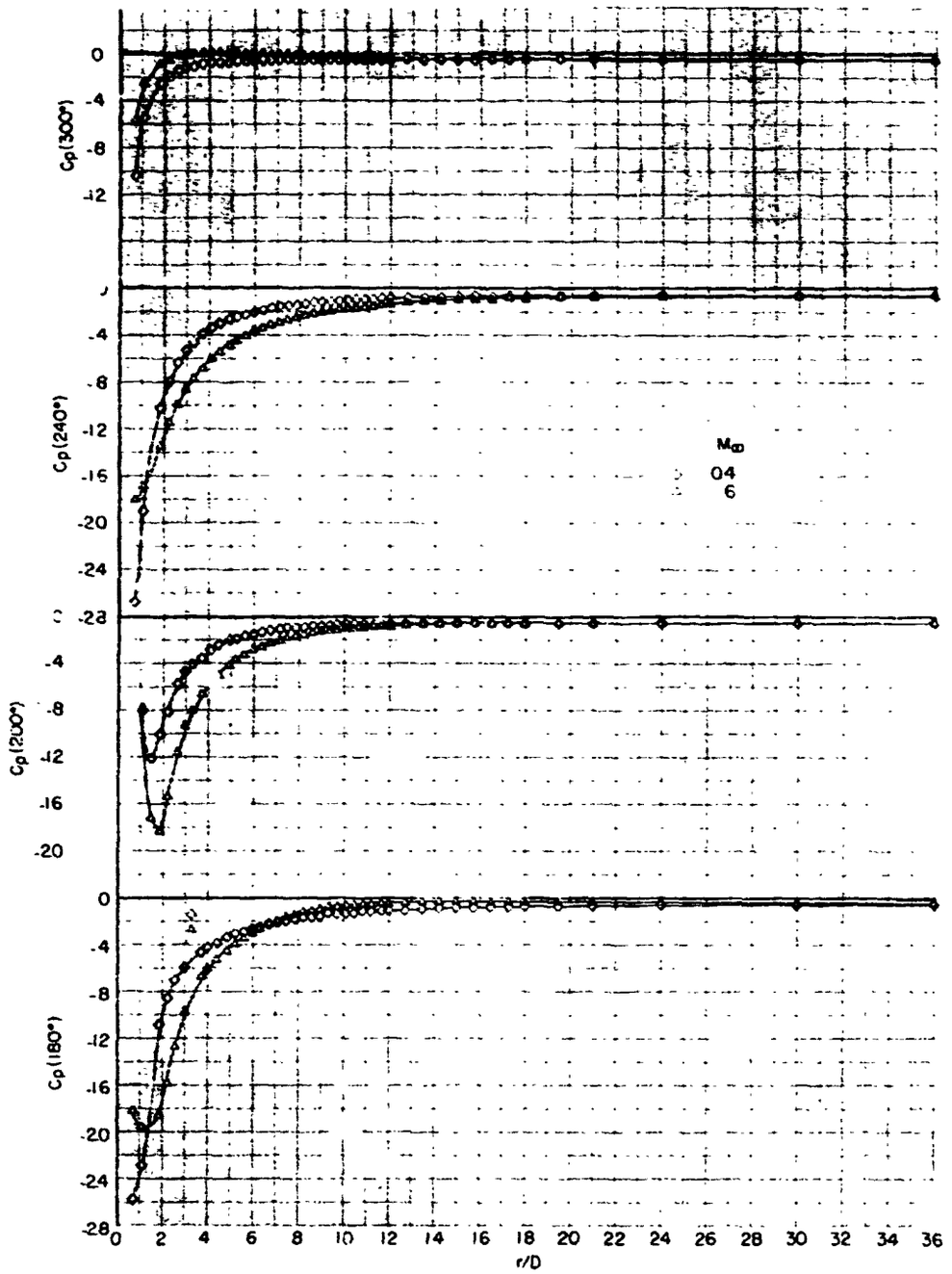

Figure 8.- Concluded.

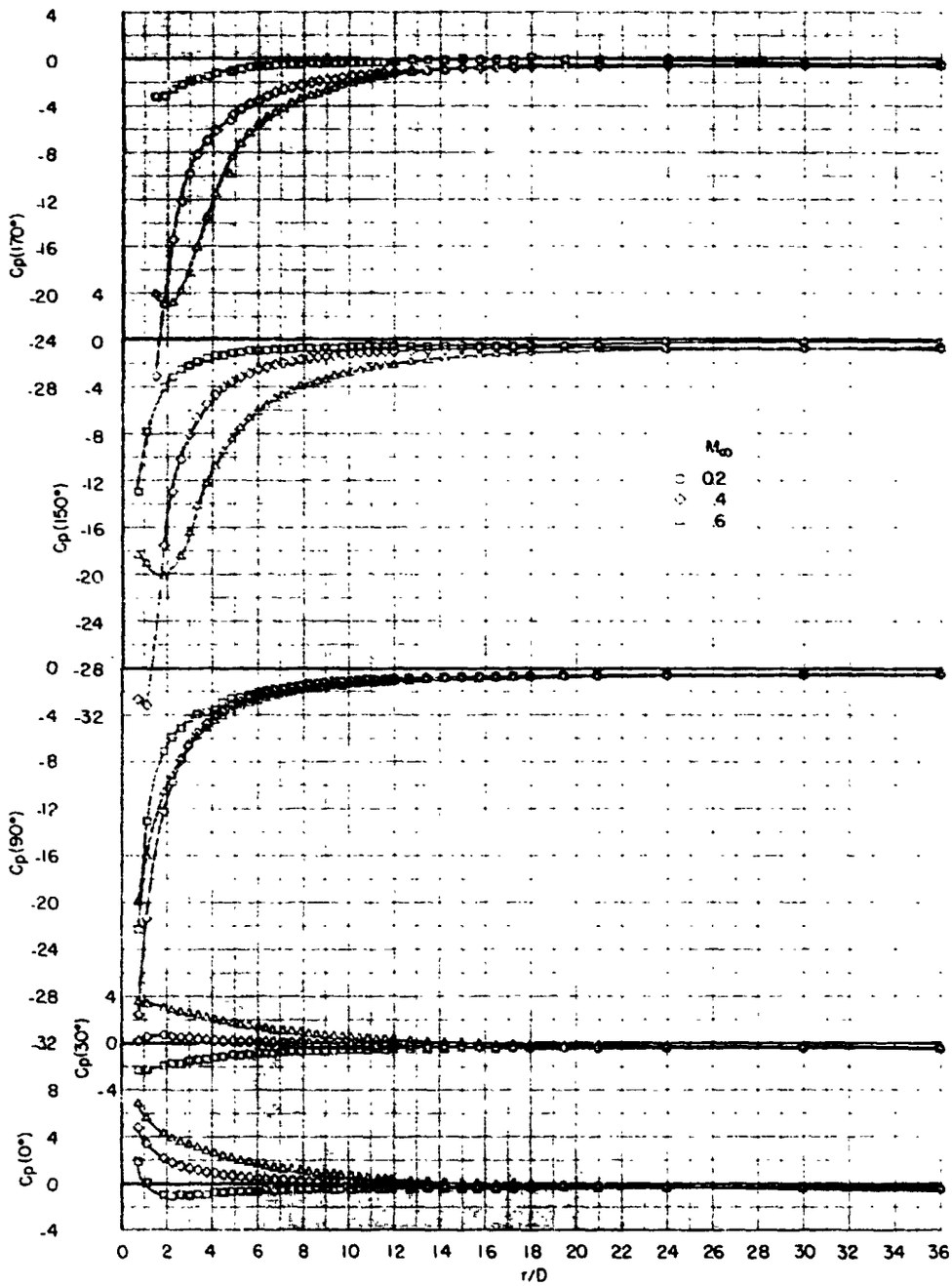

Figure 9.- Induced static-pressure coefficients on the flat plate for $\bar{Q}_{mom} = 41.4$.

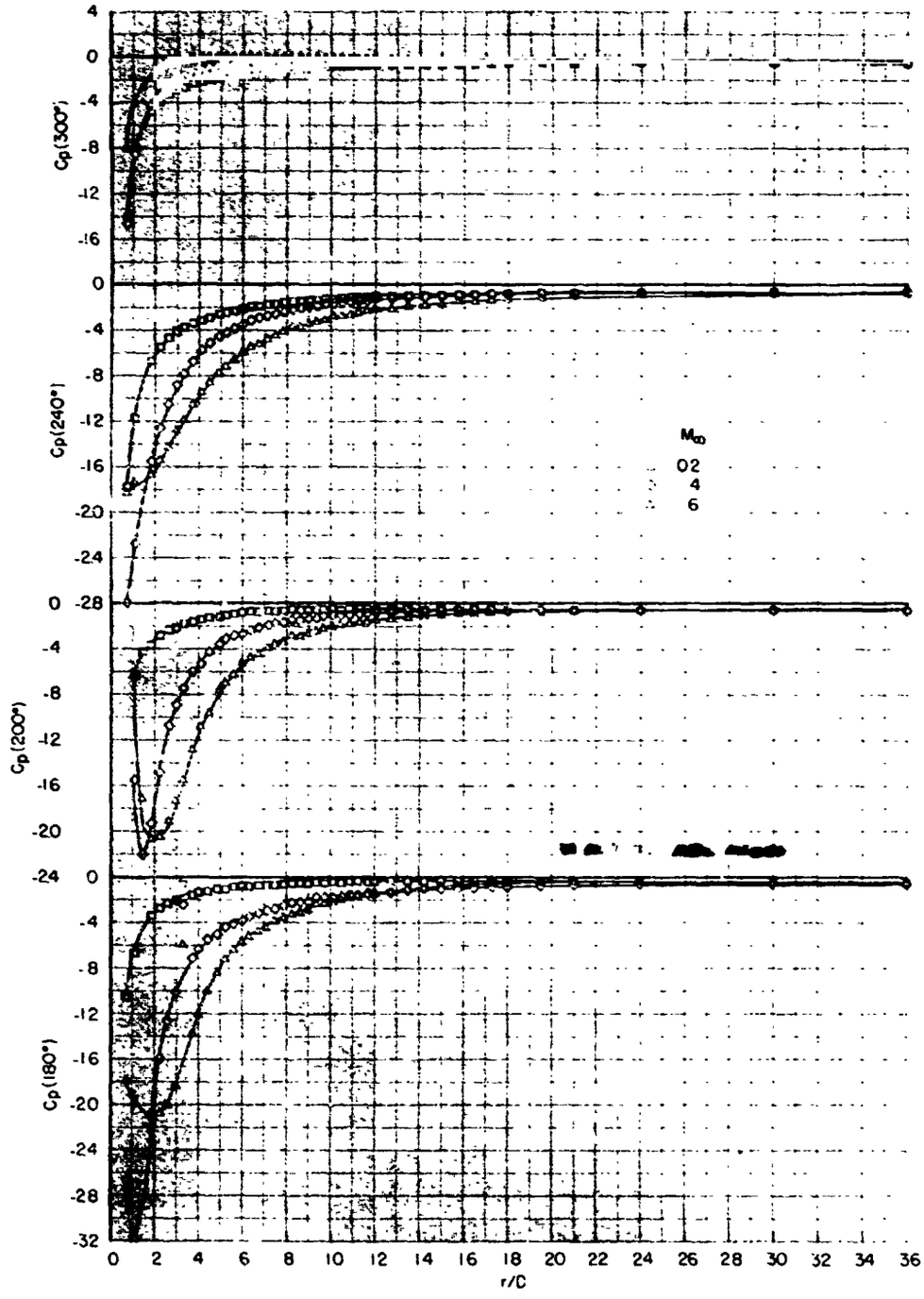

Figure 9.- Concluded.

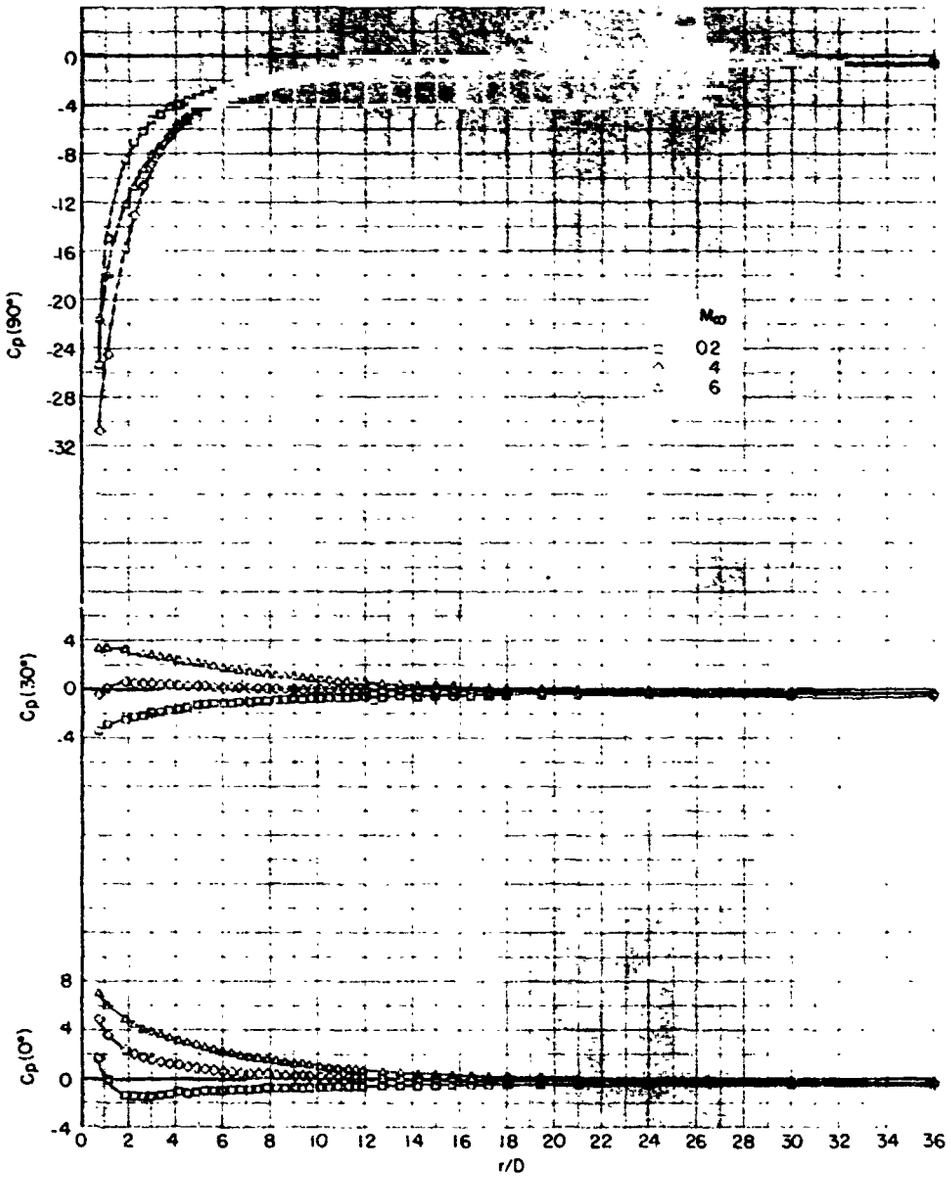

Figure 10.- Induced static-pressure coefficients on the flat plate for $\bar{Q}_{mom} = 60.4$.

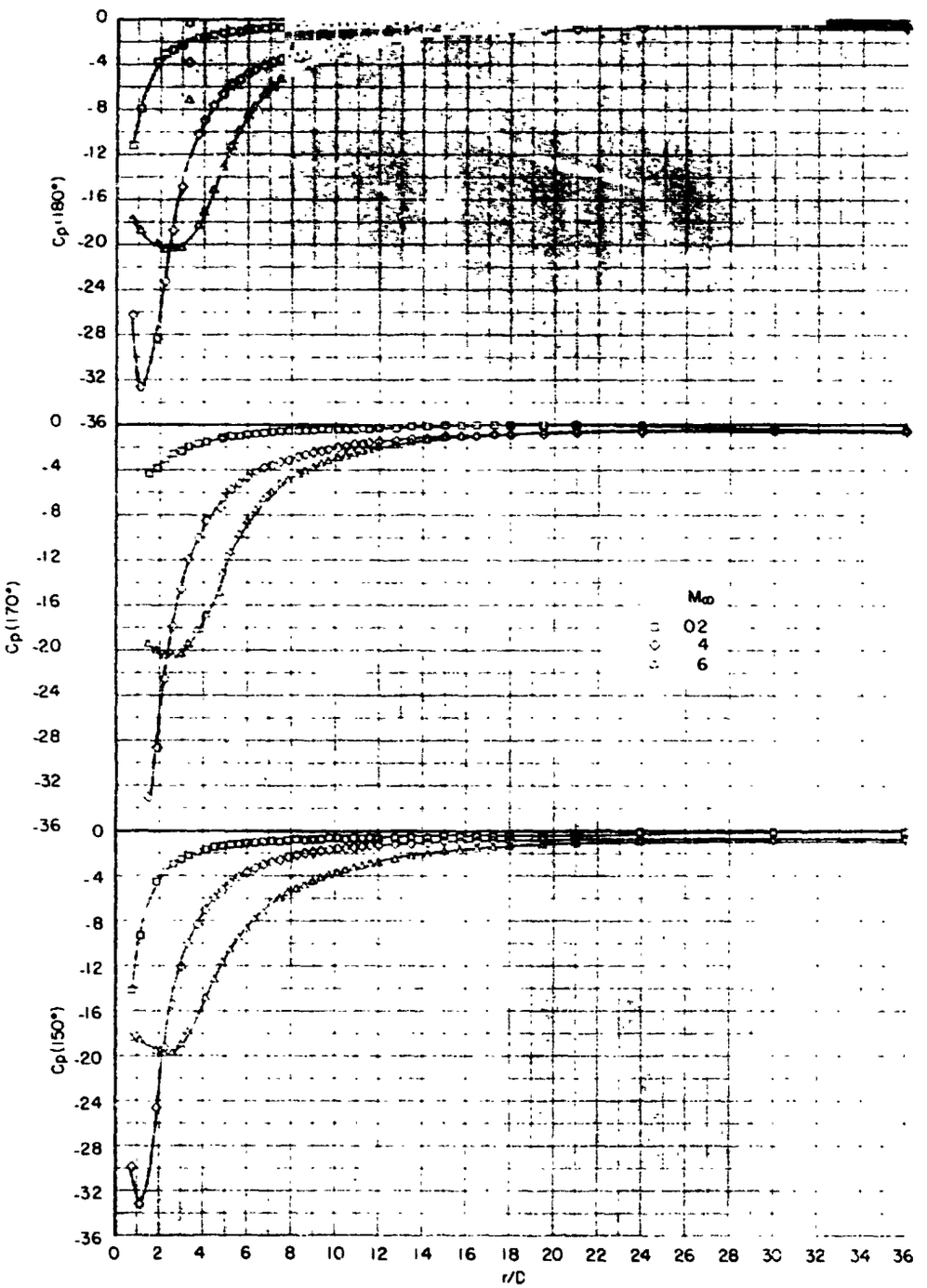

Figure 10.- Continued.

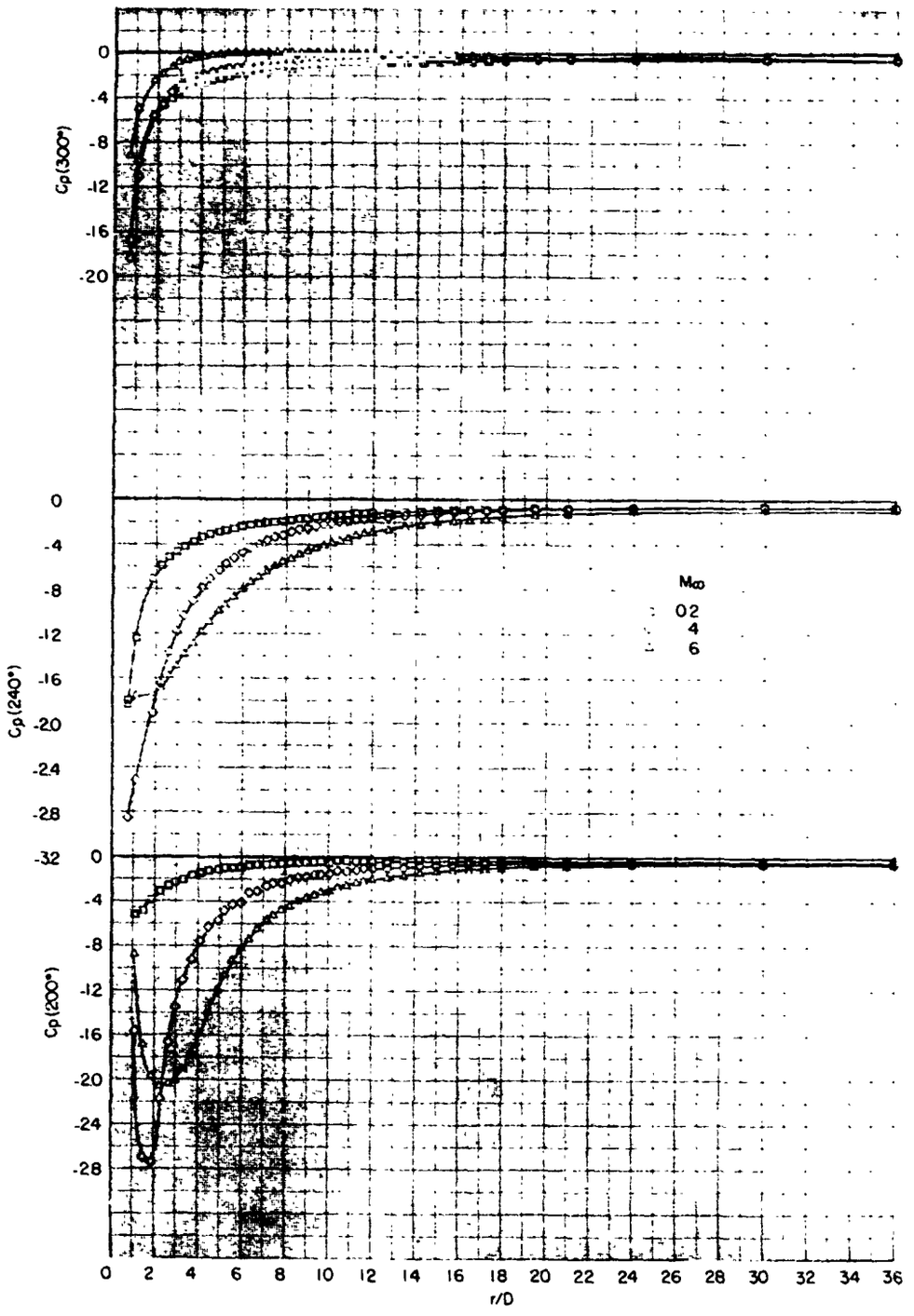

Figure 10.- Concluded.

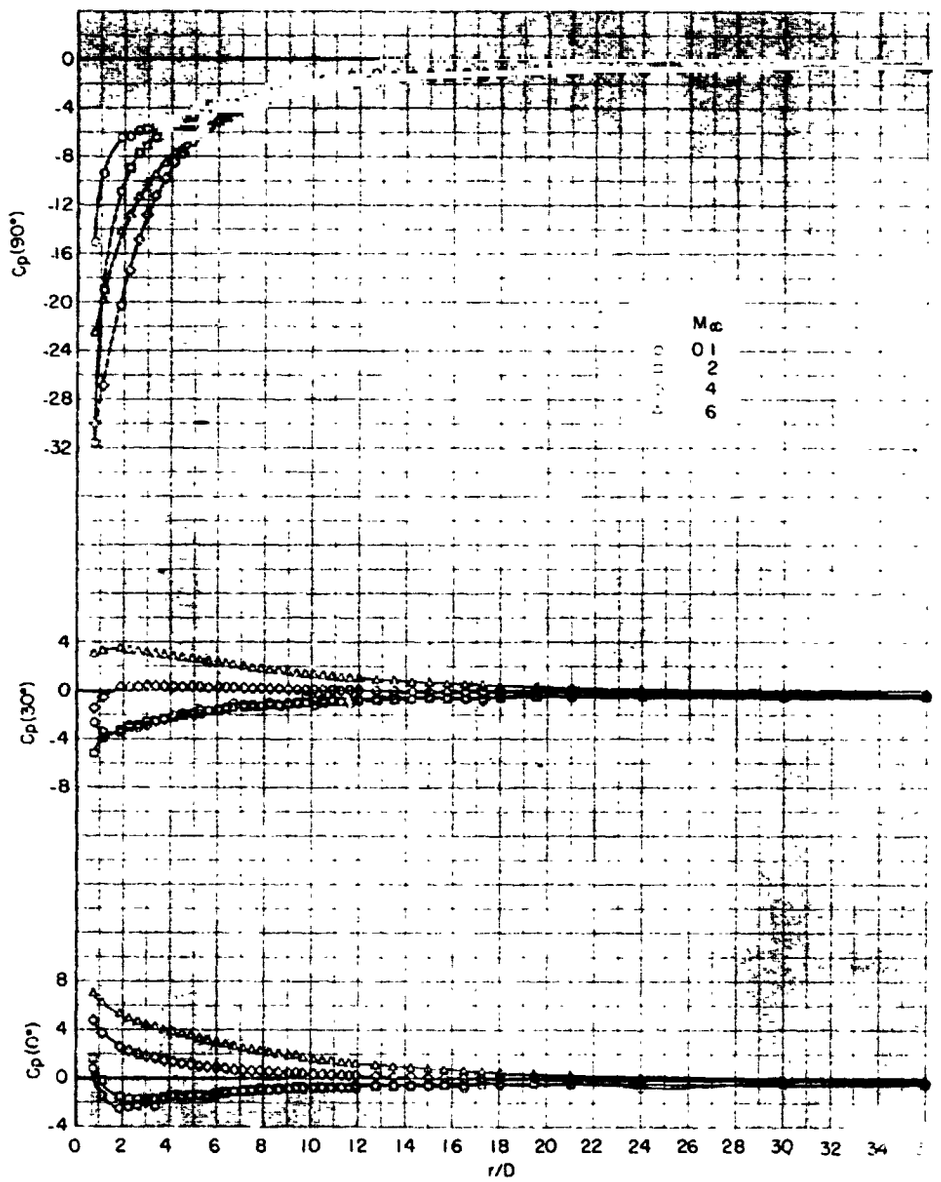

Figure 11.- Induced static-pressure coefficients on the flat plate for $Q_{mom} = 101.2$.

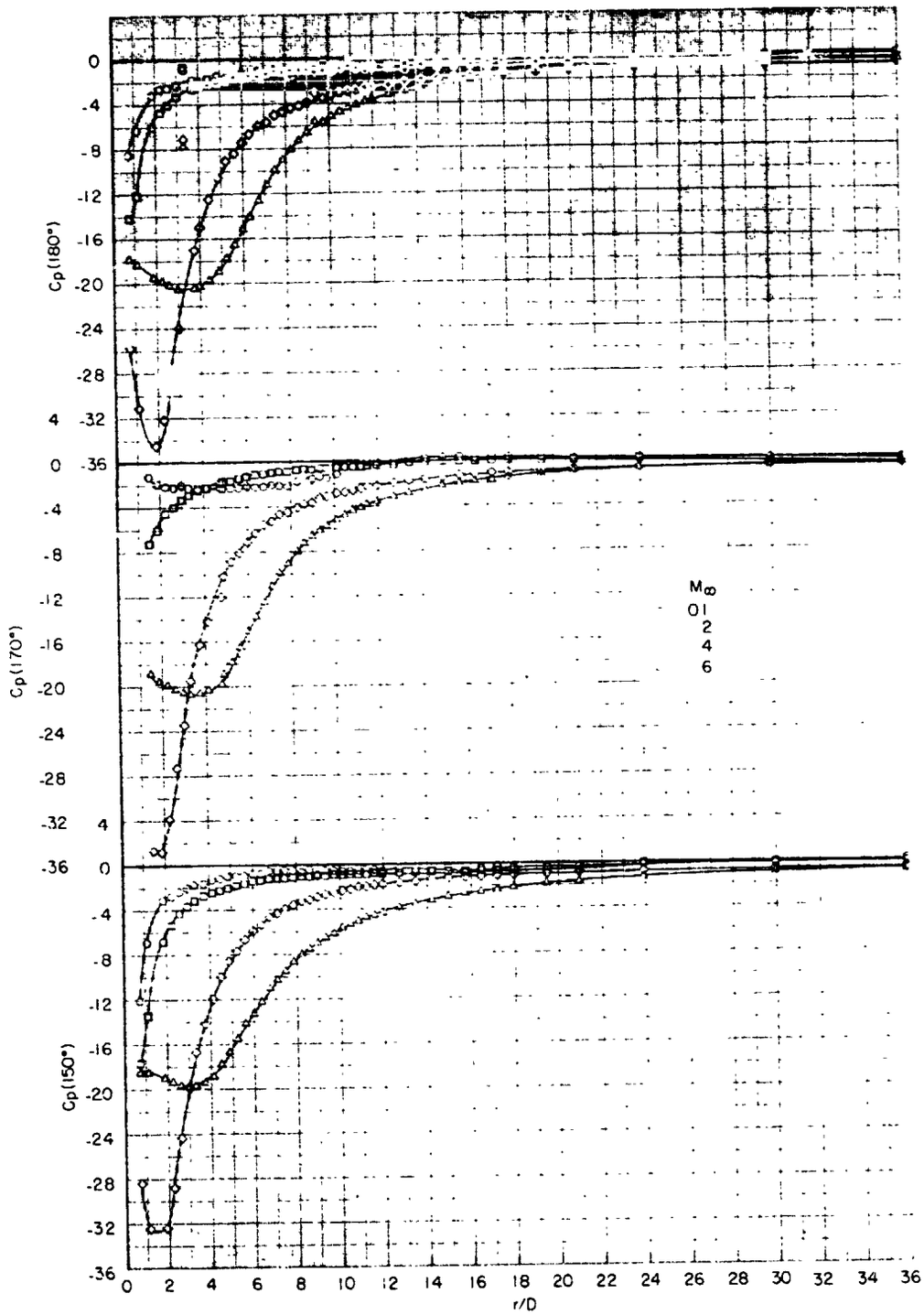

Figure 11.- Continued.

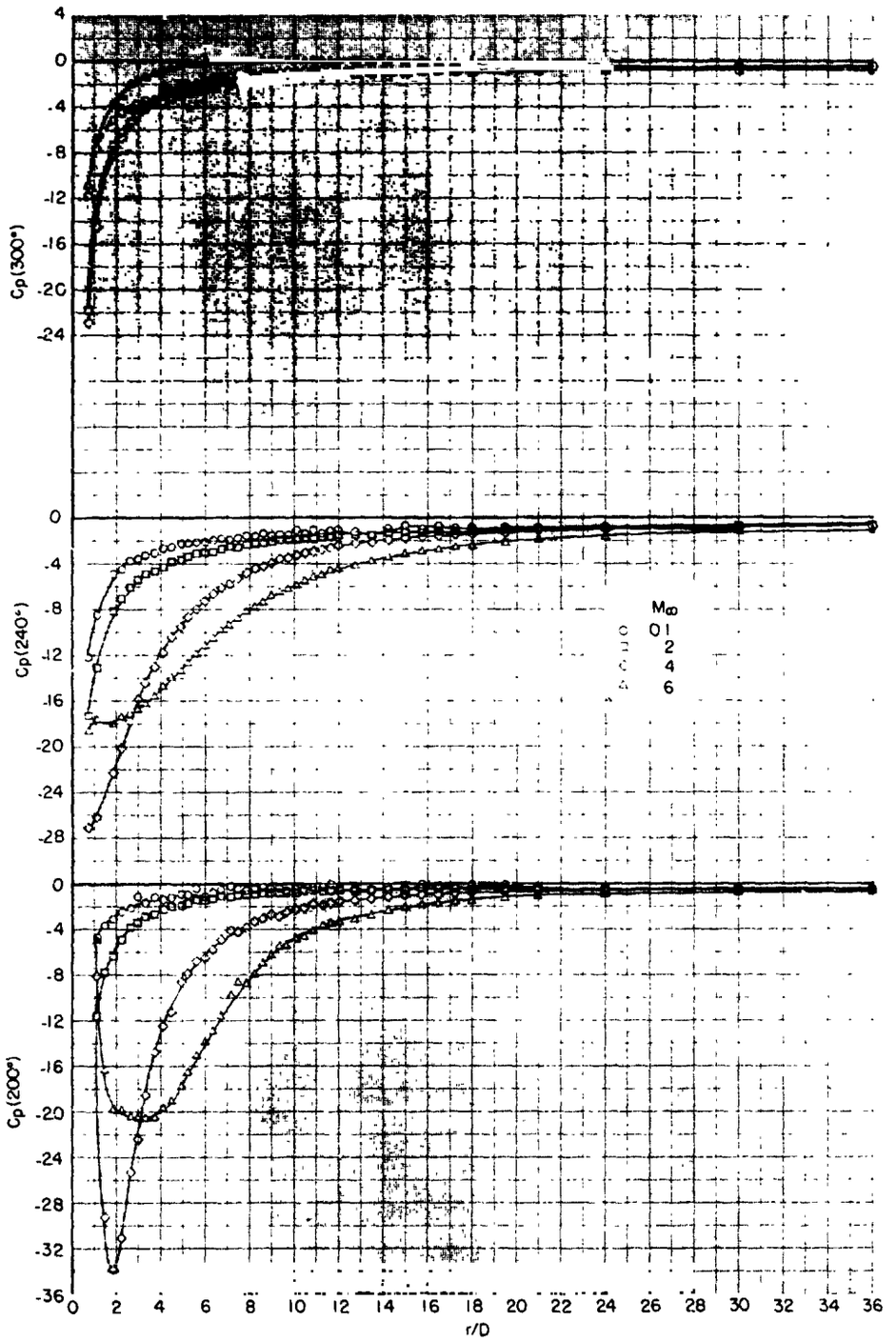

Figure 11.- Concluded.

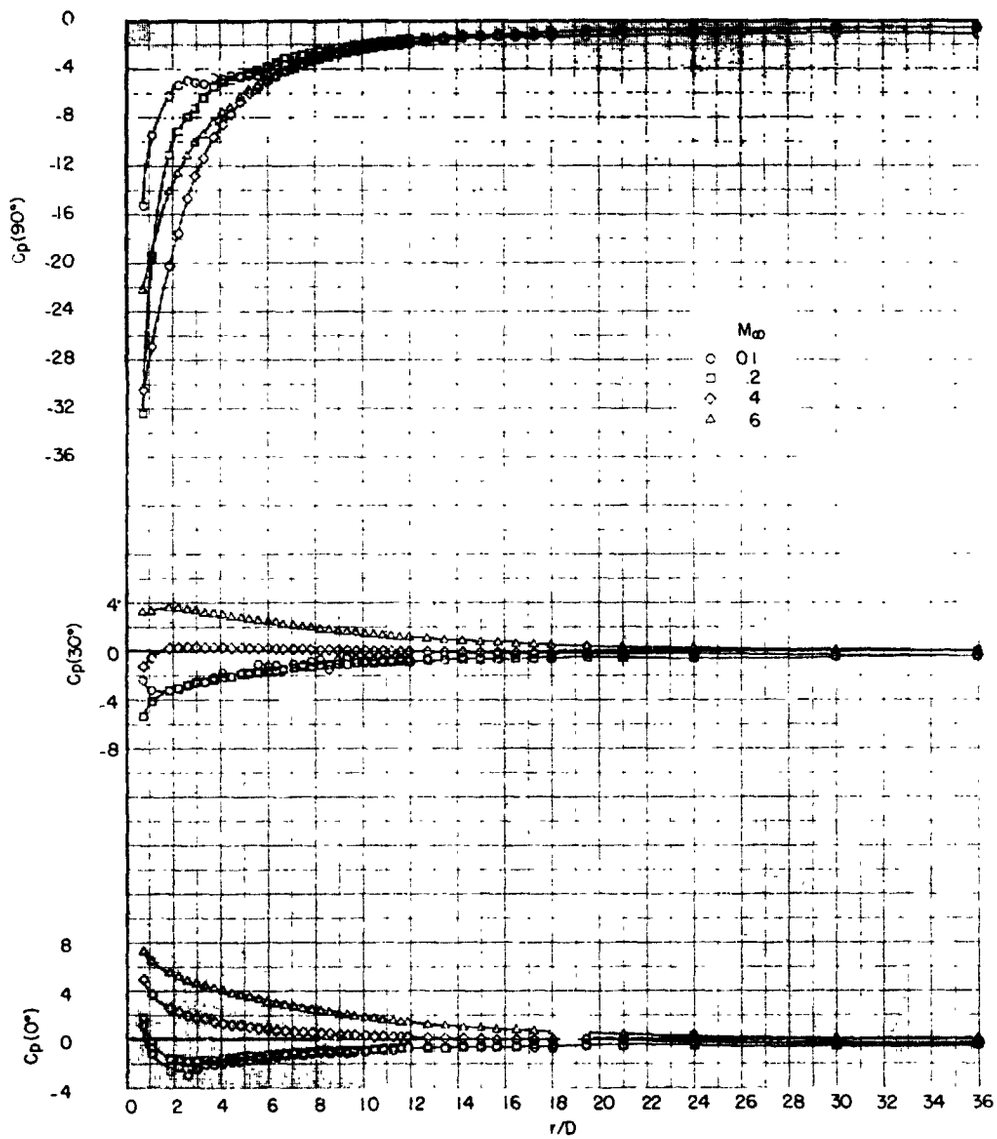

Figure 12.- Induced static-pressure coefficients on the flat plate for $\bar{Q}_{mom} = 104.9$.

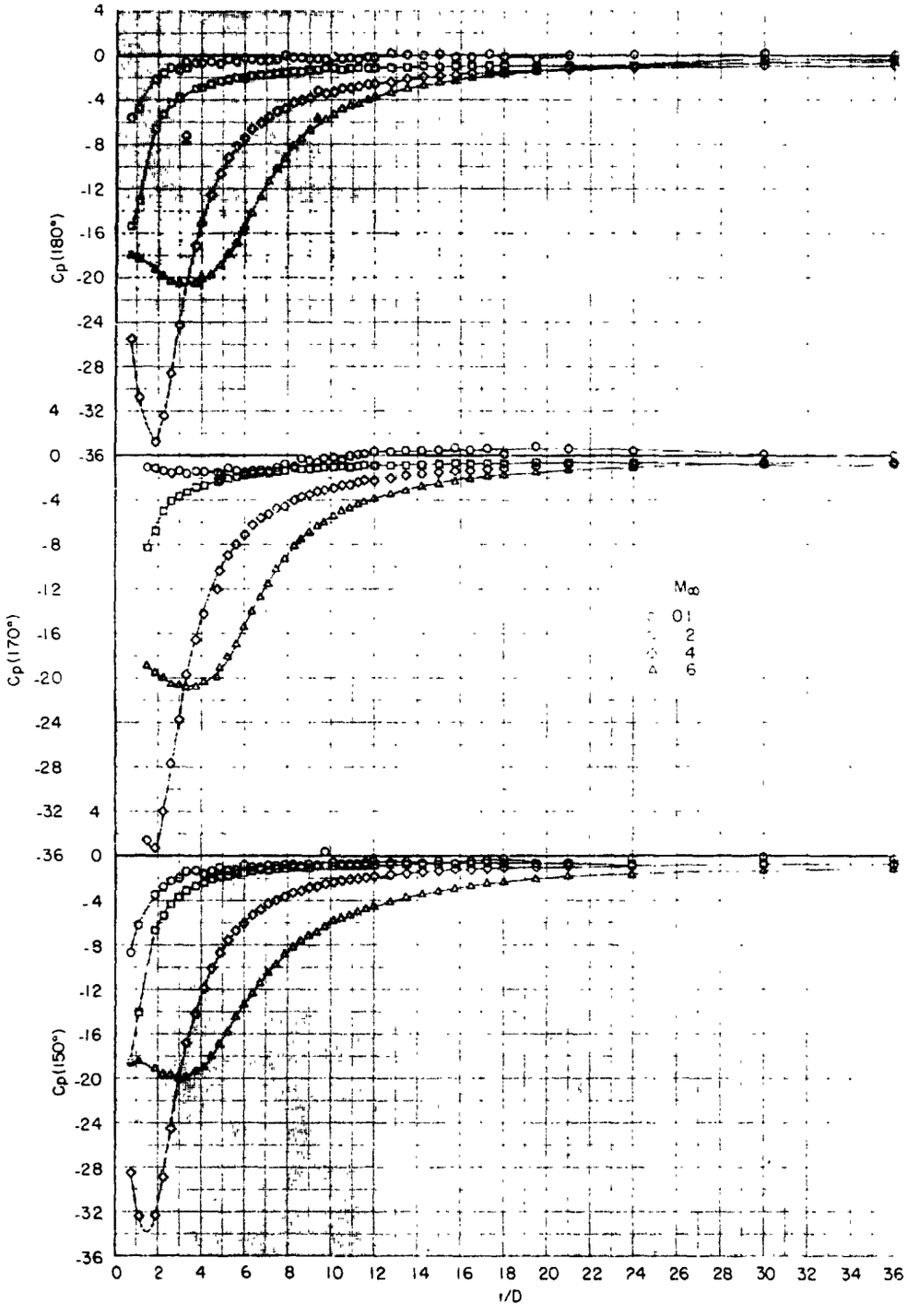

Figure 12.- Continued.

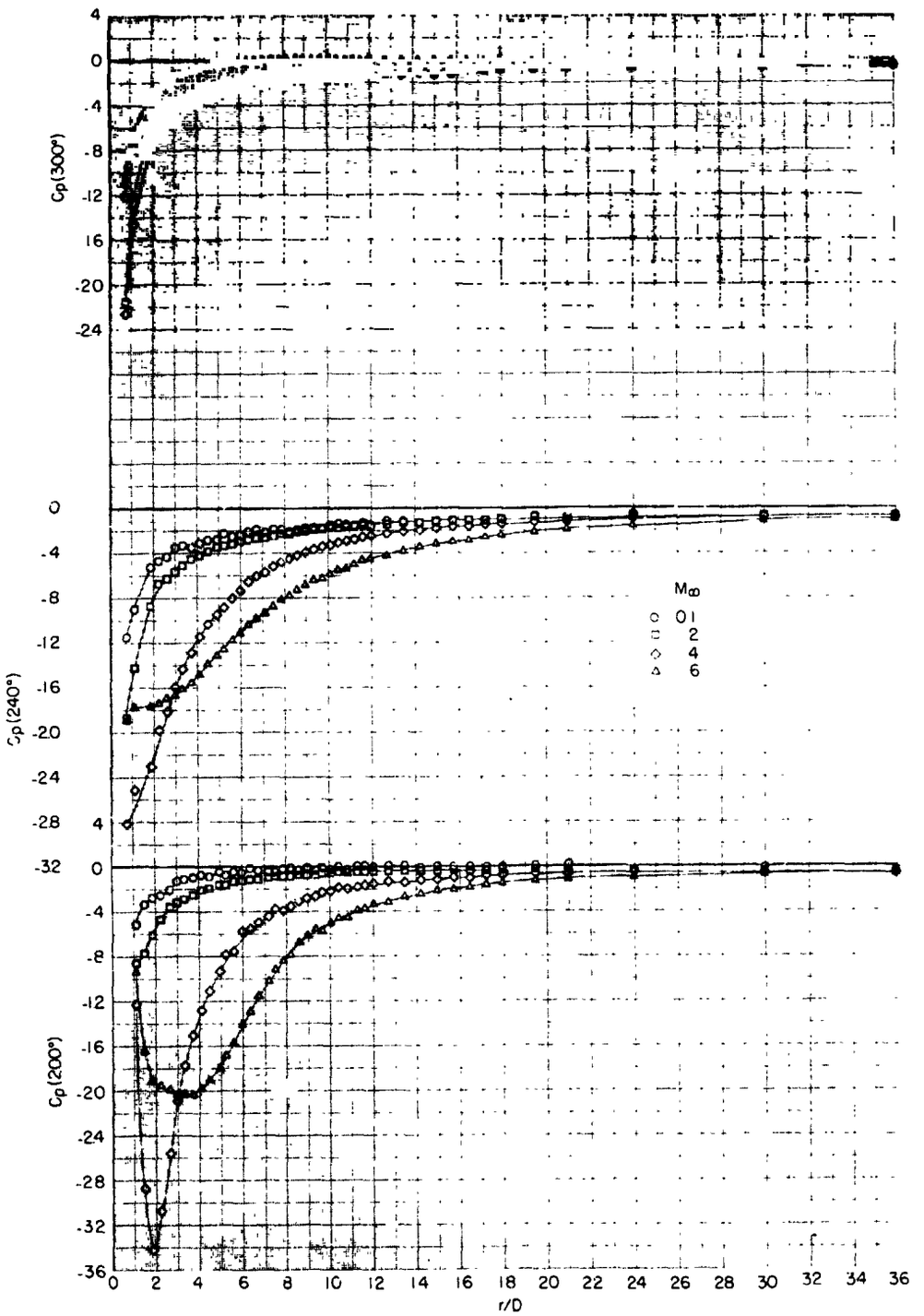

Figure 12.- Concluded.

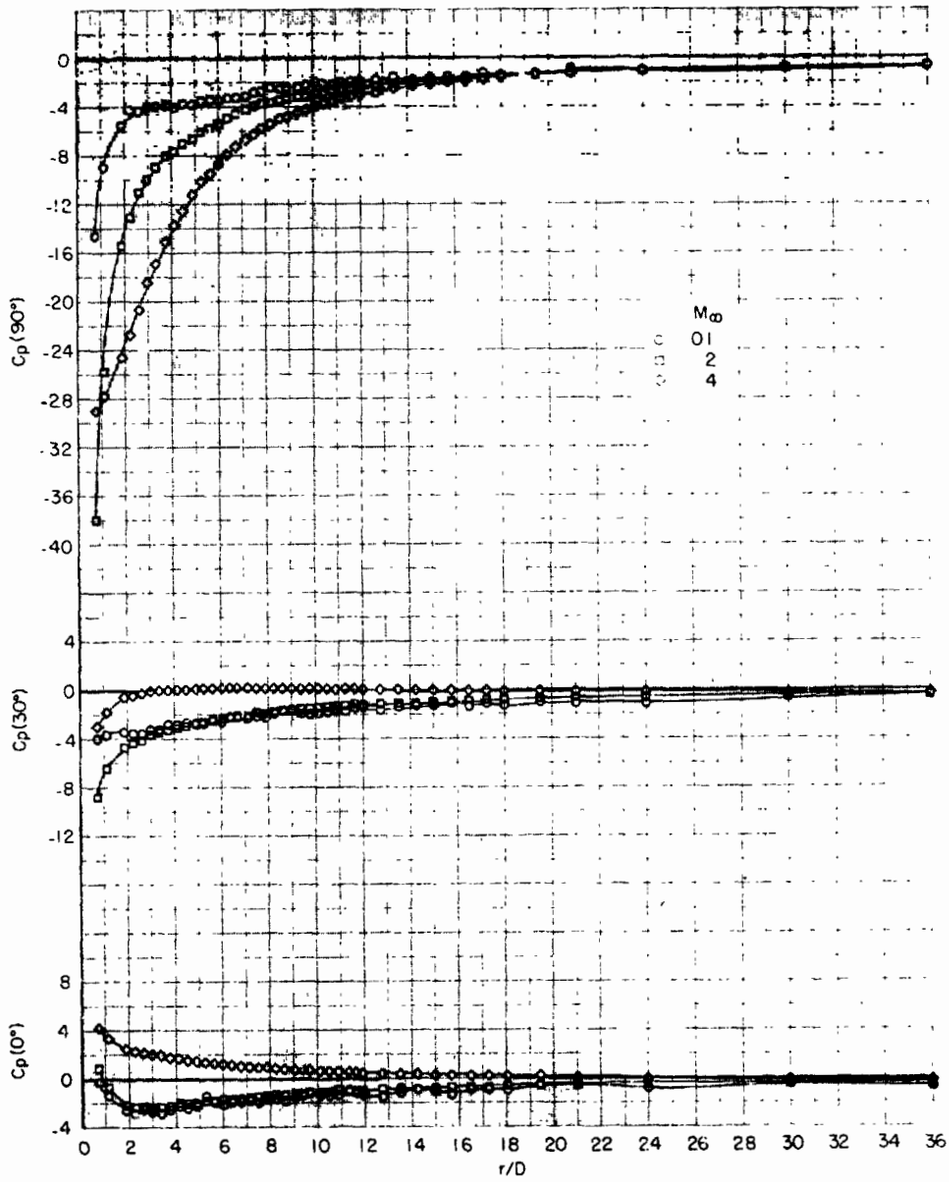

Figure 13.- Induced static-pressure coefficients on the flat plate for $\bar{Q}_{mom} = 203.0$.

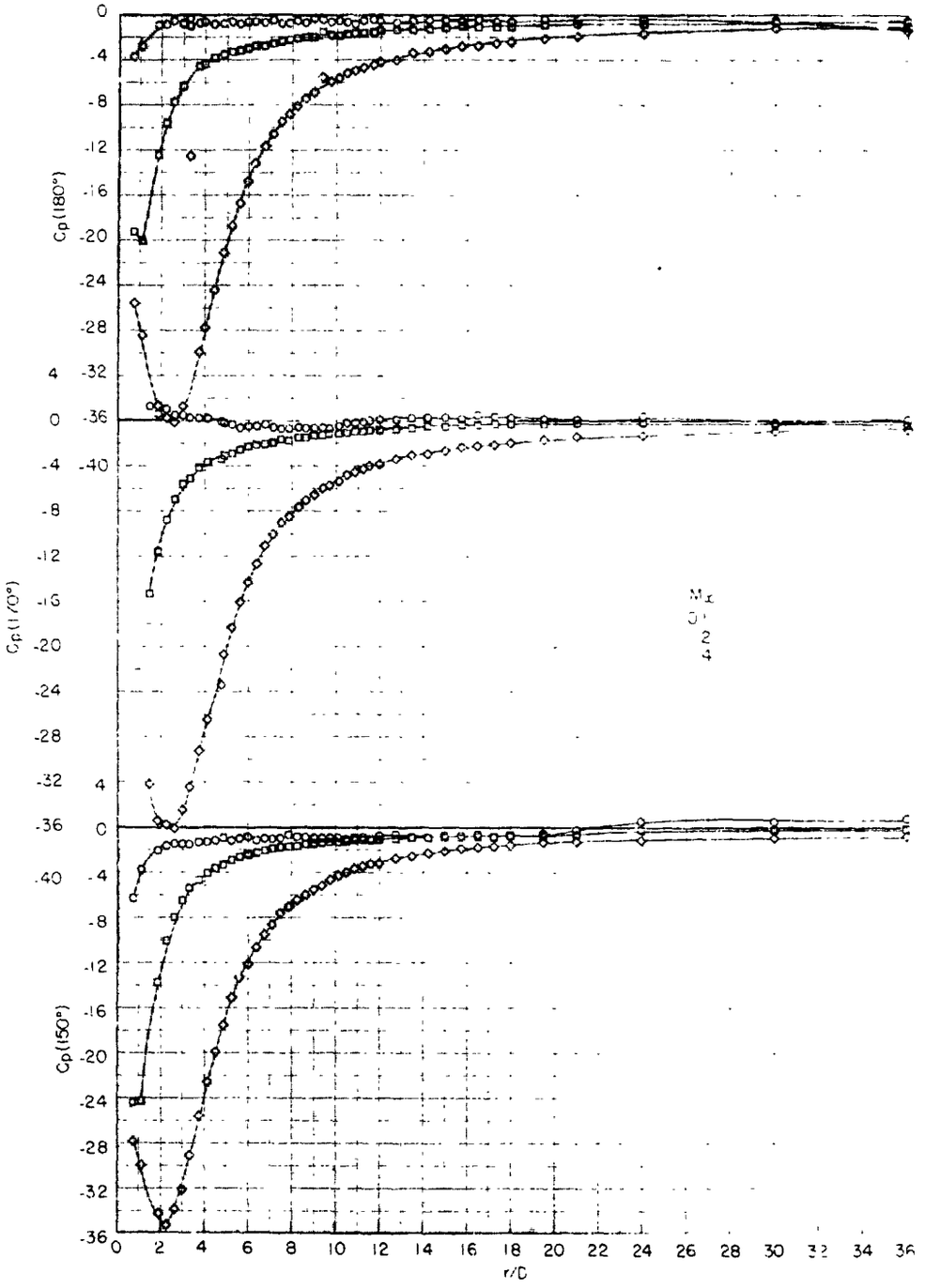

Figure 13.- Continued.

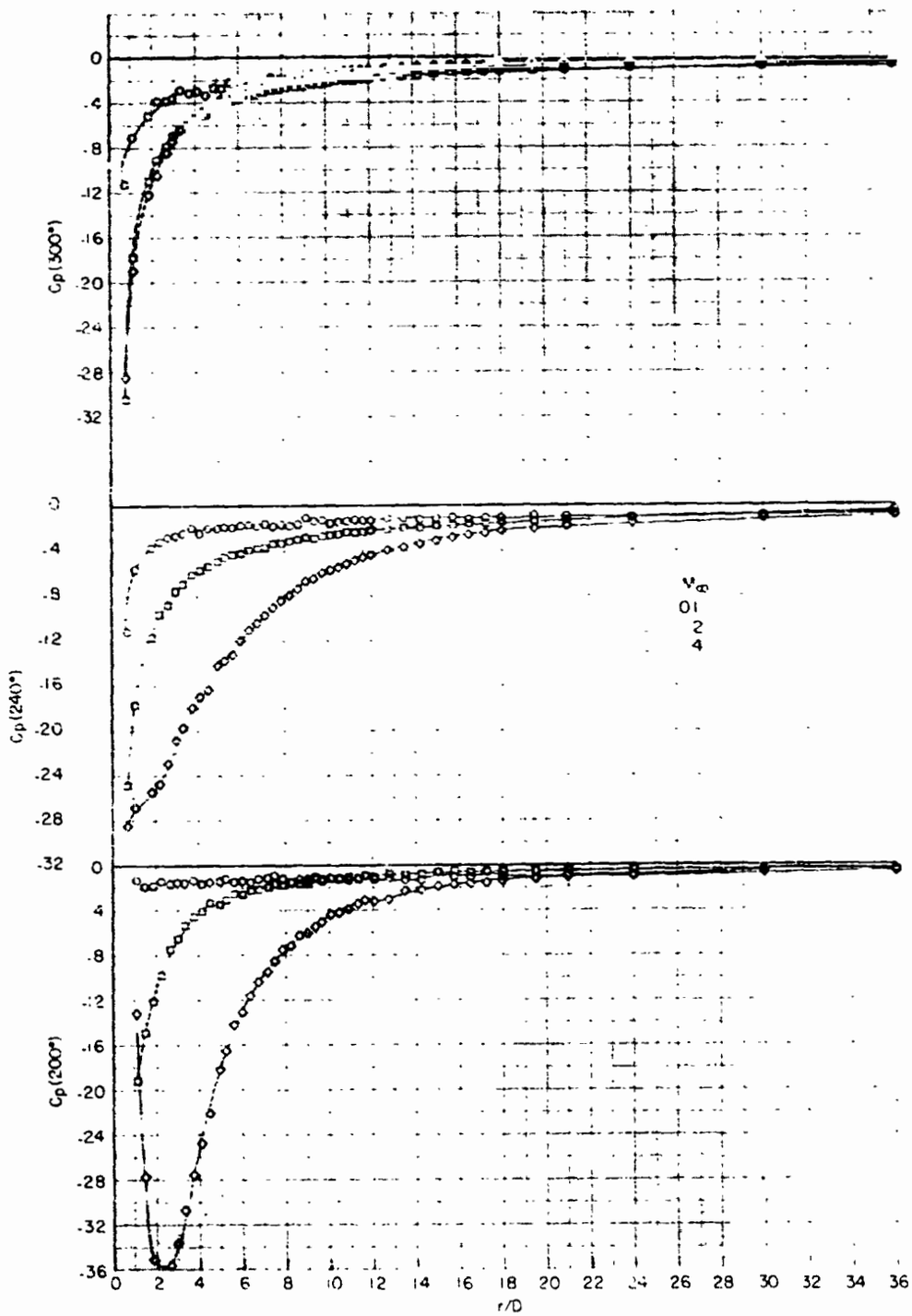

Figure 13.- Concluded.

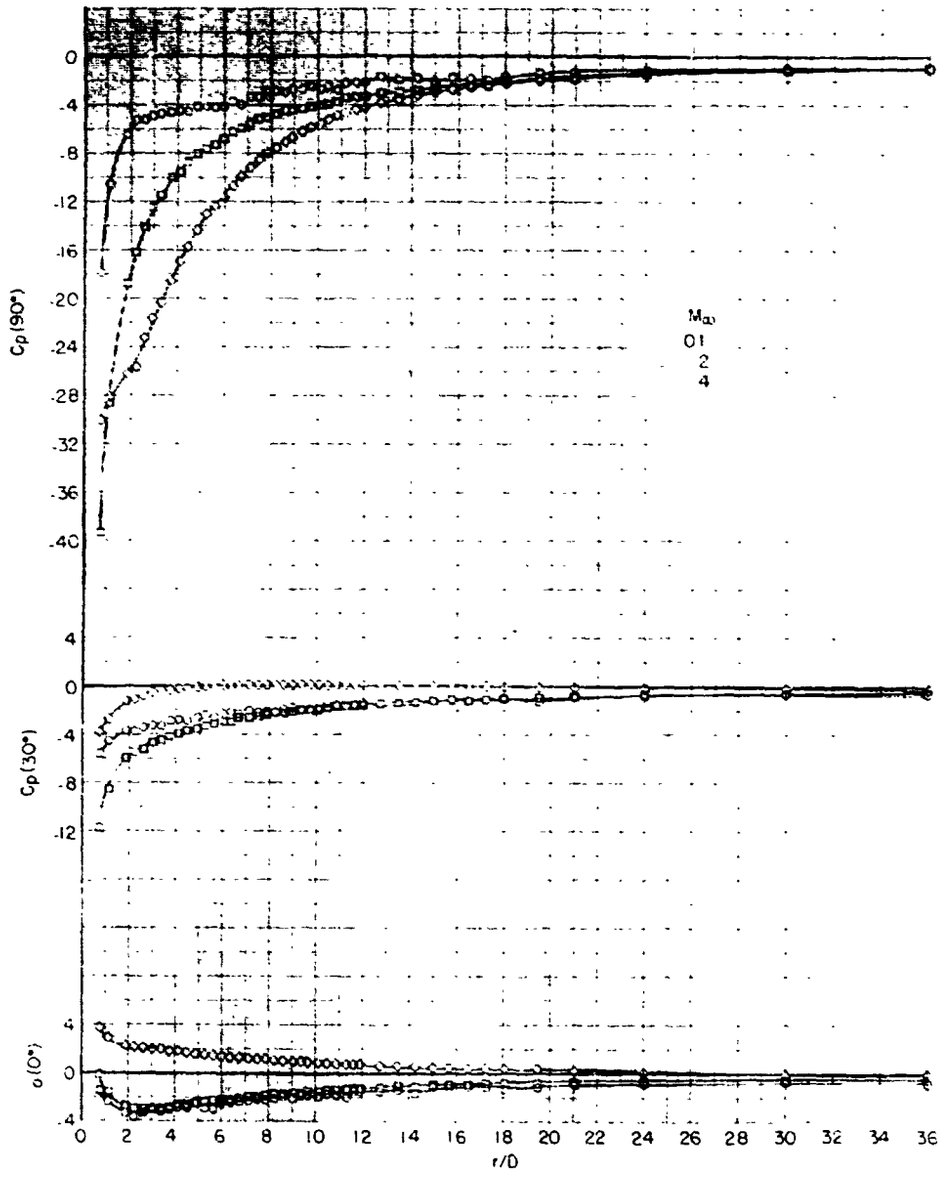

Figure 14.- Induced static-pressure cofficients on the flat plate for $\bar{Q}_{mom} = 308.7$.

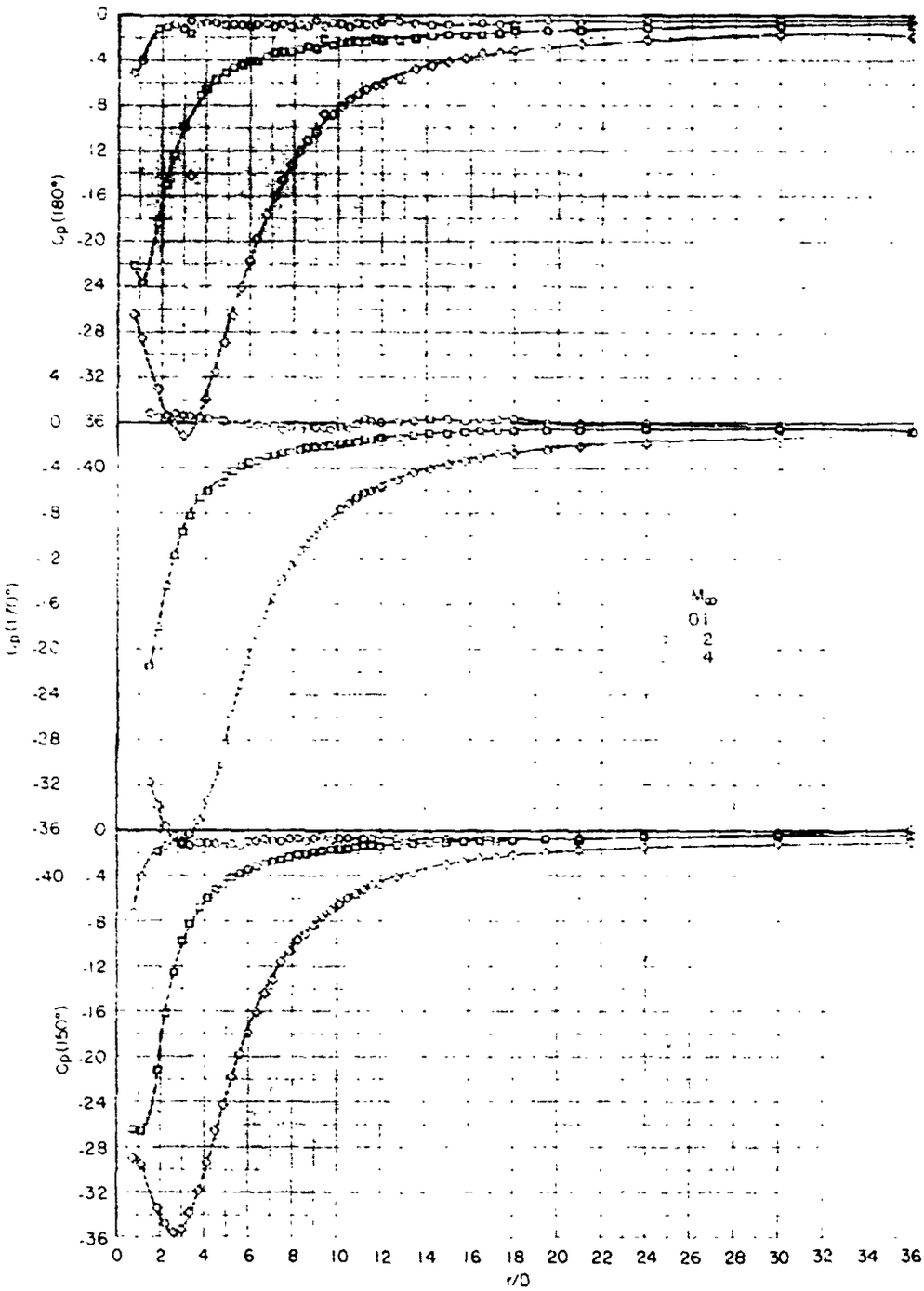

Figure 14.- Continued.

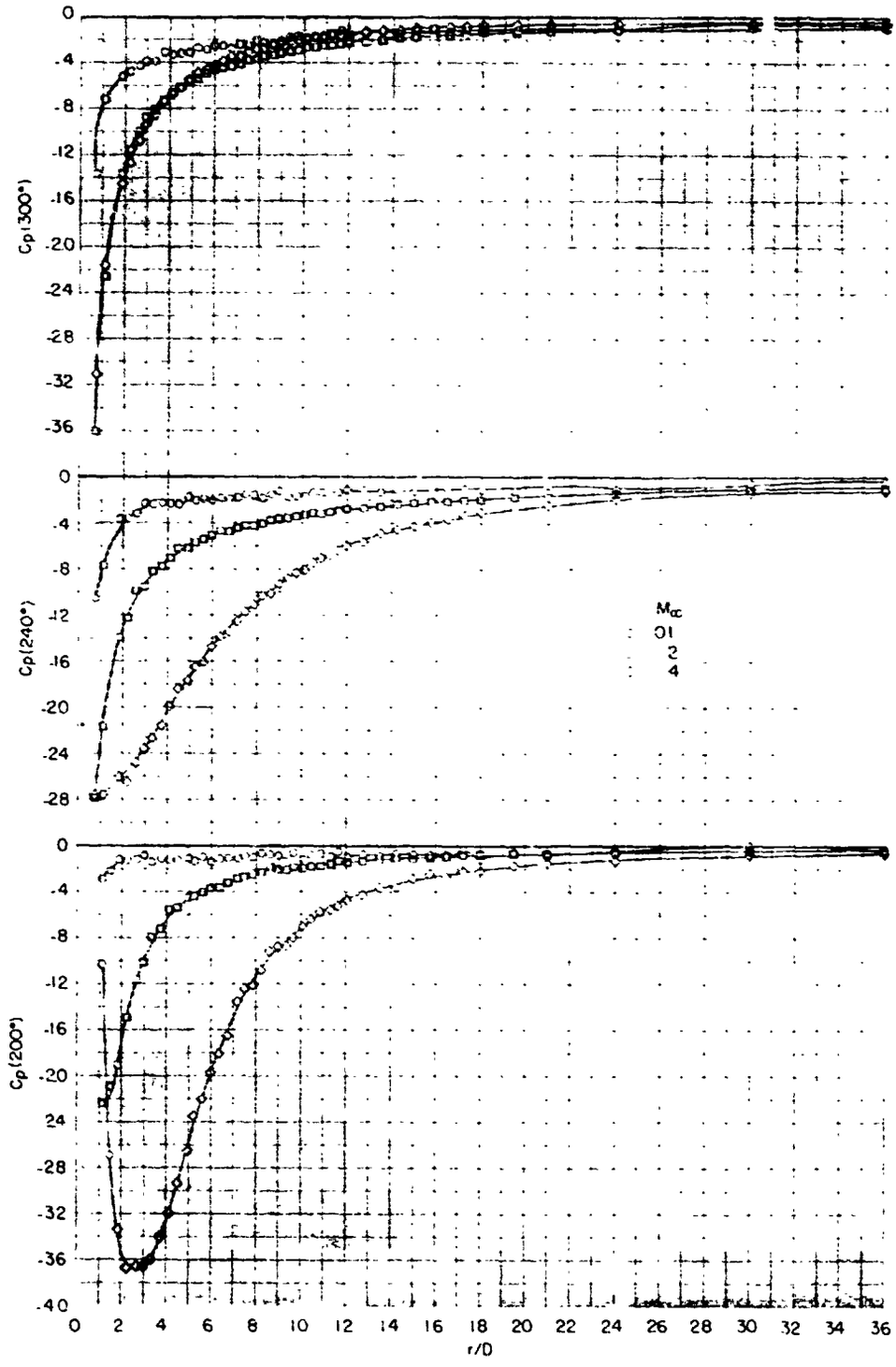

Figure 14.- Concluded.

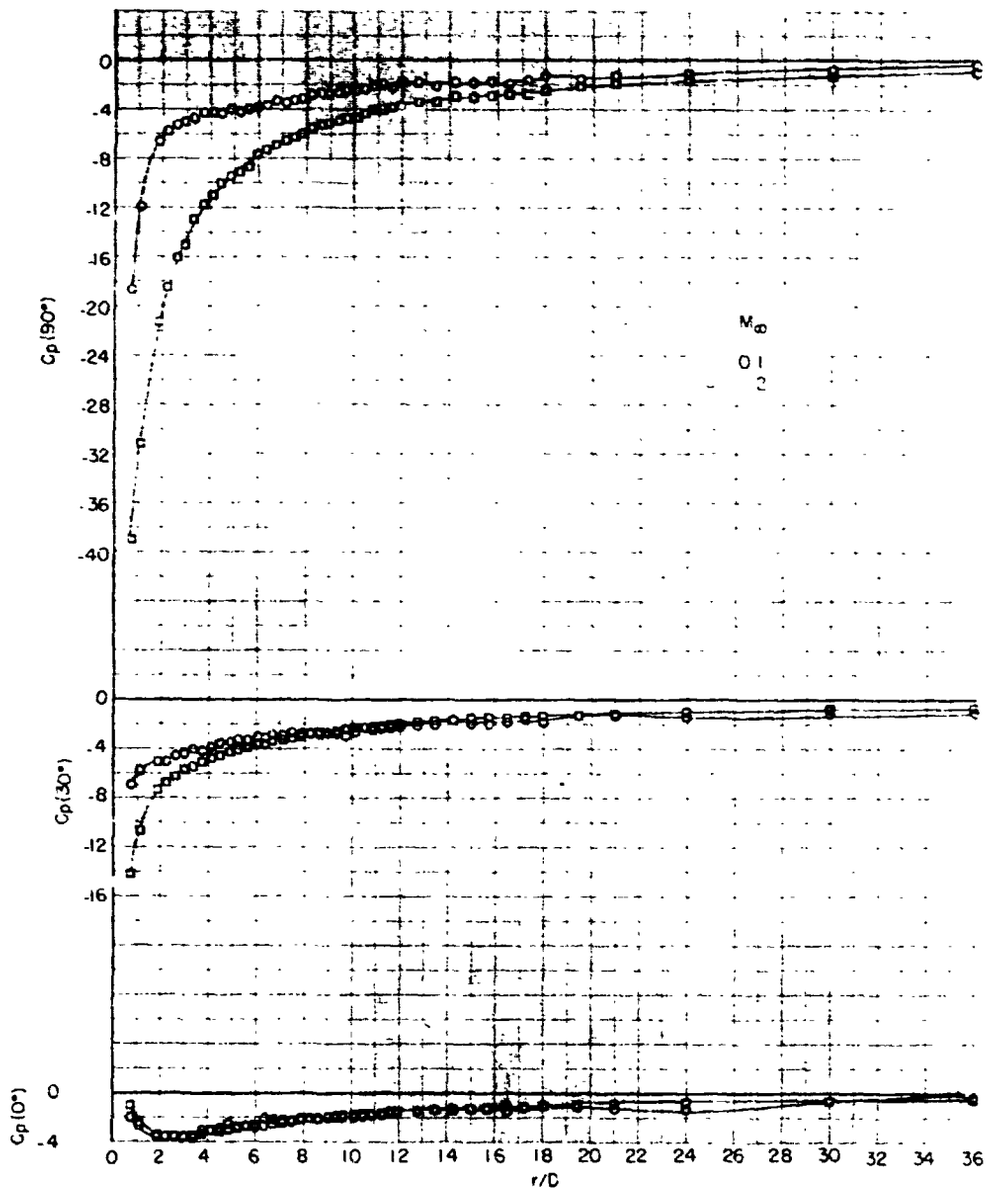

Figure 15.- Induced static-pressure coefficients on the flat plate for $\bar{Q}_{mom} = 415.6$.

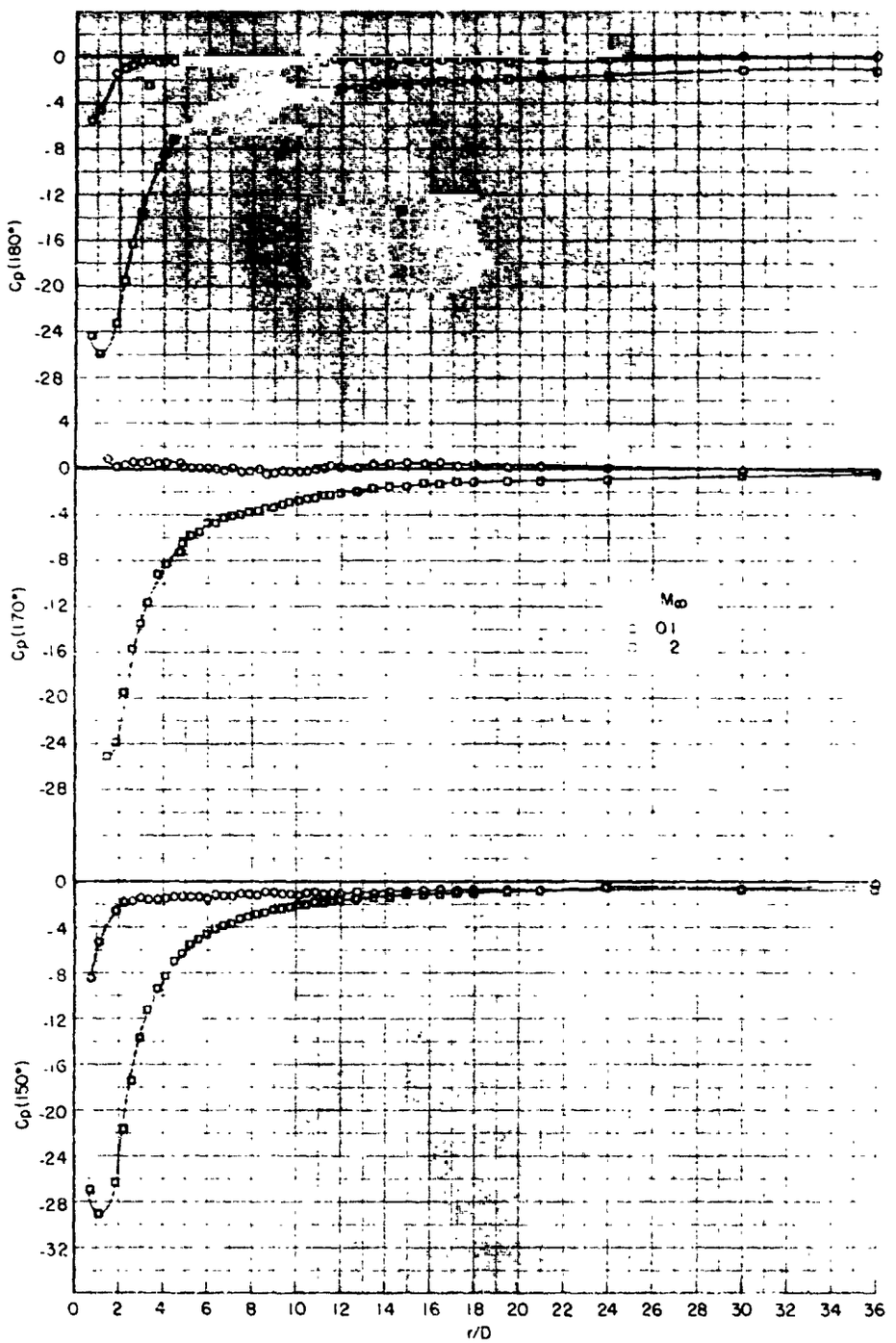

Figure 15.- Continued.

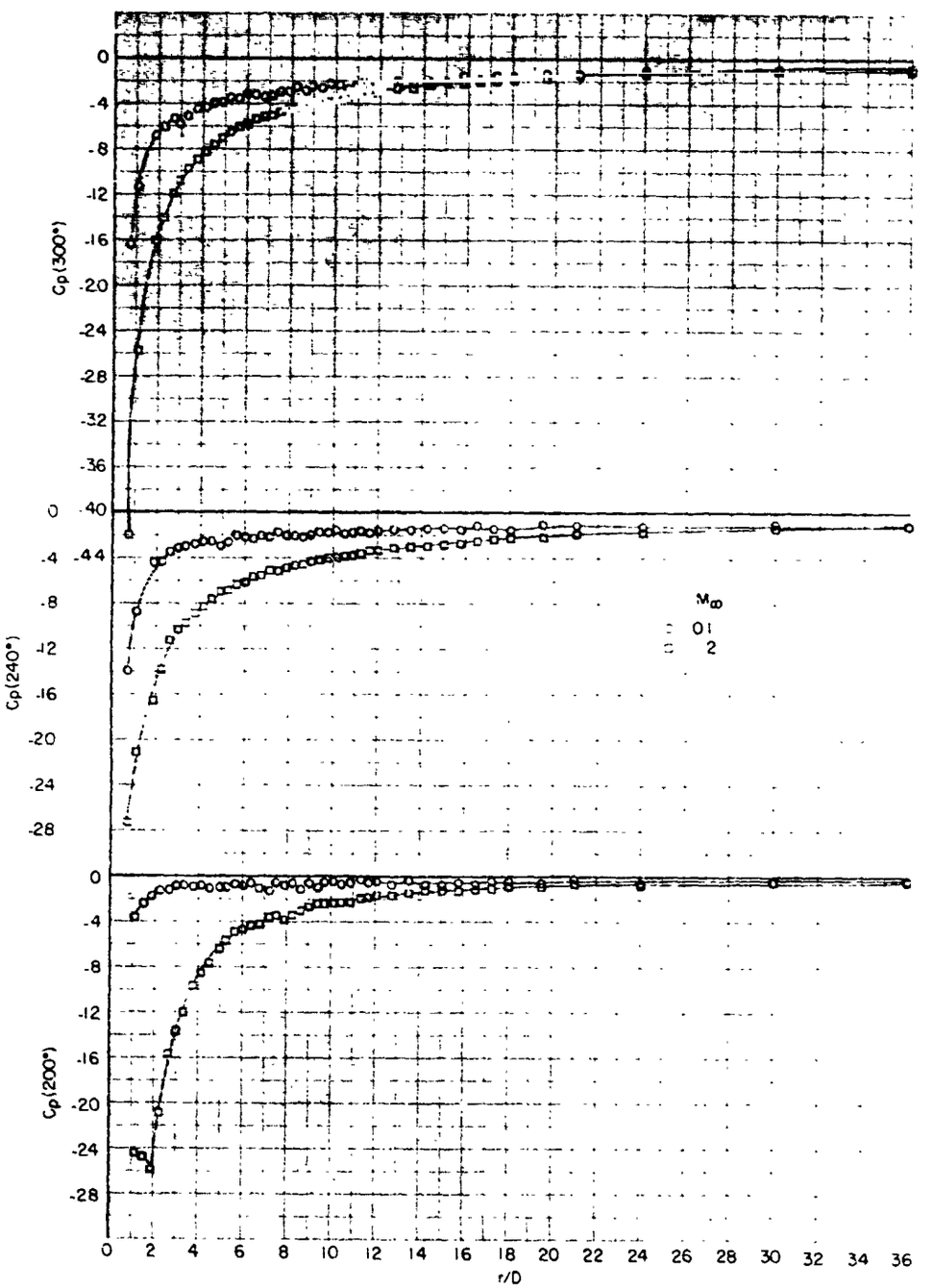

Figure 15.- Concluded.

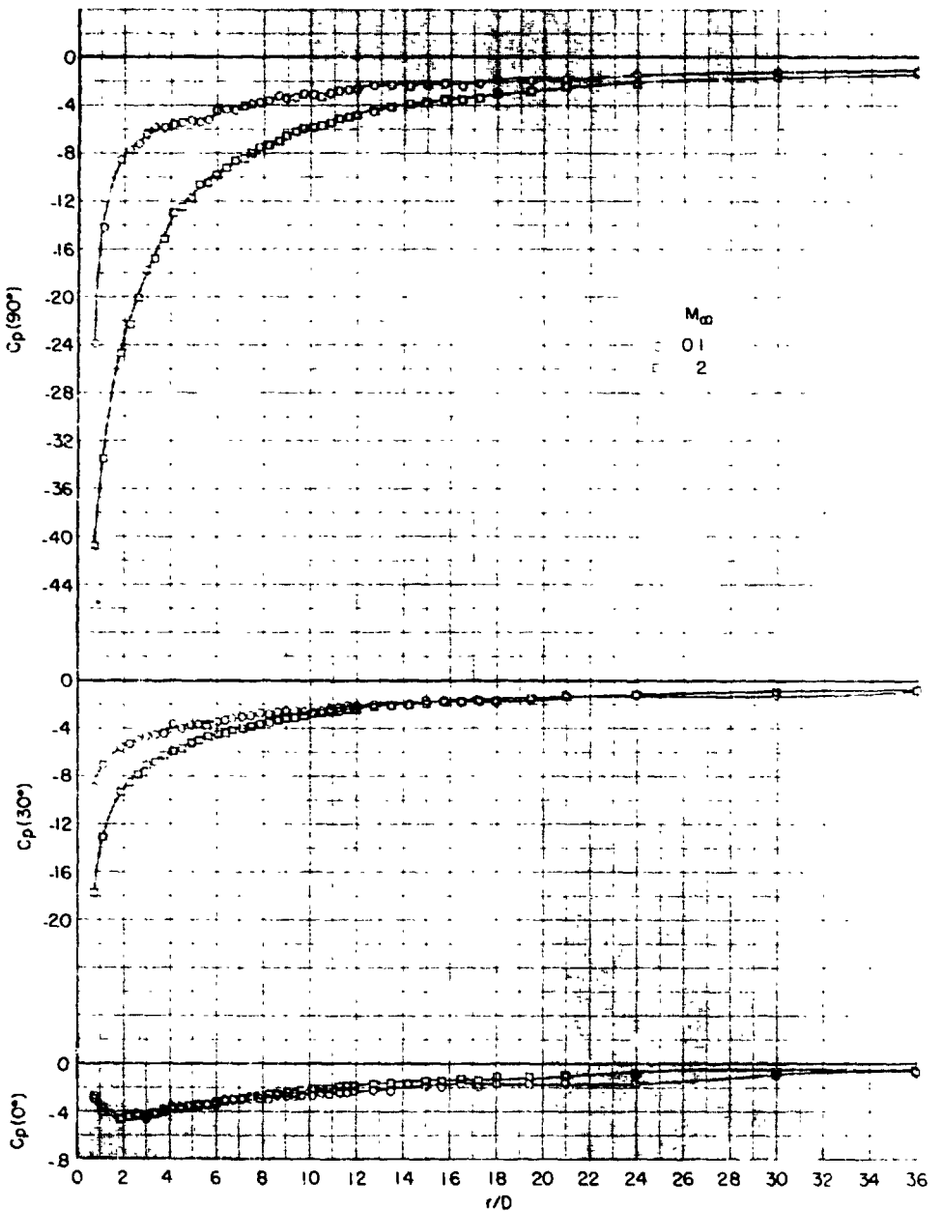

Figure 16.- Induced static-pressure coefficients on the flat plate for $\bar{Q}_{mom} = 619.5$.

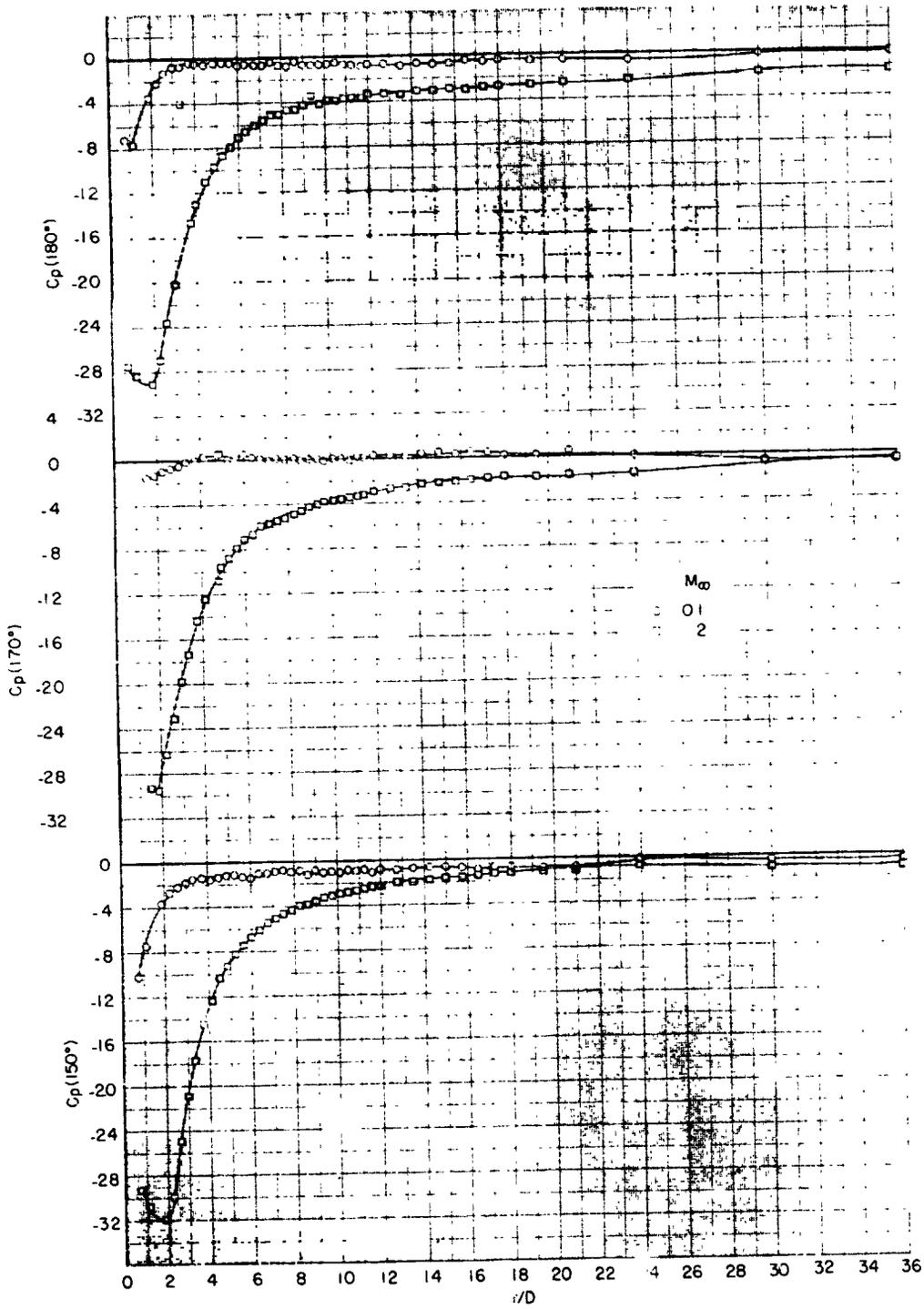

Figure 16.- Continued.

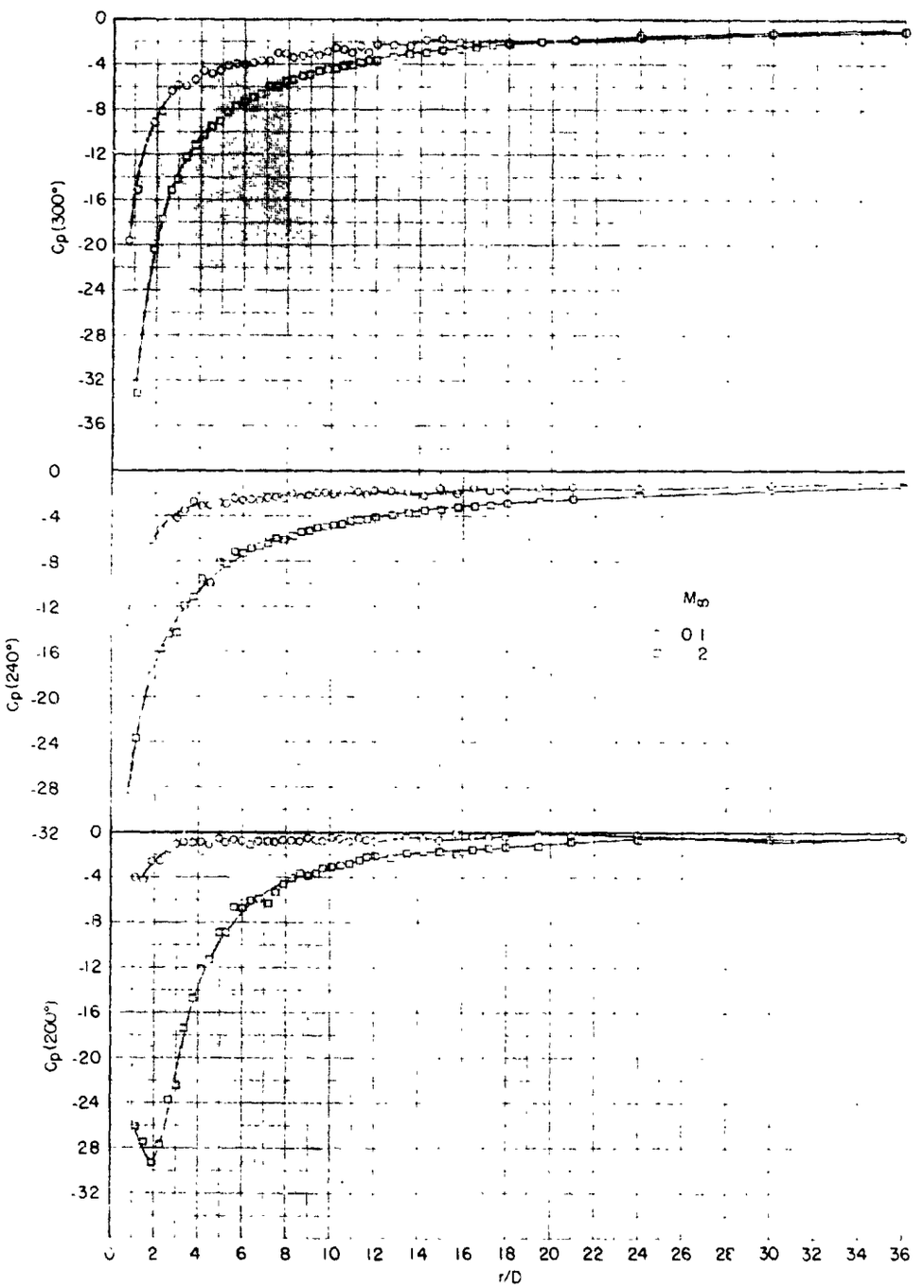

Figure 16.- Concluded.

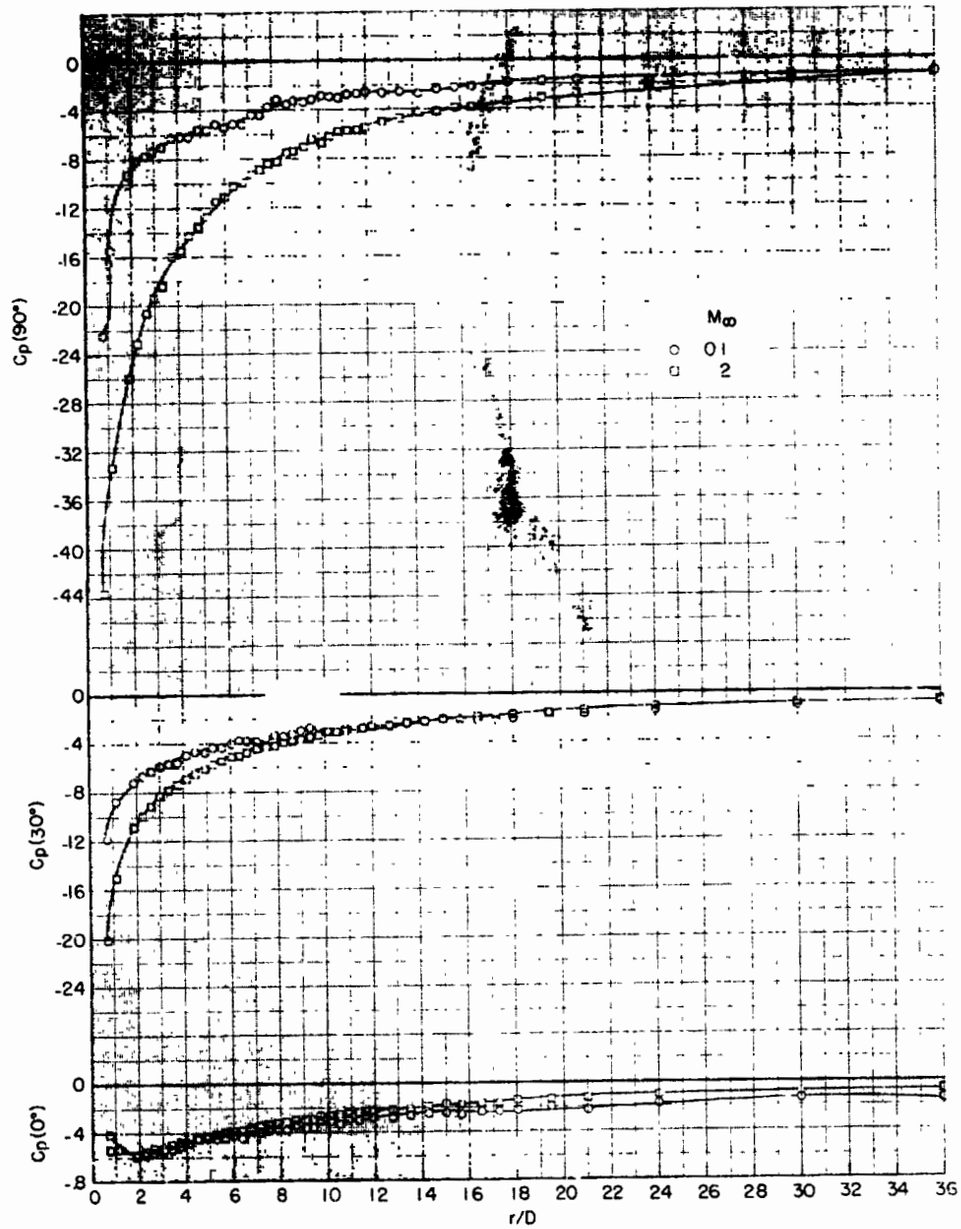

Figure 17.- Induced static-pressure coefficients on the flat plate for $\bar{Q}_{mom} = 829.9$.

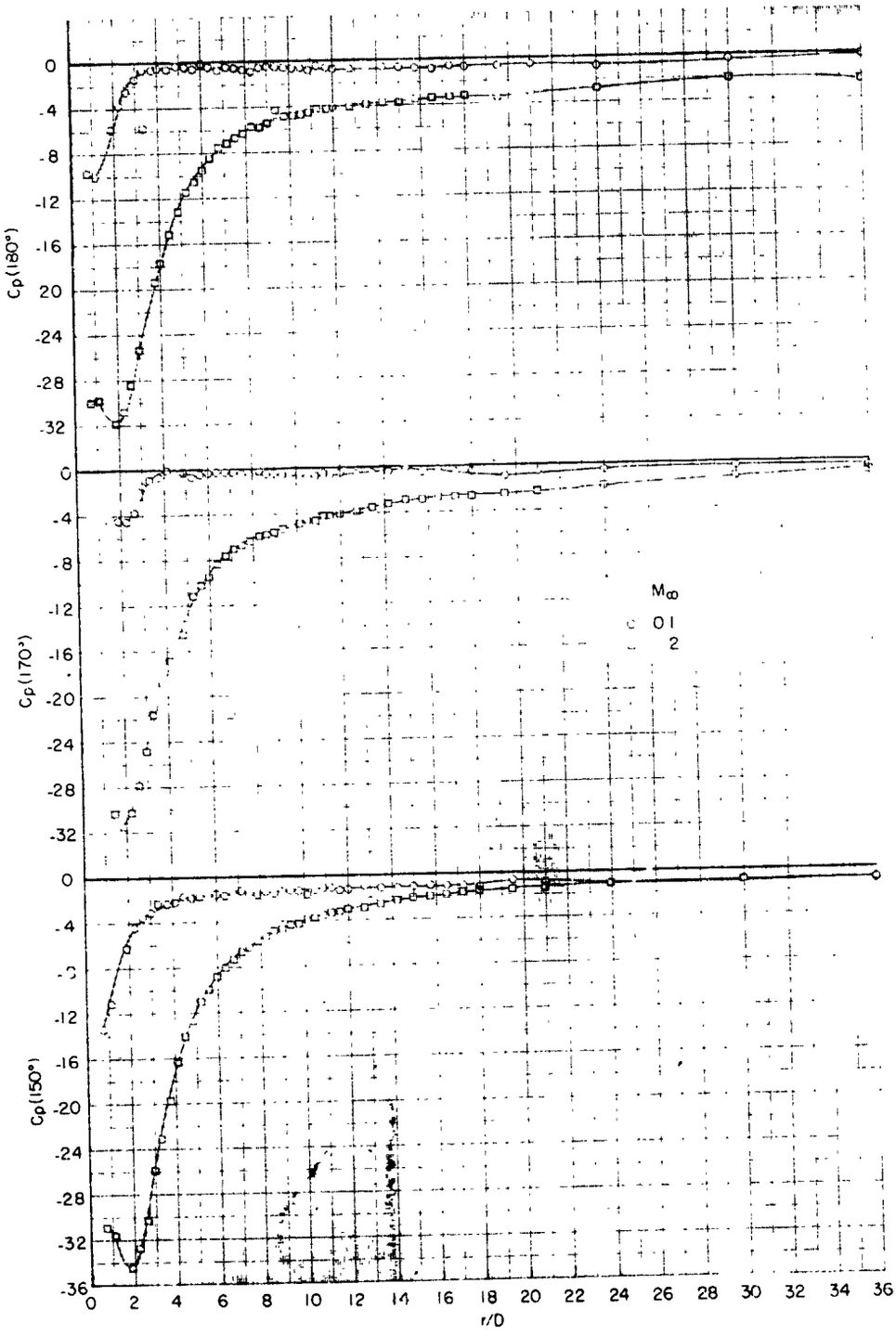

Figure 17.- Continued.

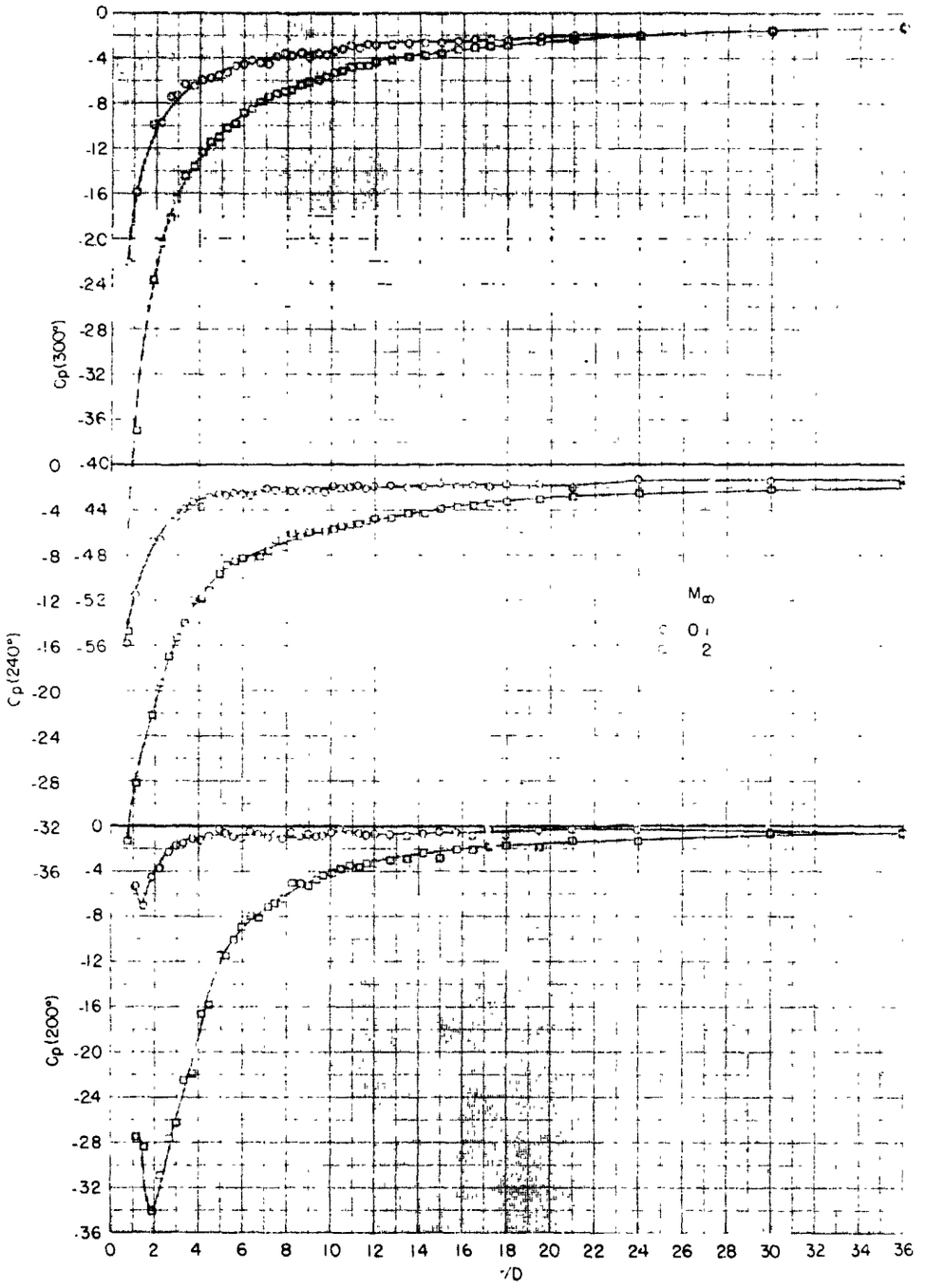

Figure 17.- Concluded.

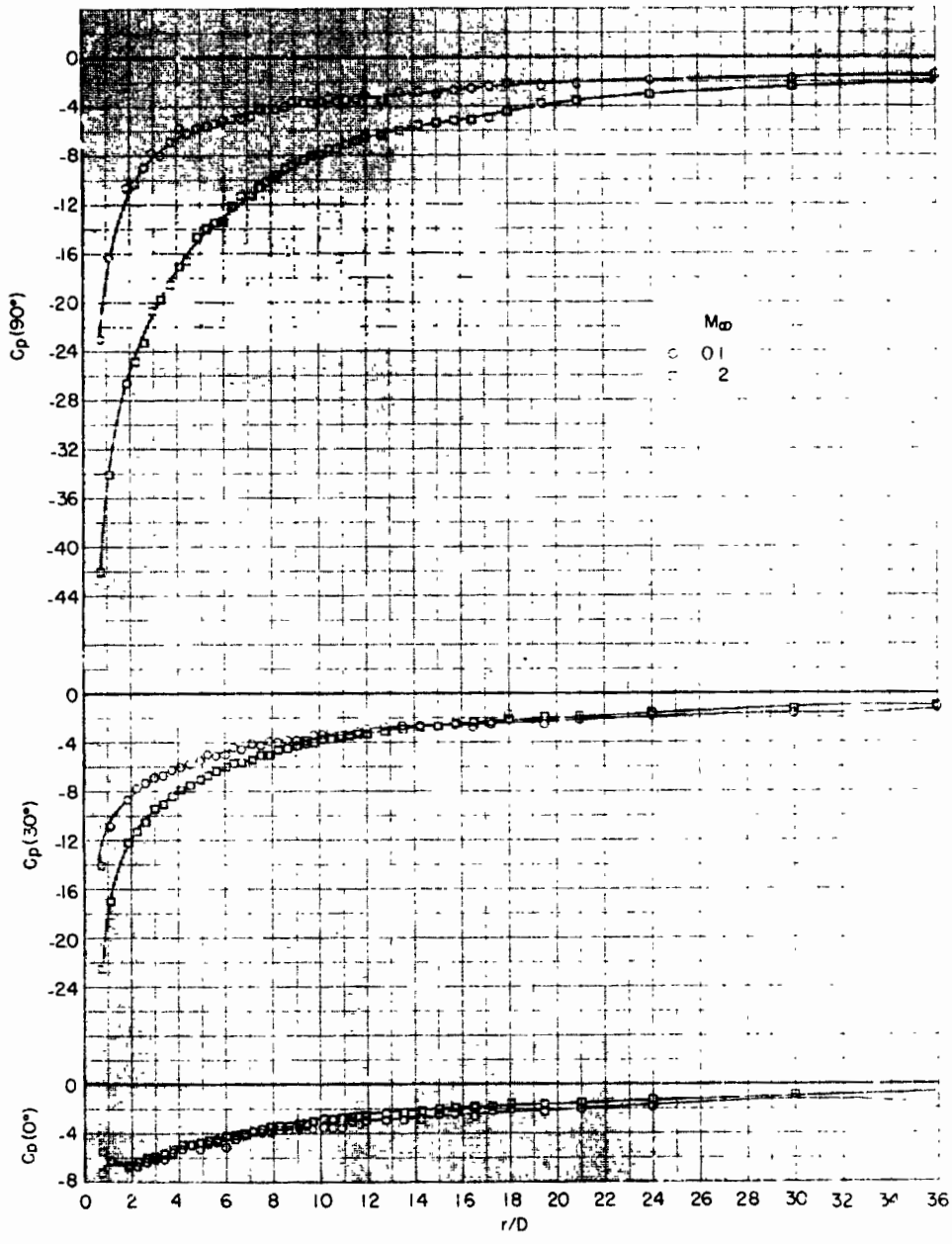

Figure 18.- Induced static-pressure coefficients on the flat plate for $\bar{Q}_{mom} = 1052.3$

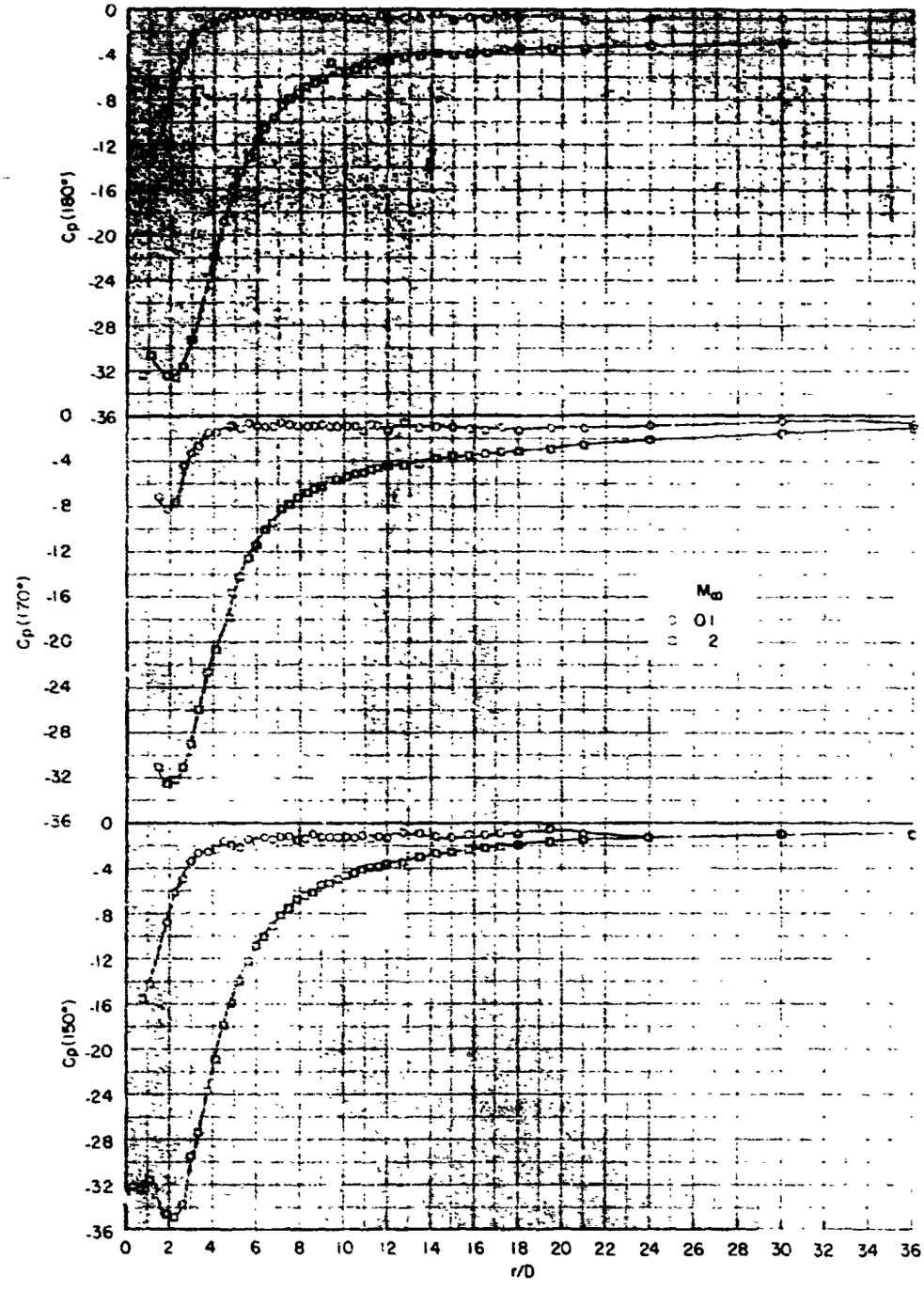

Figure 18.- Continued.

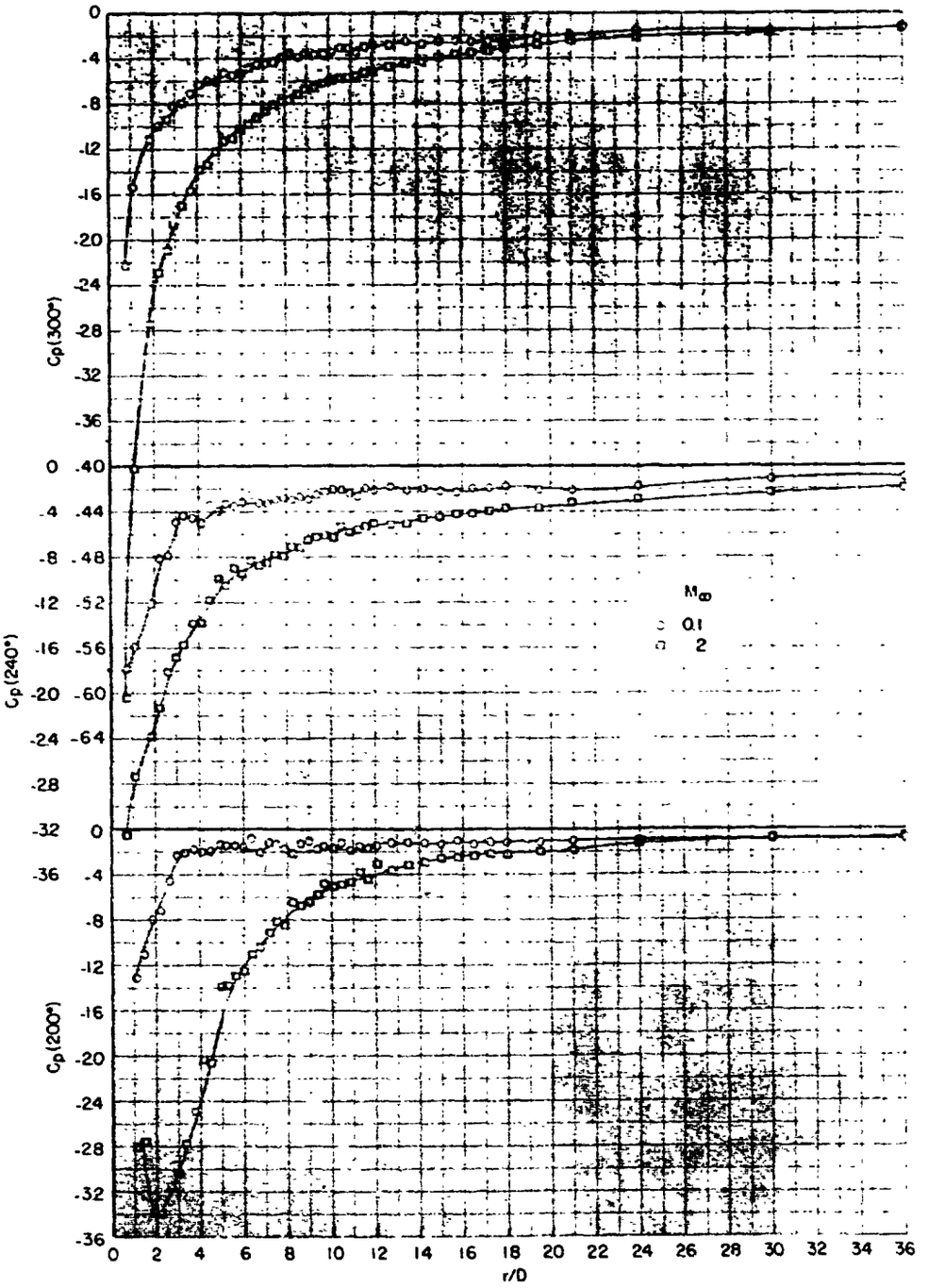

Figure 18.- Concluded.

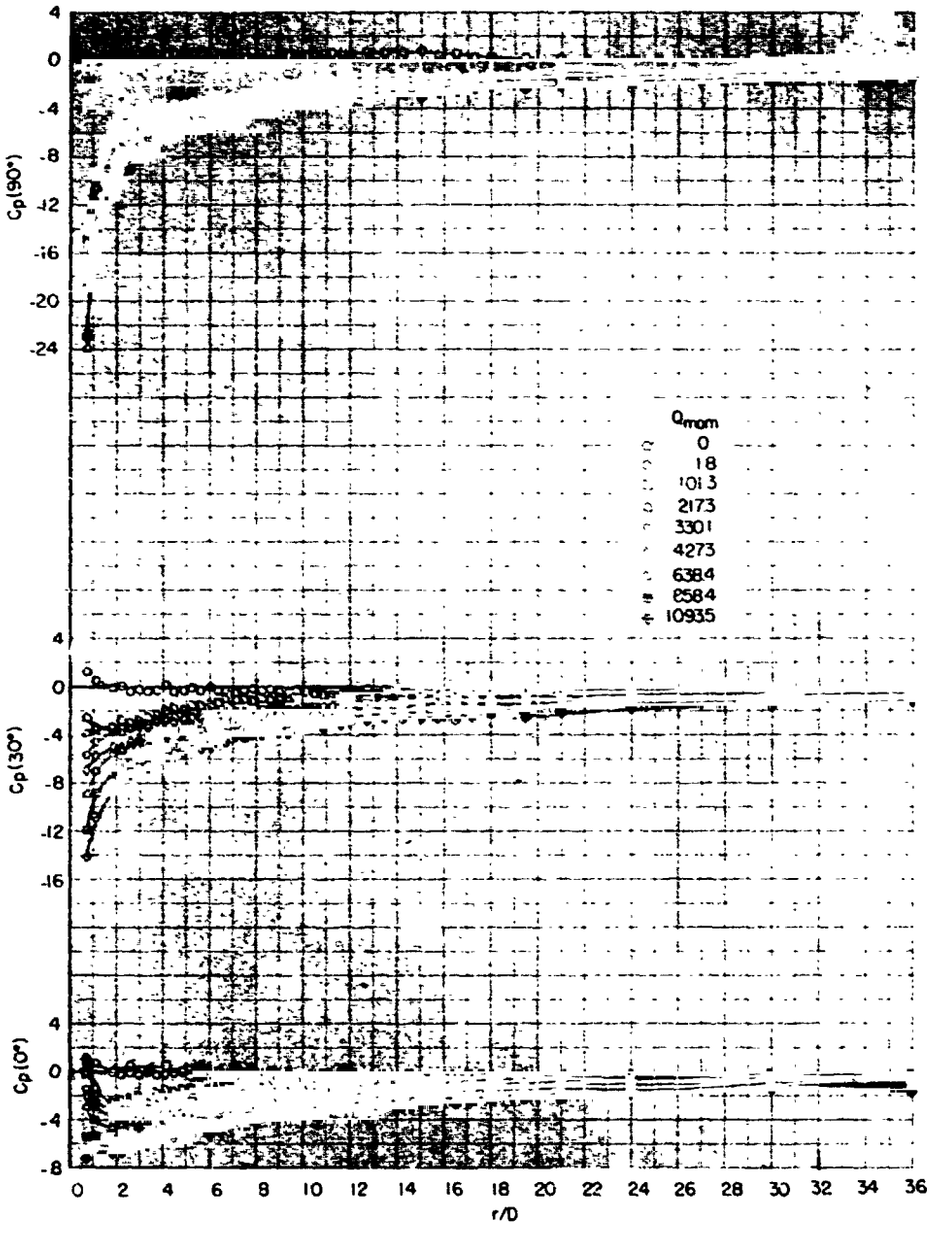

Figure 19.- Induced static-pressure coefficients on the flat plate for $M_\infty = 0.1$.

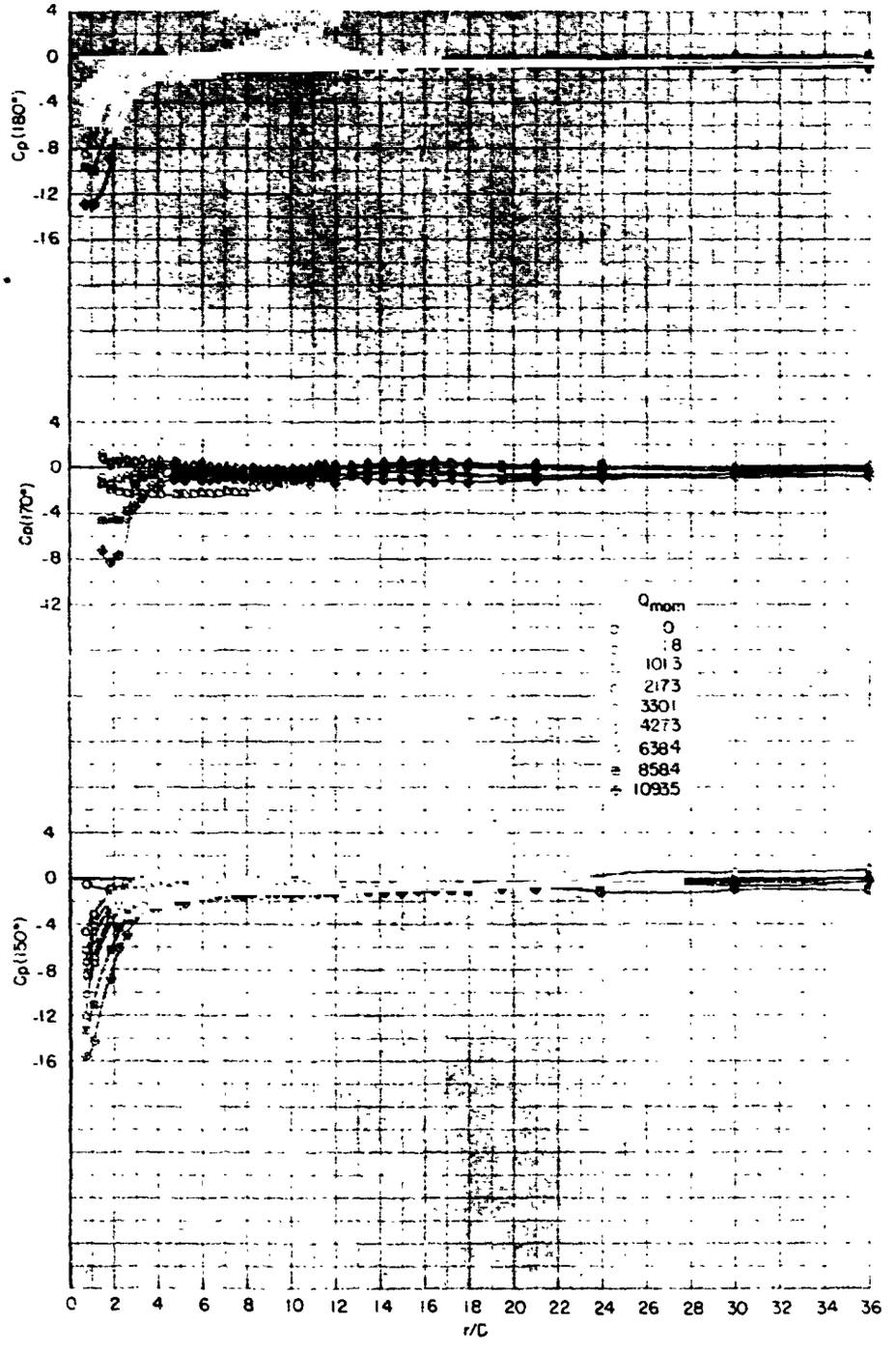

Figure 19.- Continued.

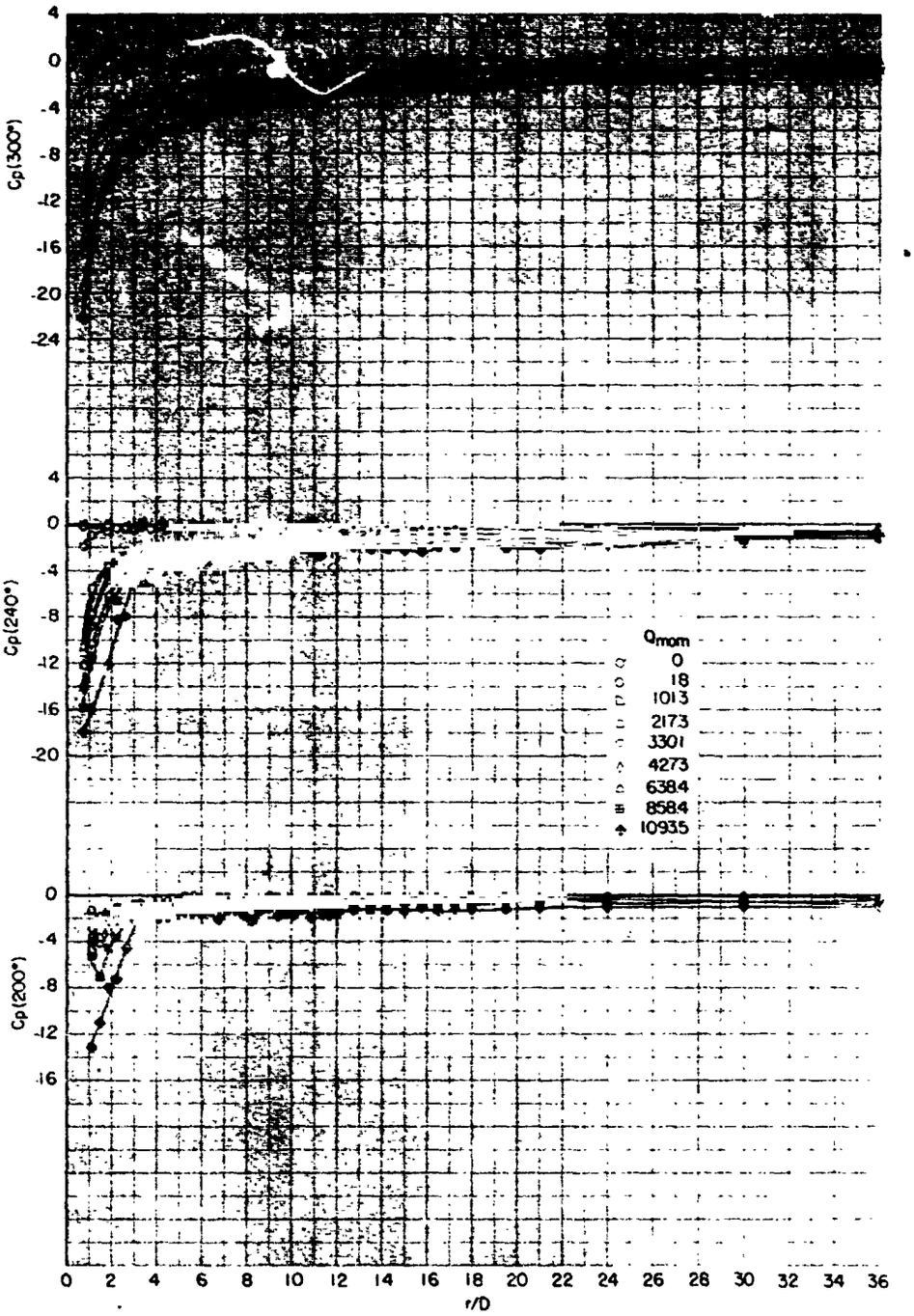

Figure 19.- Concluded.

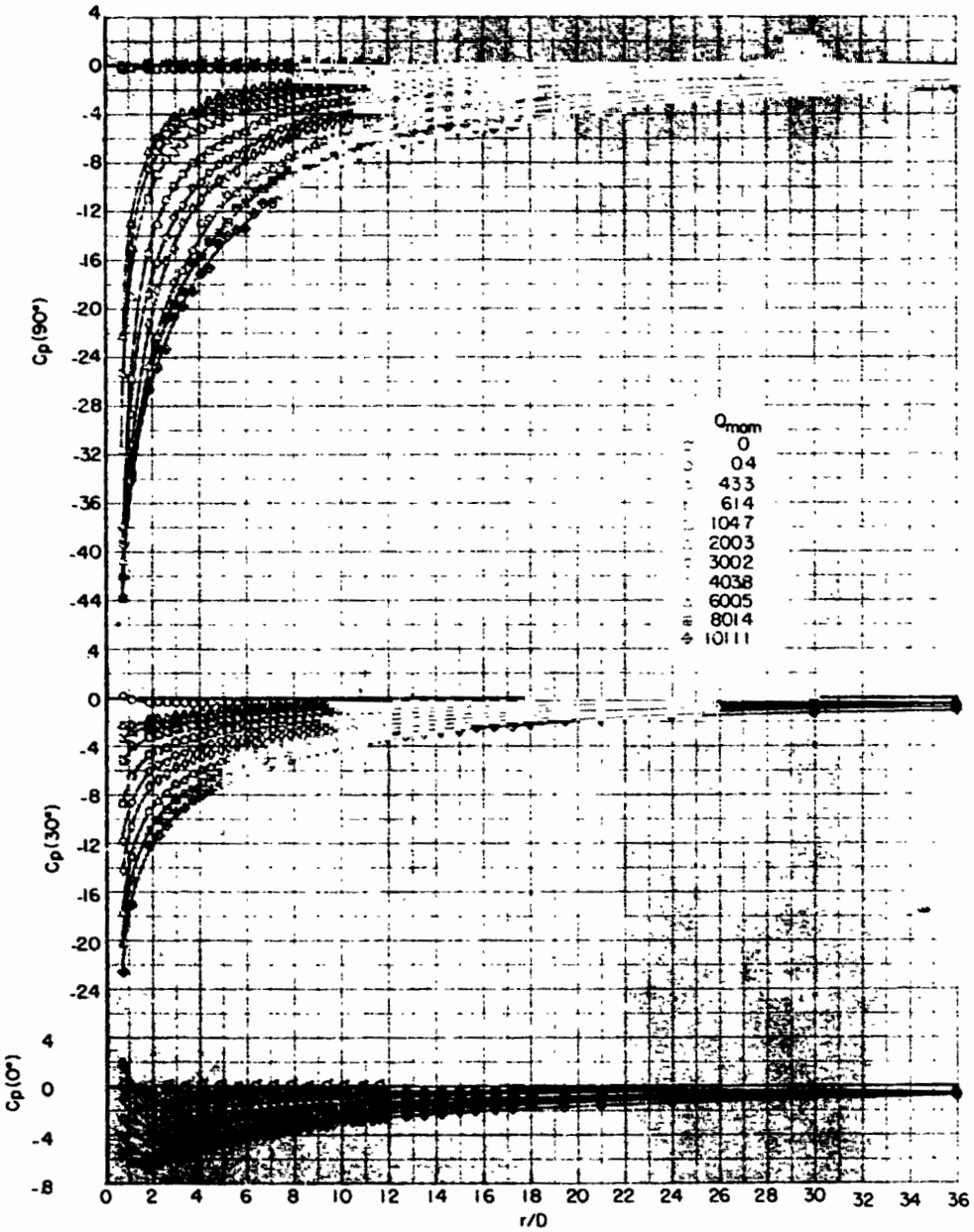

Figure 20.- Induced static-pressure coefficients on the flat plate for $M_\infty = 0.2$.

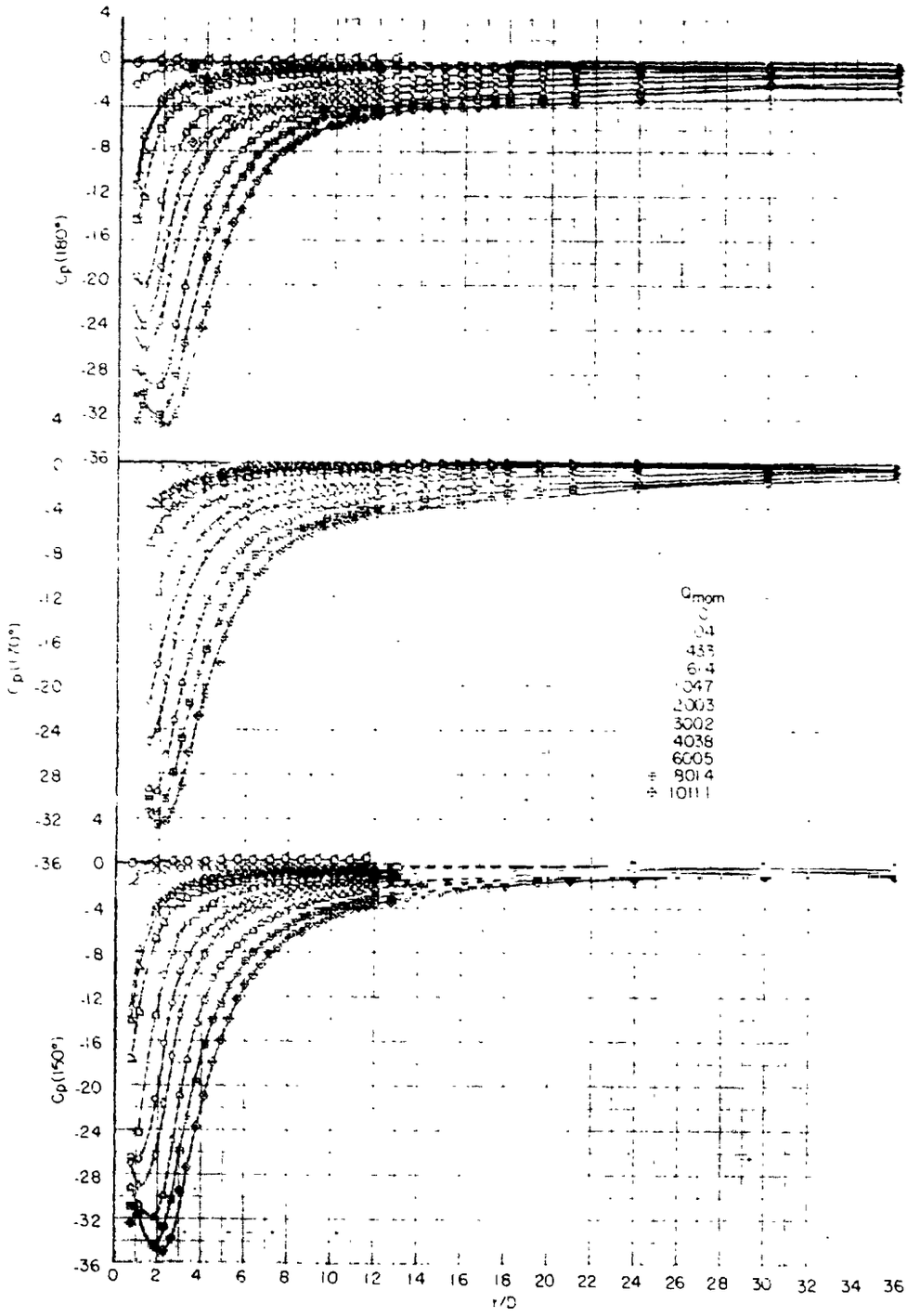

Figure 20.- Continued.

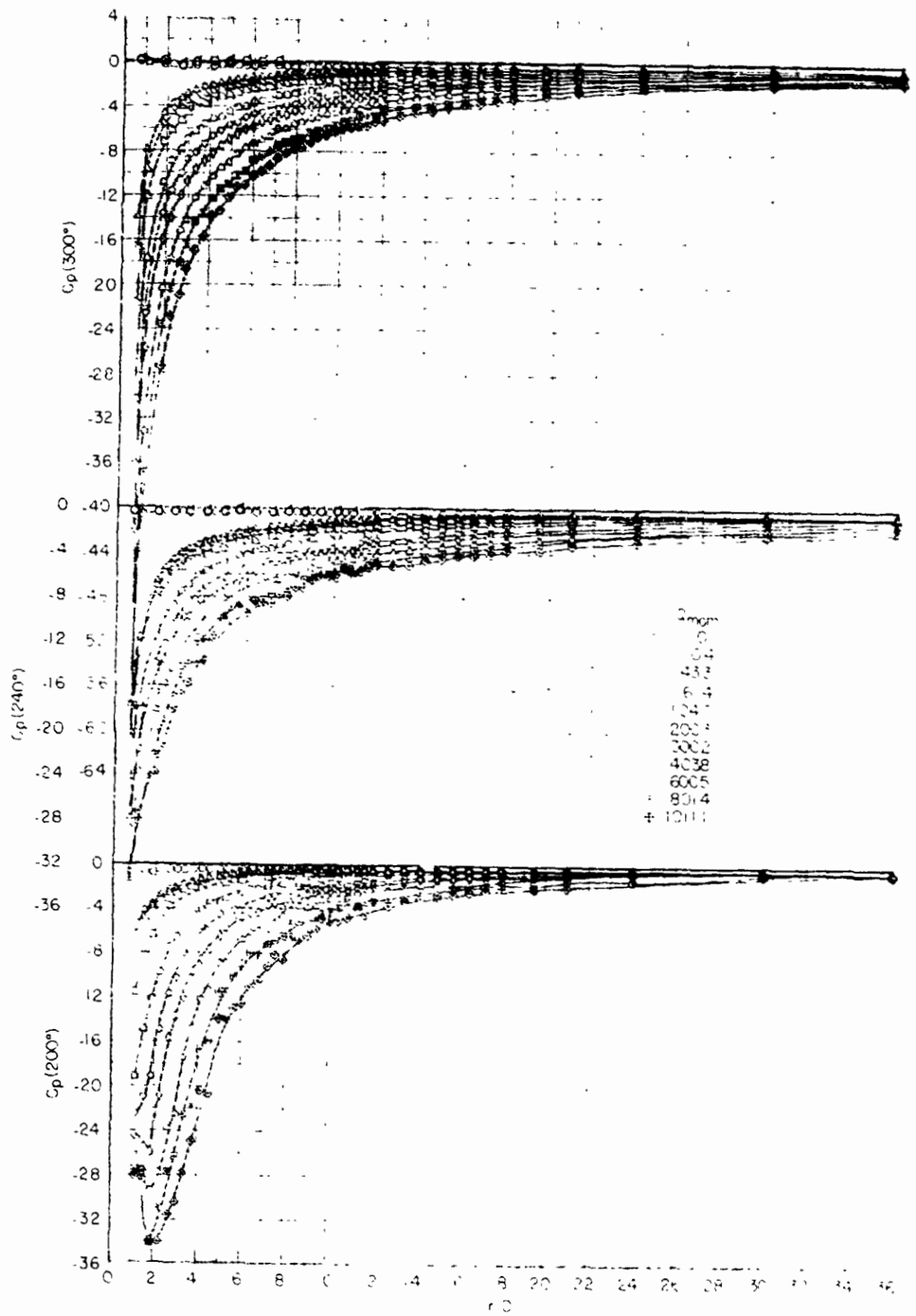

Figure 20.- Concluded.

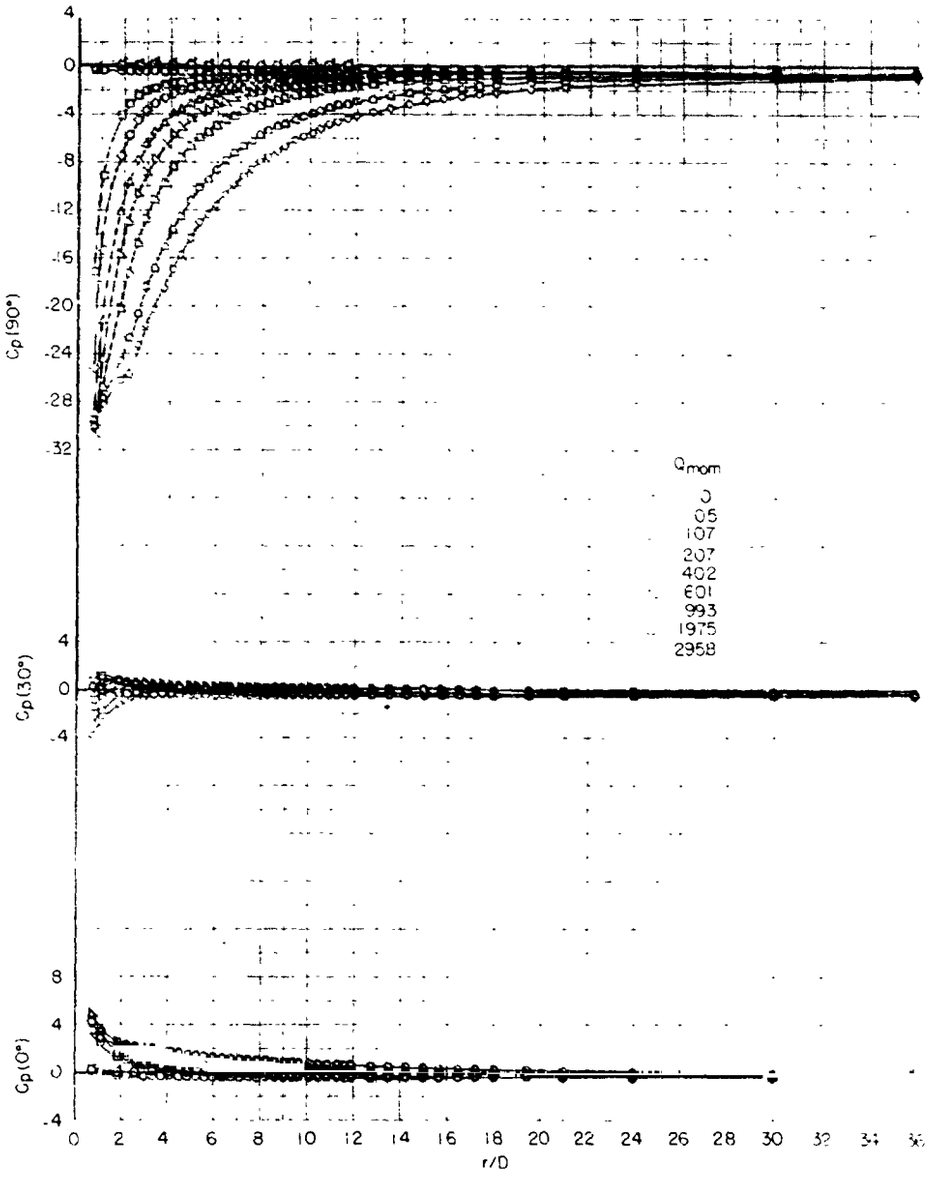

Figure 21.- Induced static-pressure coefficients on the flat plate for $M_\infty = 0.4$.

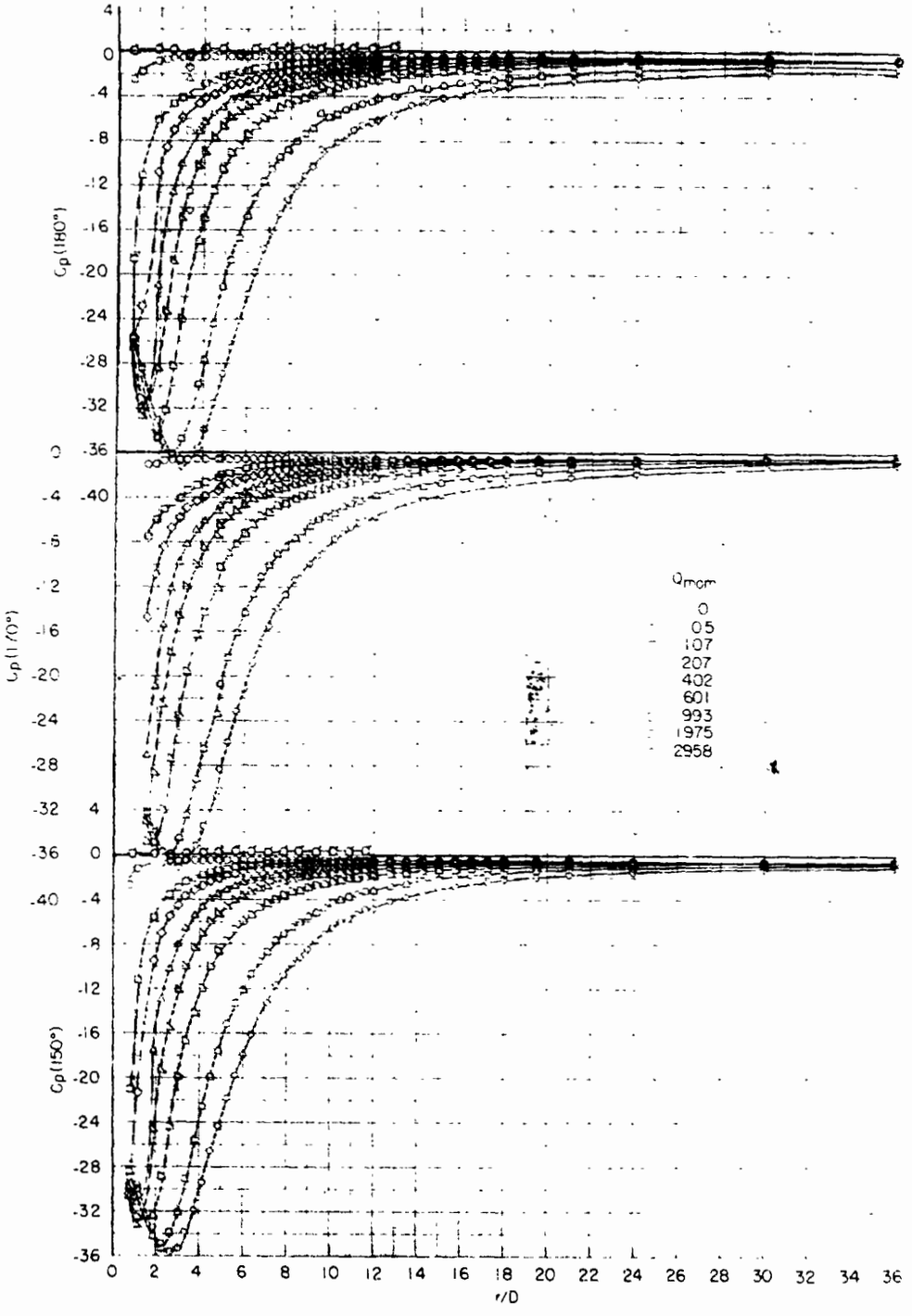

Figure 21.- Continued.

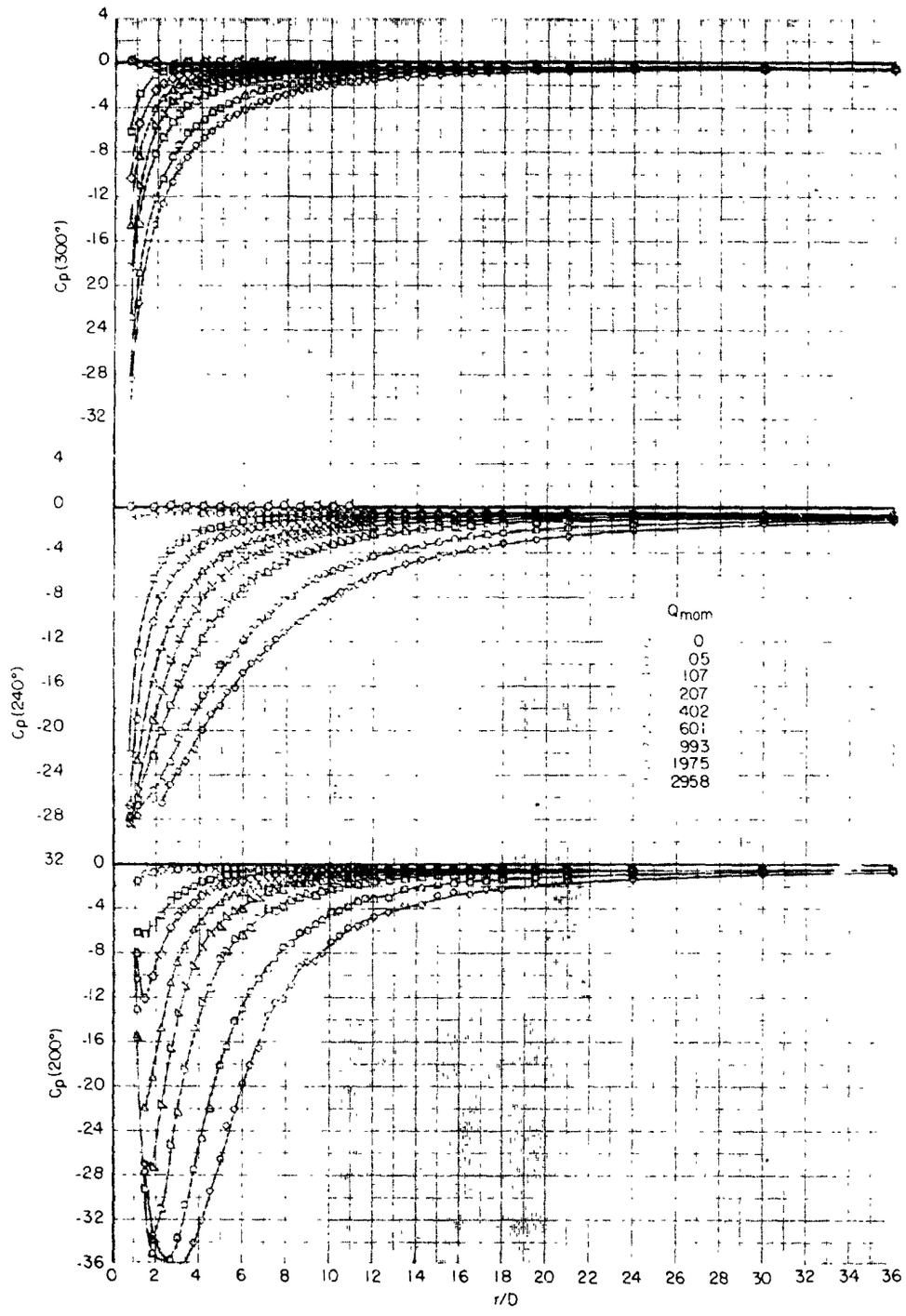

Figure 21.- Concluded.

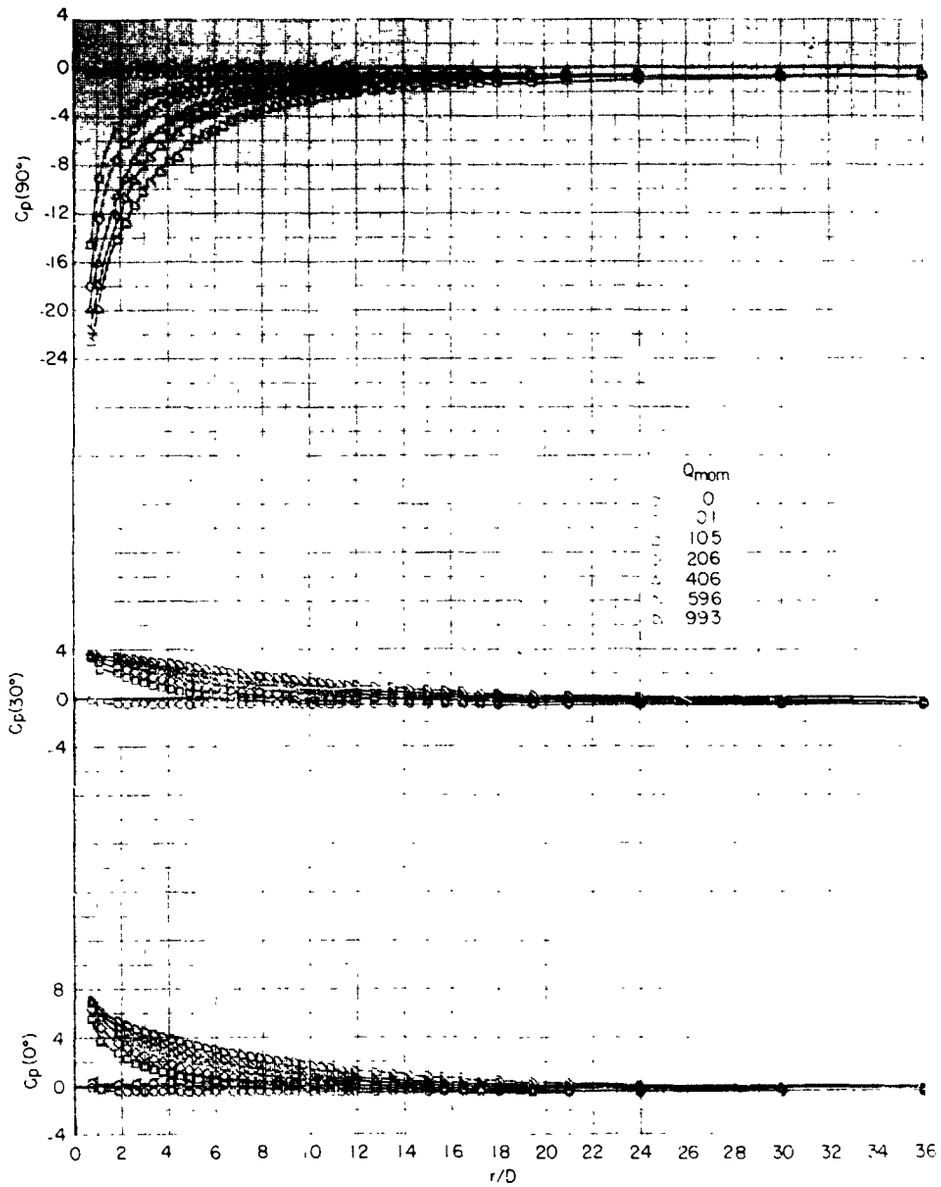

Figure 22.- Induced static-pressure coefficients on the flat plate for $M_\infty = 0.6$.

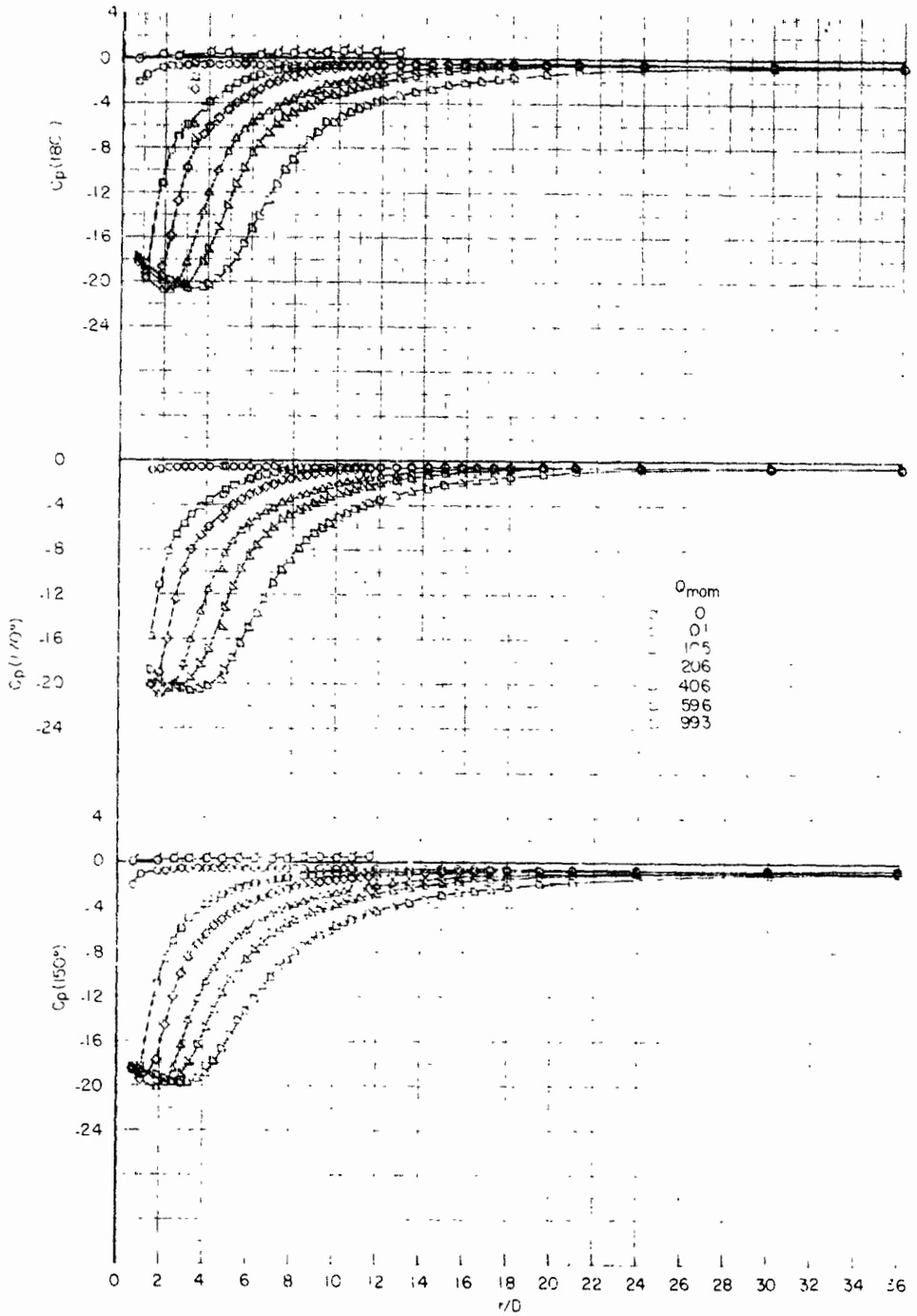

Figure 22.- Continued.

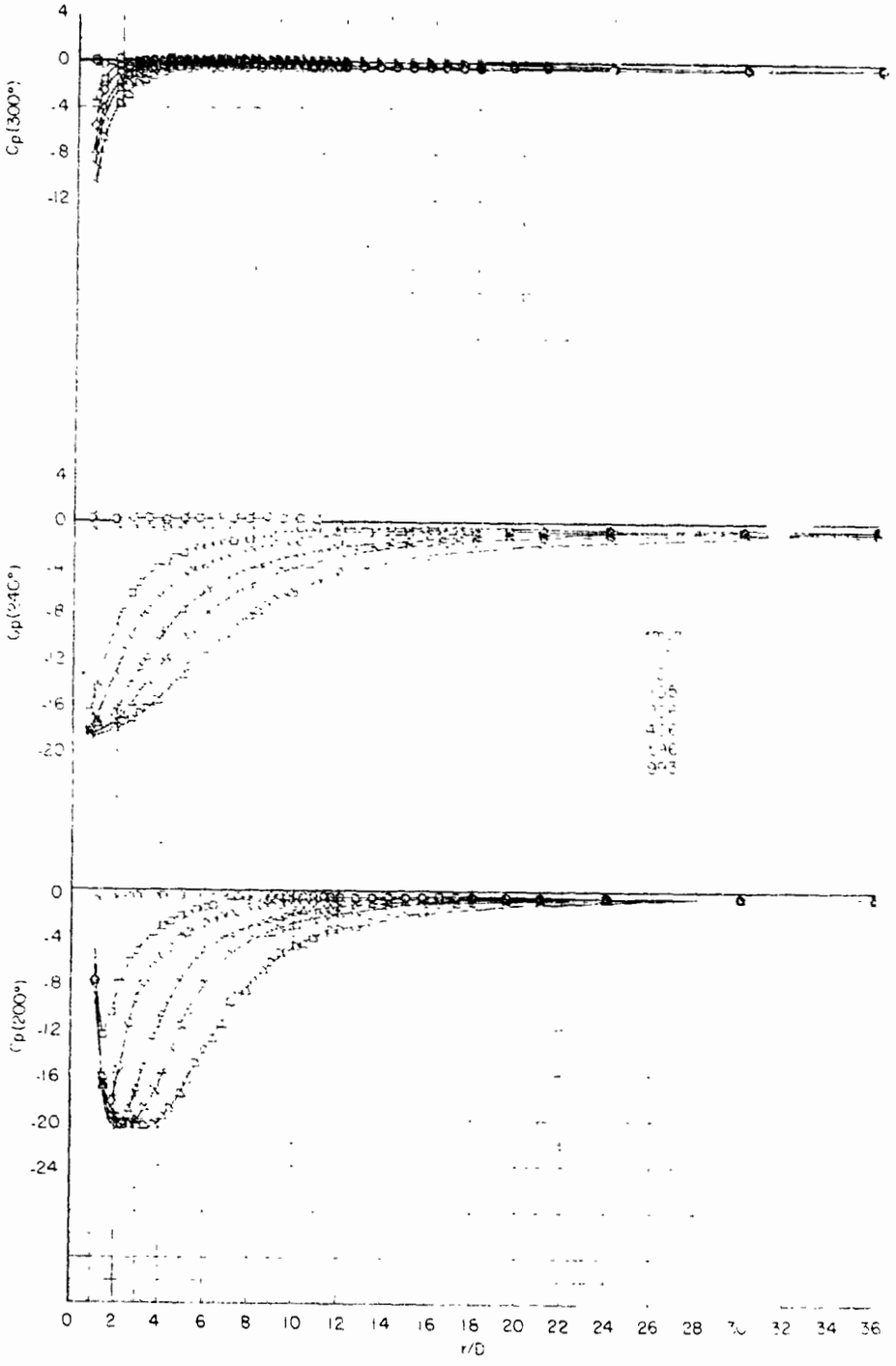

Figure 22.- Concluded.

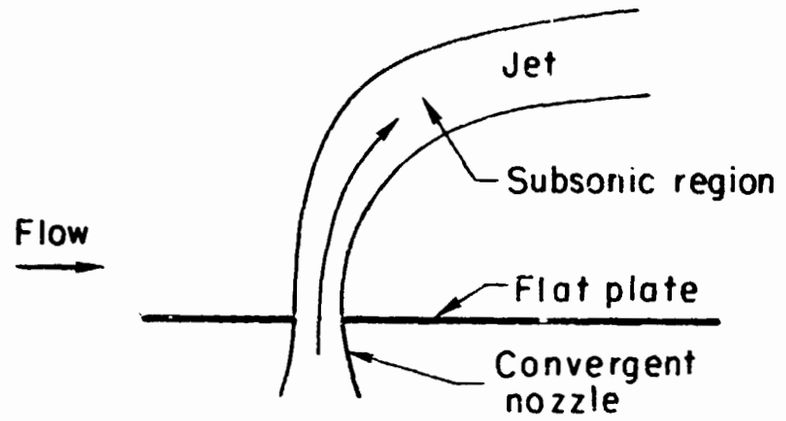

(a) Fully expanded jet, $\left(\frac{p_j}{p_\infty}\right)_{exit} \approx 1.0$.

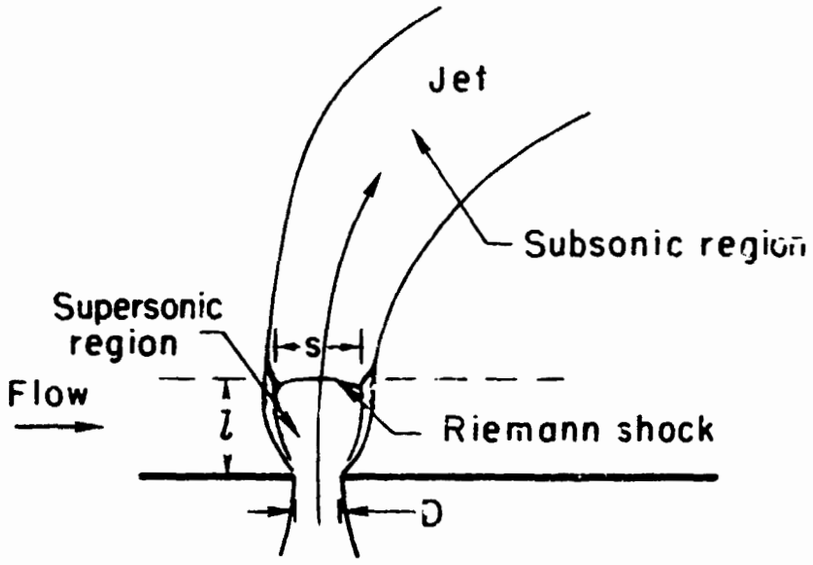

(b) Underexpanded jet, $\left(\frac{p_j}{p_\infty}\right)_{exit} > 1.0$.

Figure 23.- Schematic of a sonic jet issuing into a subsonic crossflow.

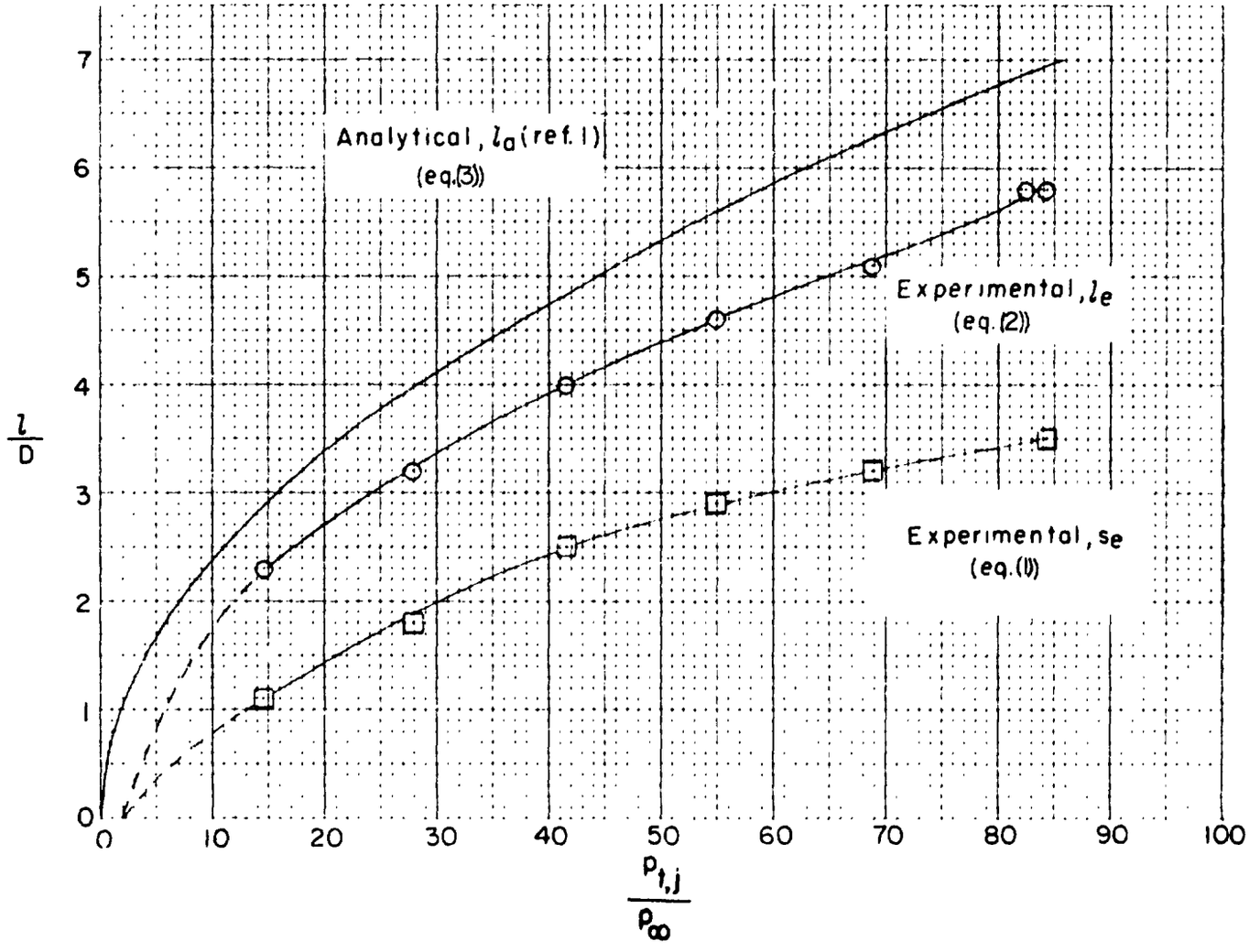

Figure 24.- Variation of Riemann shock geometry with pressure ratio $p_{t,j}/p_\infty$.

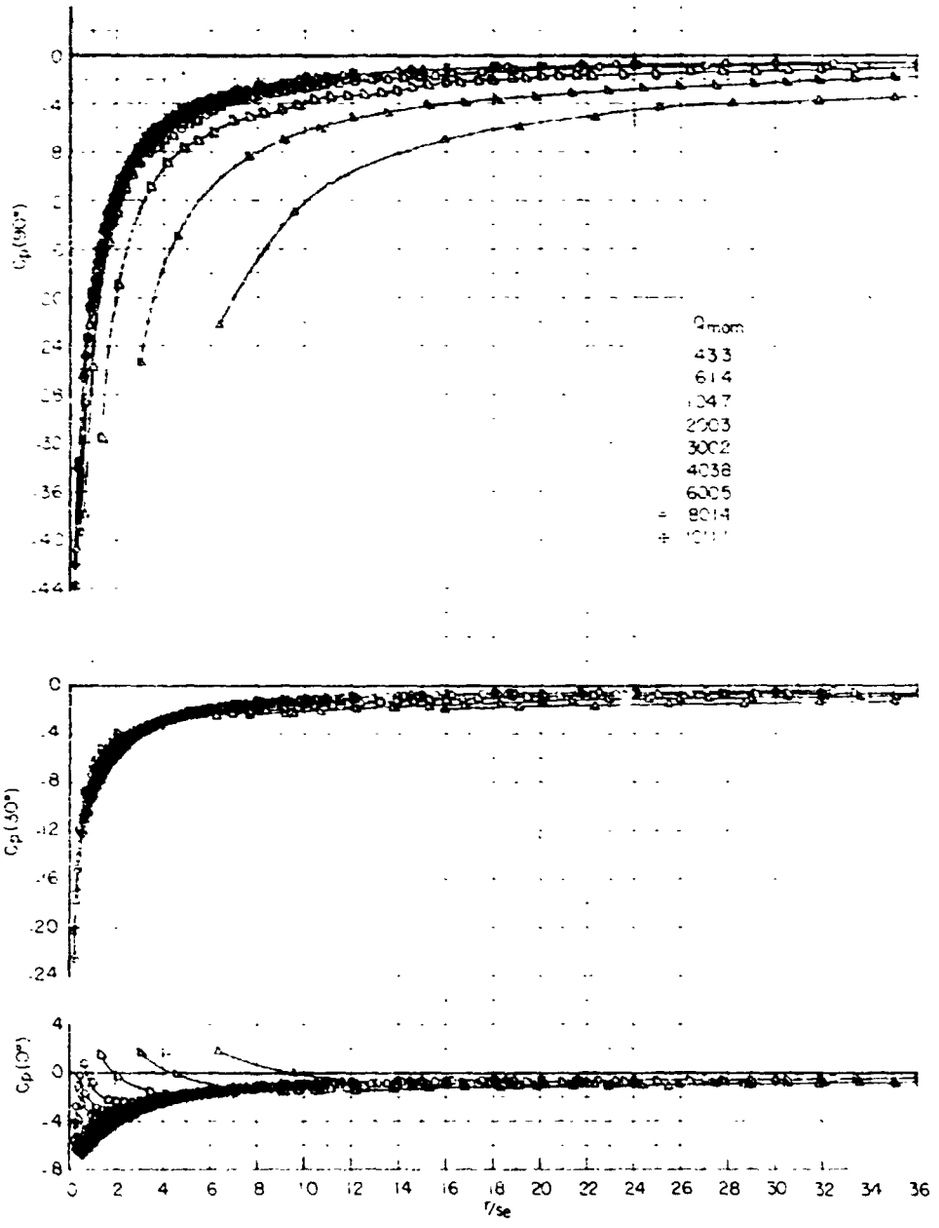

Figure 25.- Correlation of pressure data using the experimental relationship for shock diameter with $M_\infty = 0.2$.

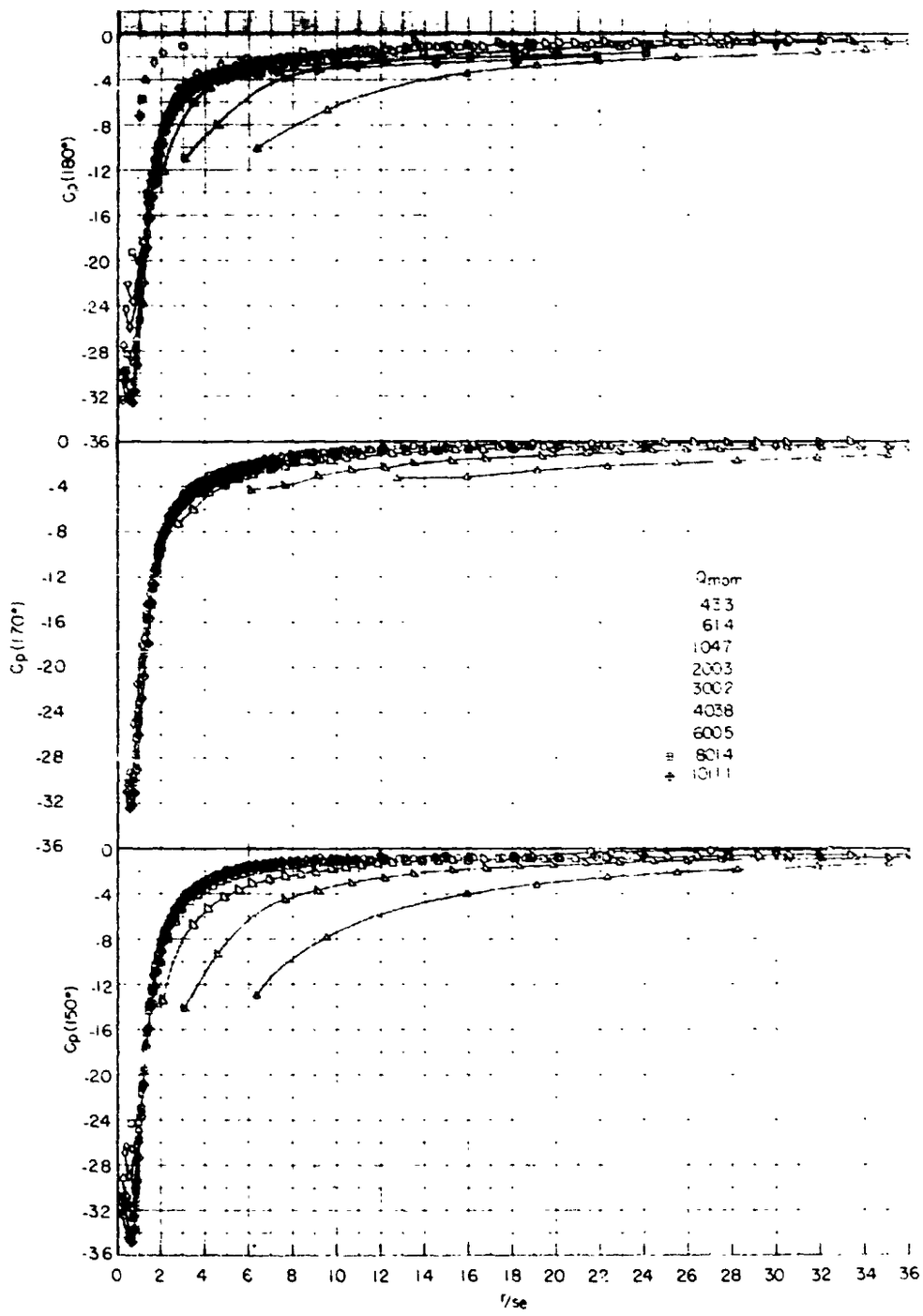

Figure 25.- Continued.

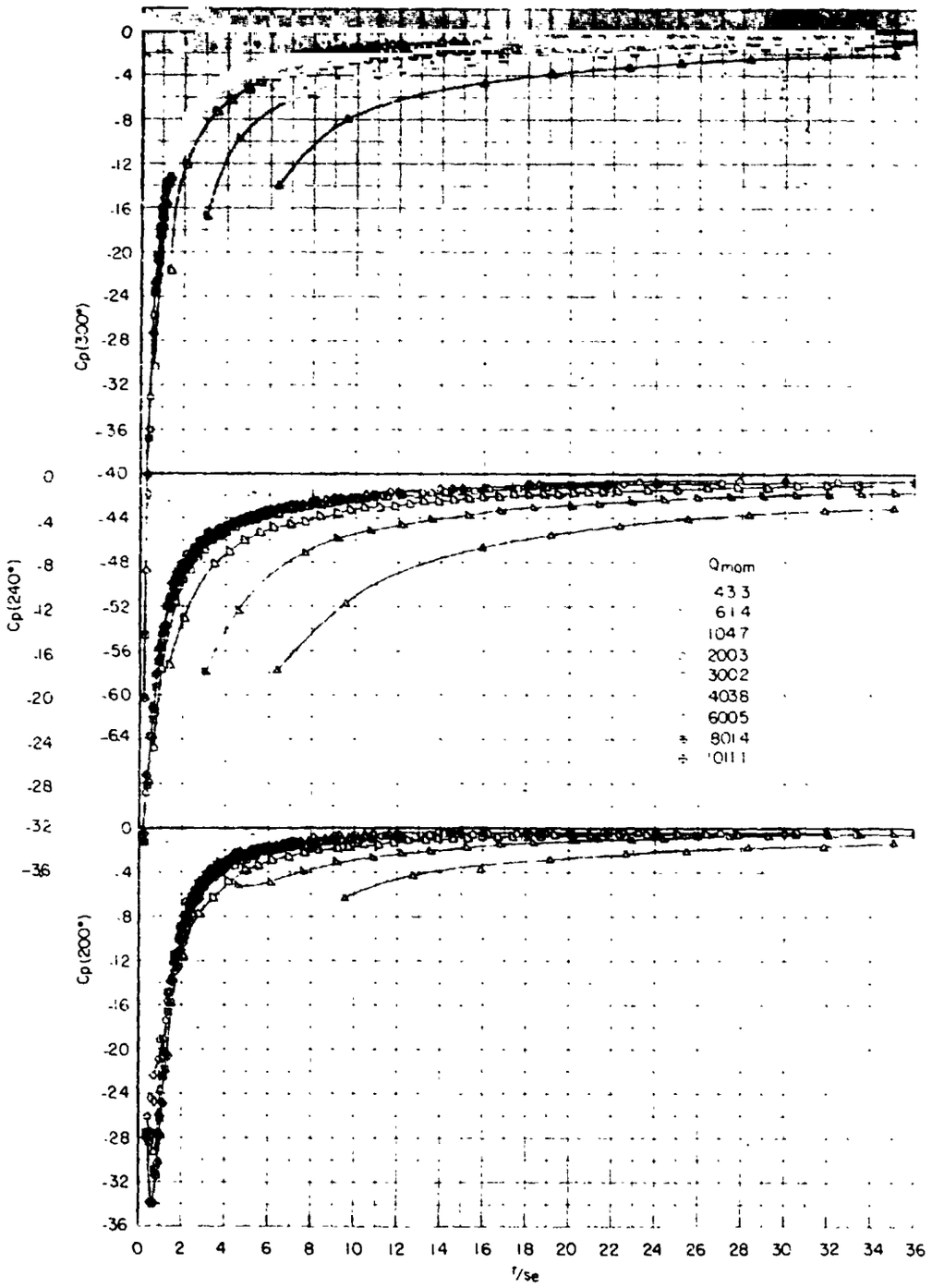

Figure 25.- Concluded.

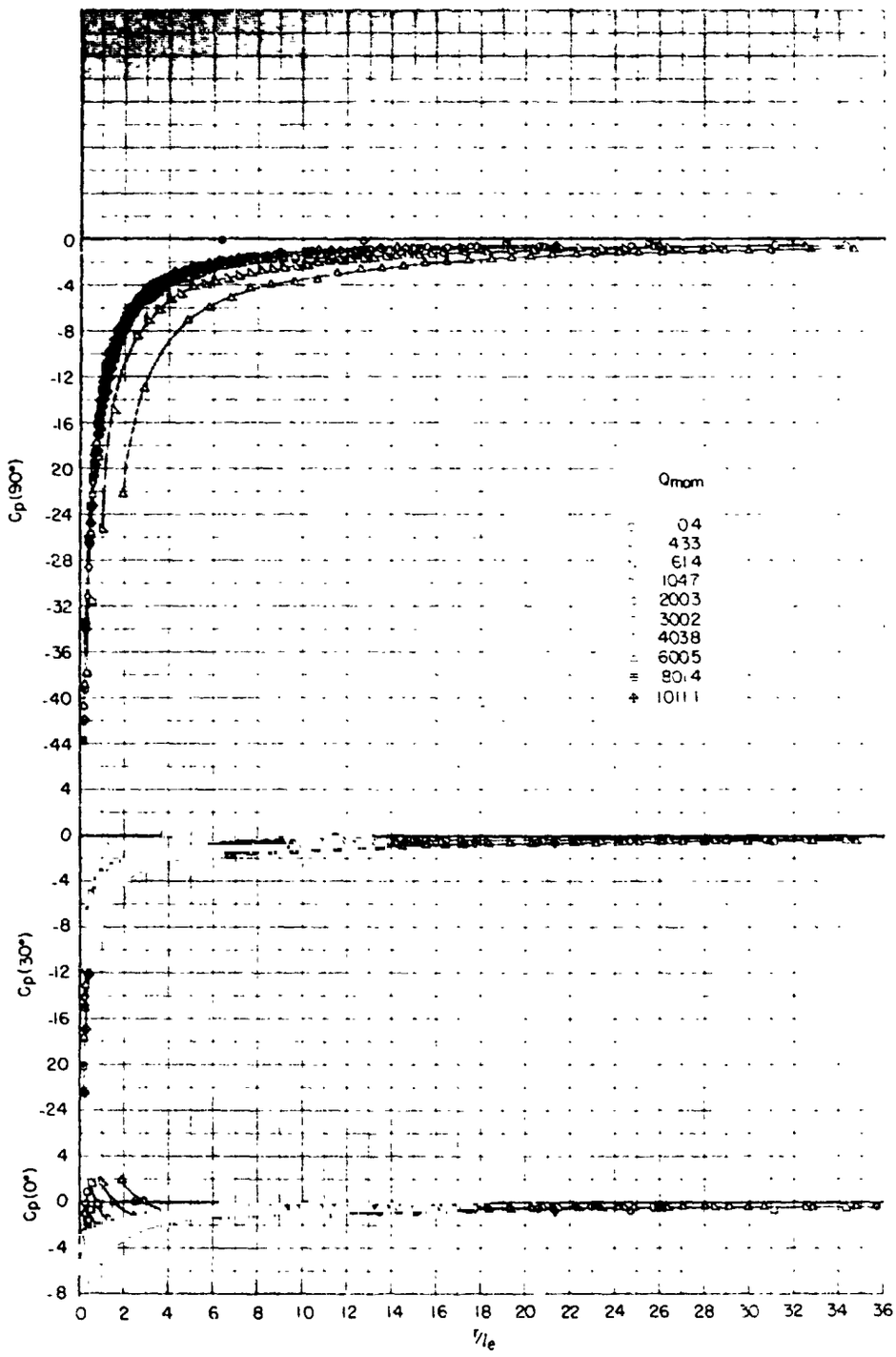

Figure 26.- Correlation of pressure data using the experimental relationship for plume length with $M_\infty = 0.2$.

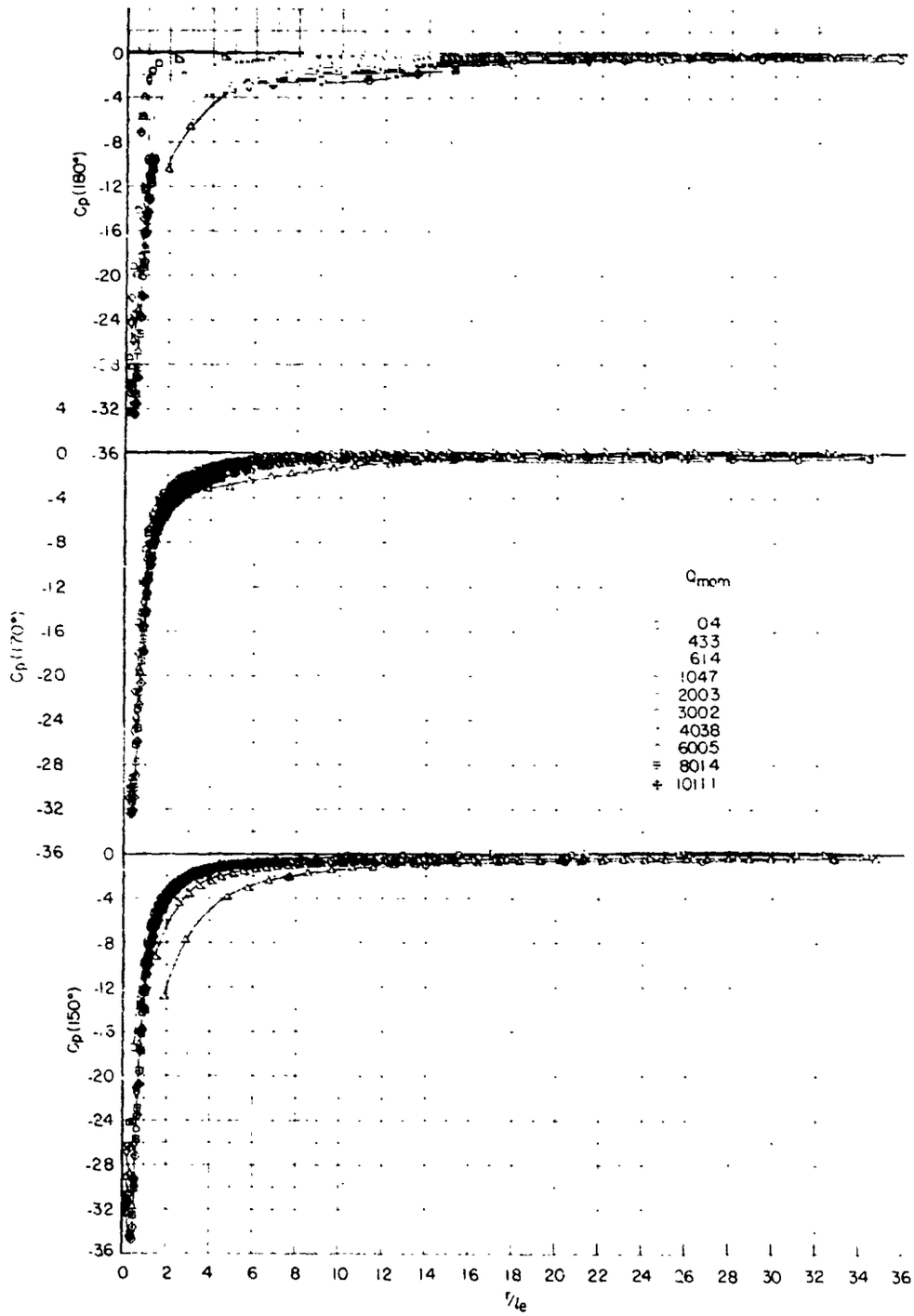

Figure 26.- Continued.

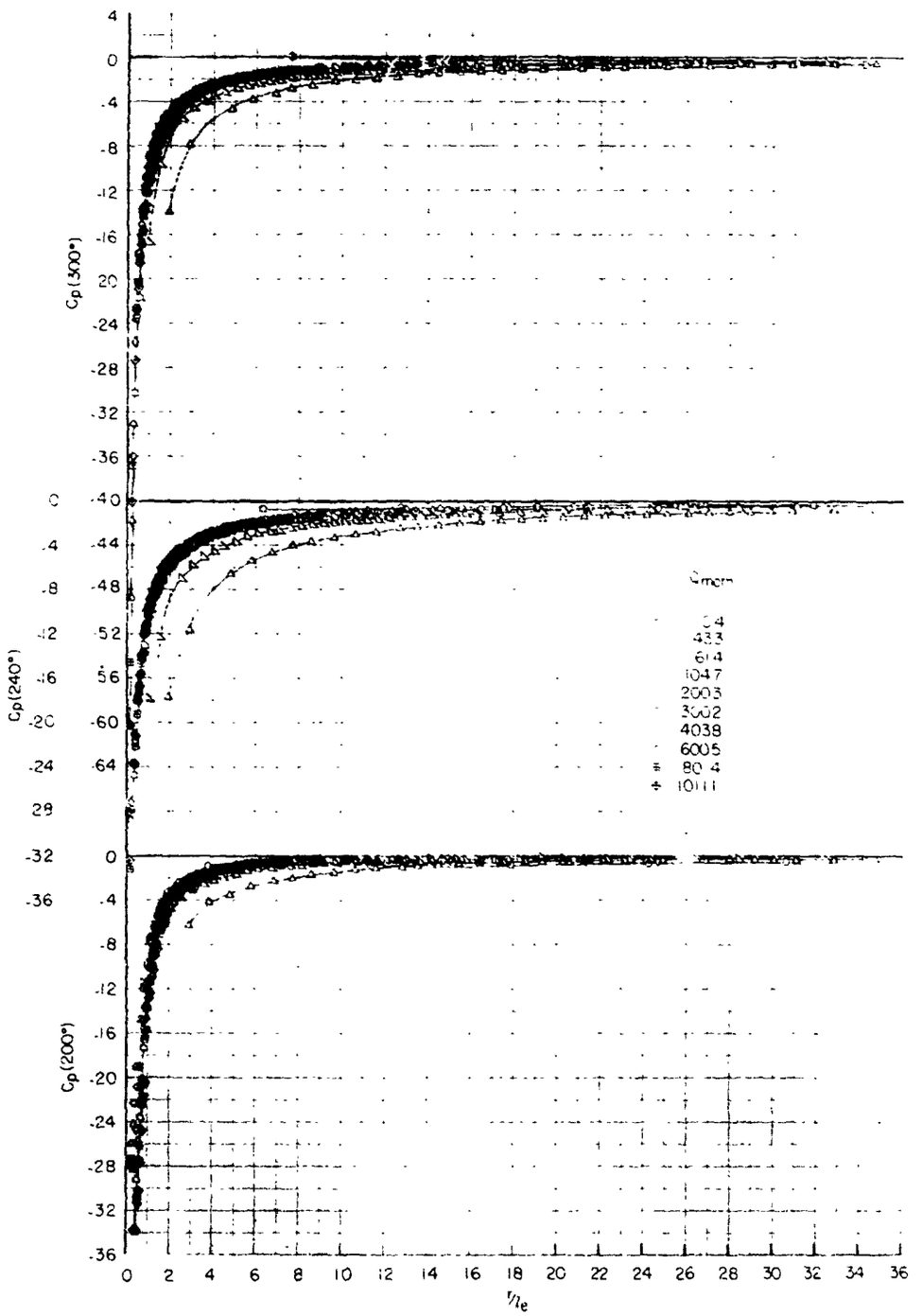

Figure 26.- Concluded.

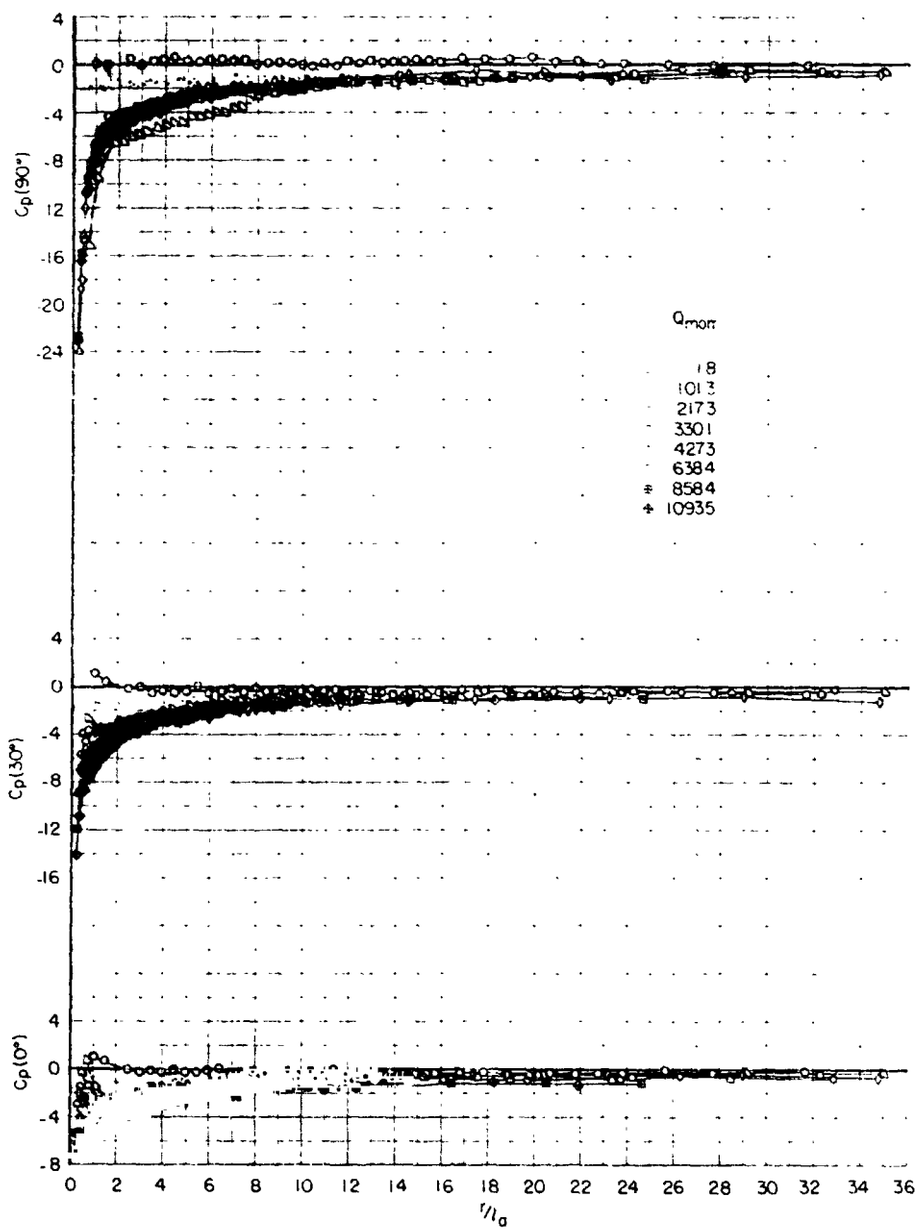

Figure 27.- Correlation of pressure data using the analytical relationship for plume length with $M_\infty = 0.1$.

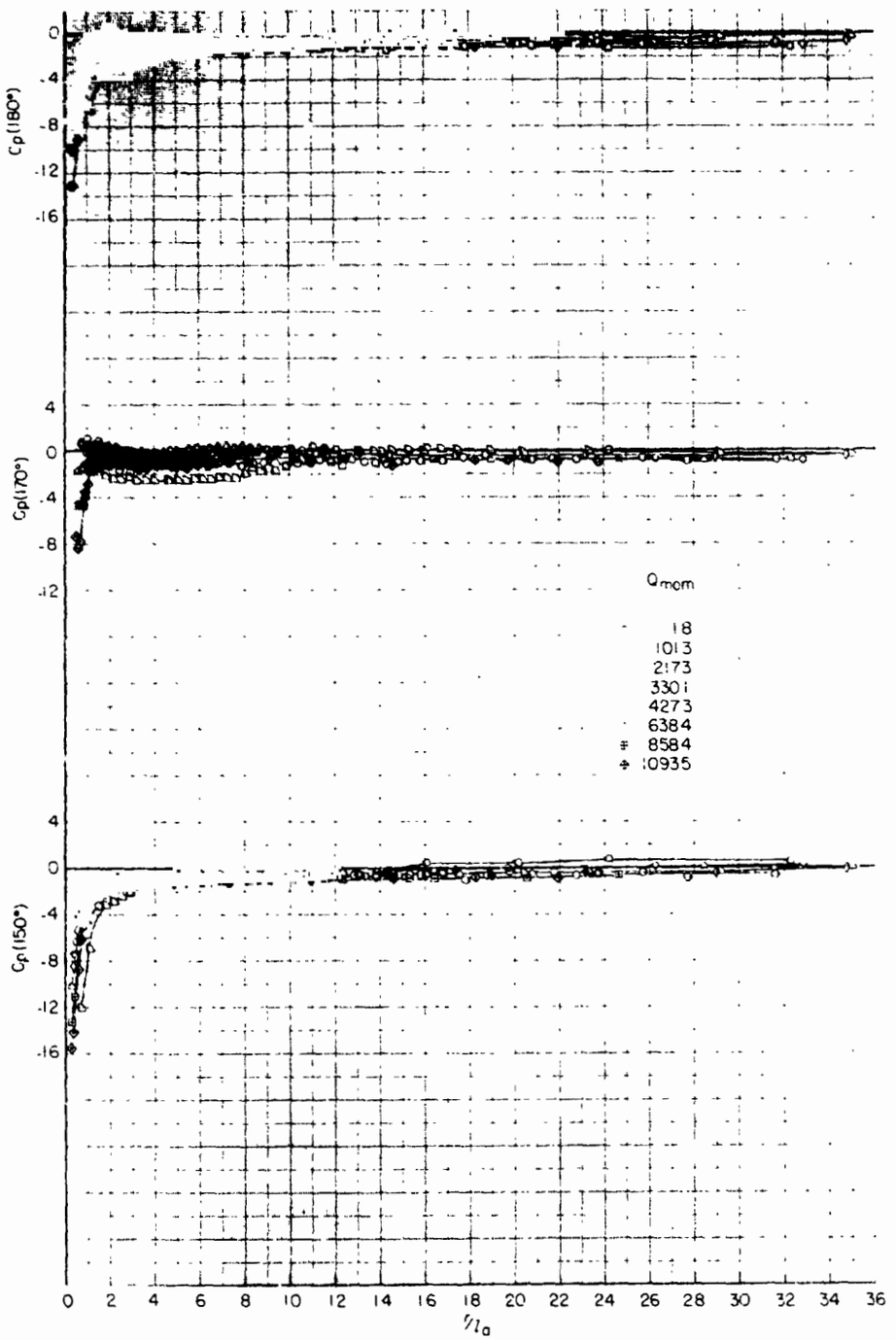

Figure 27.- Continued.

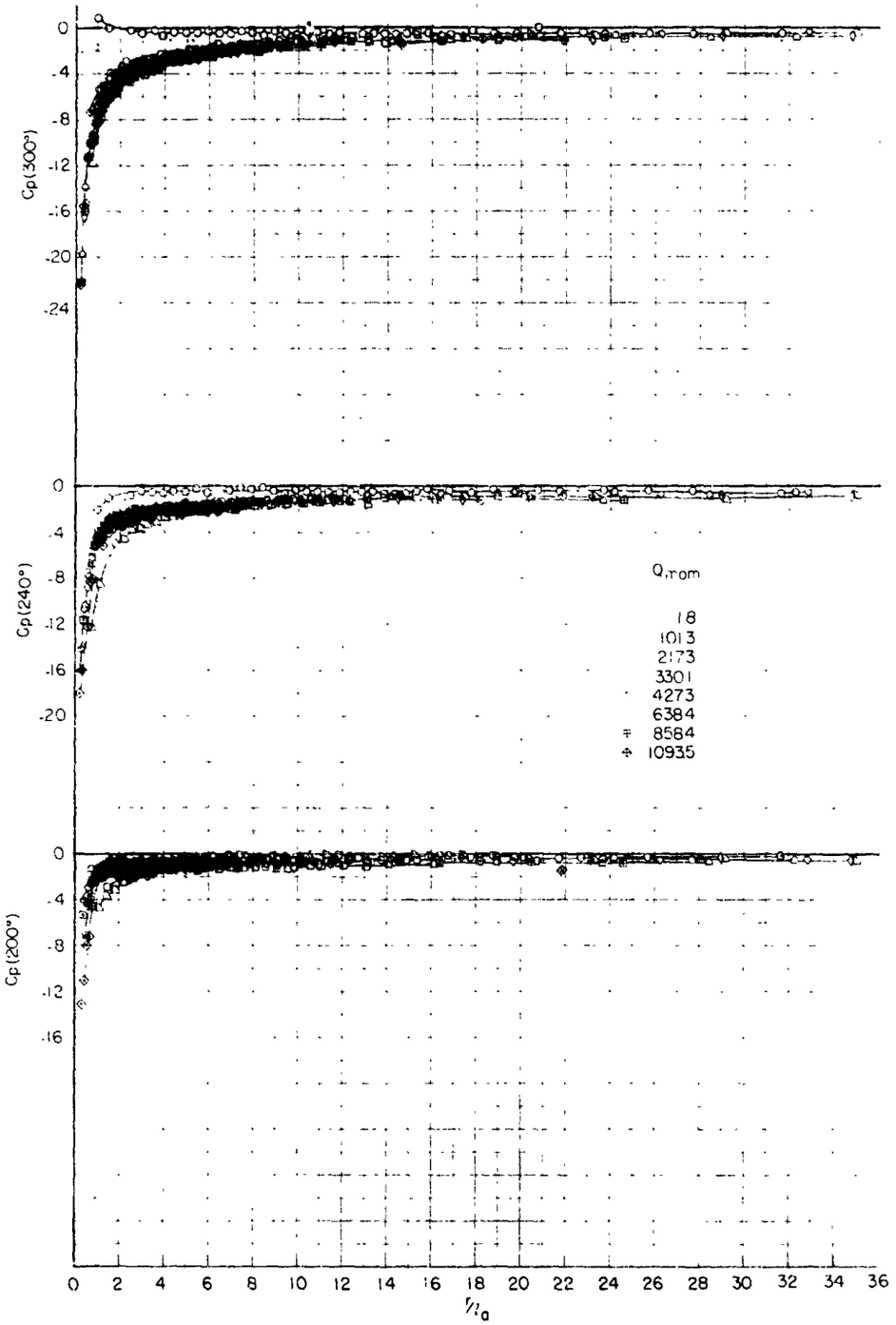

Figure 27.- Concluded.

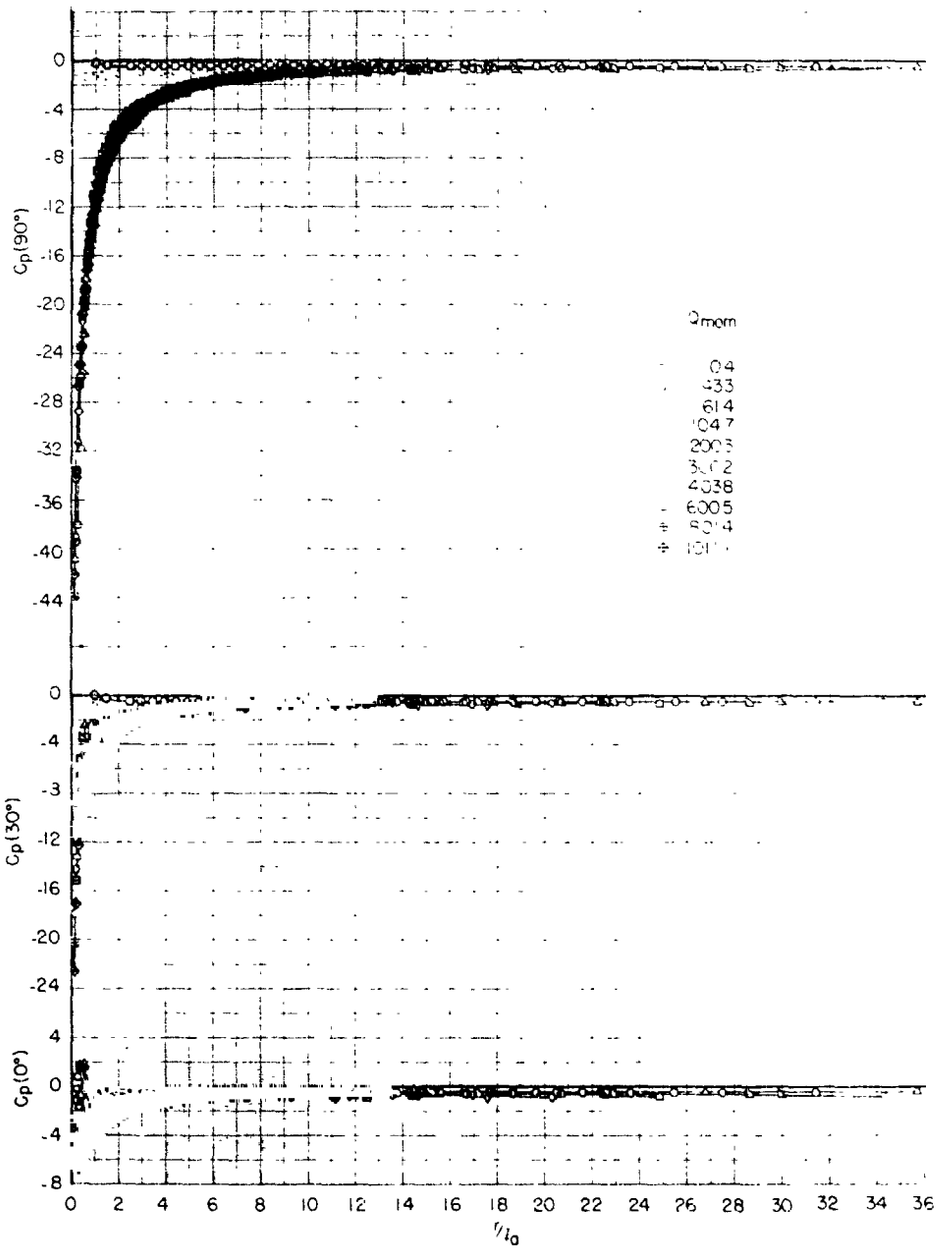

Figure 28.- Correlation of pressure data using the analytical relationship for plume length with $M_\infty = 0.2$.

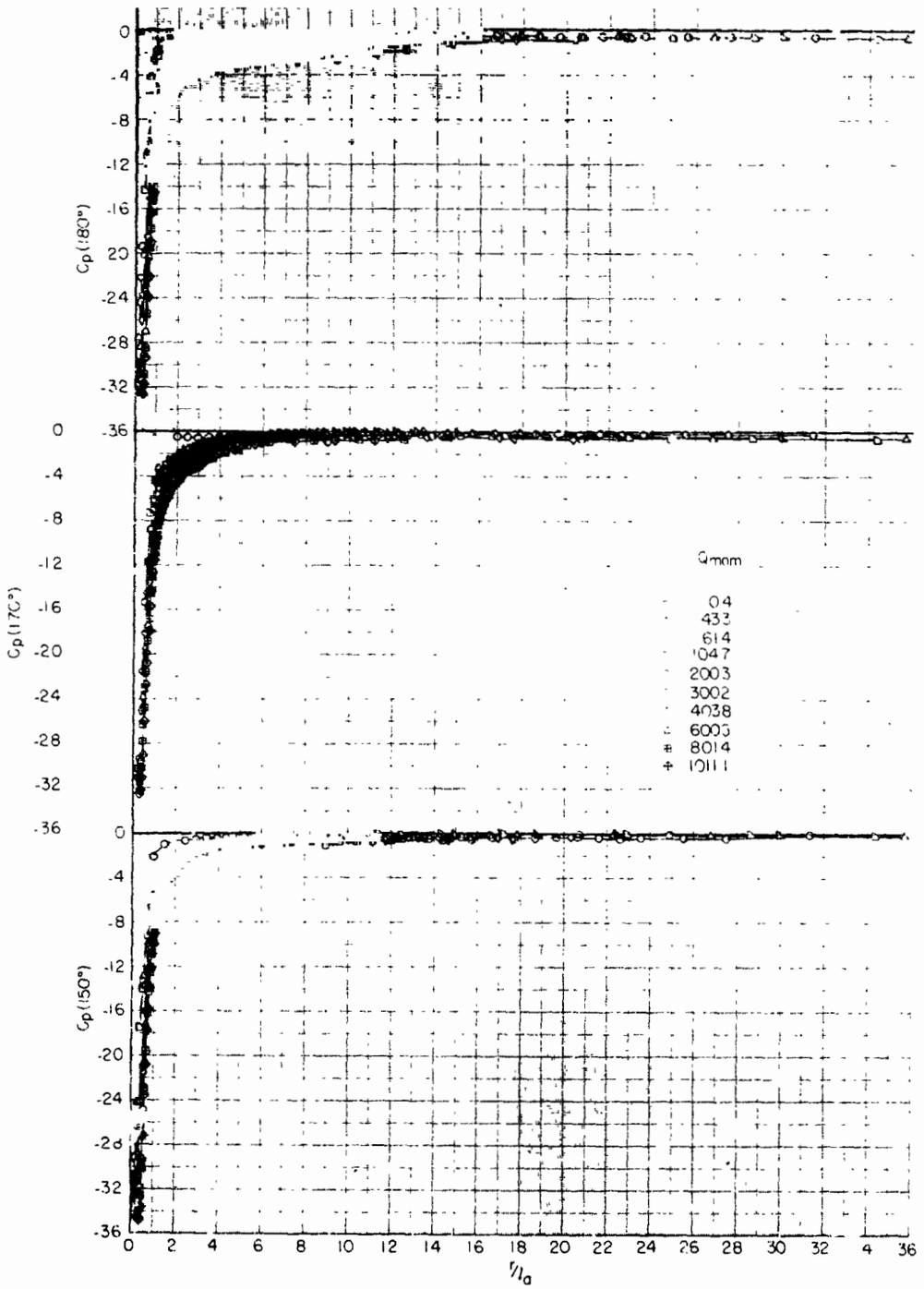

Figure 28.- Continued.

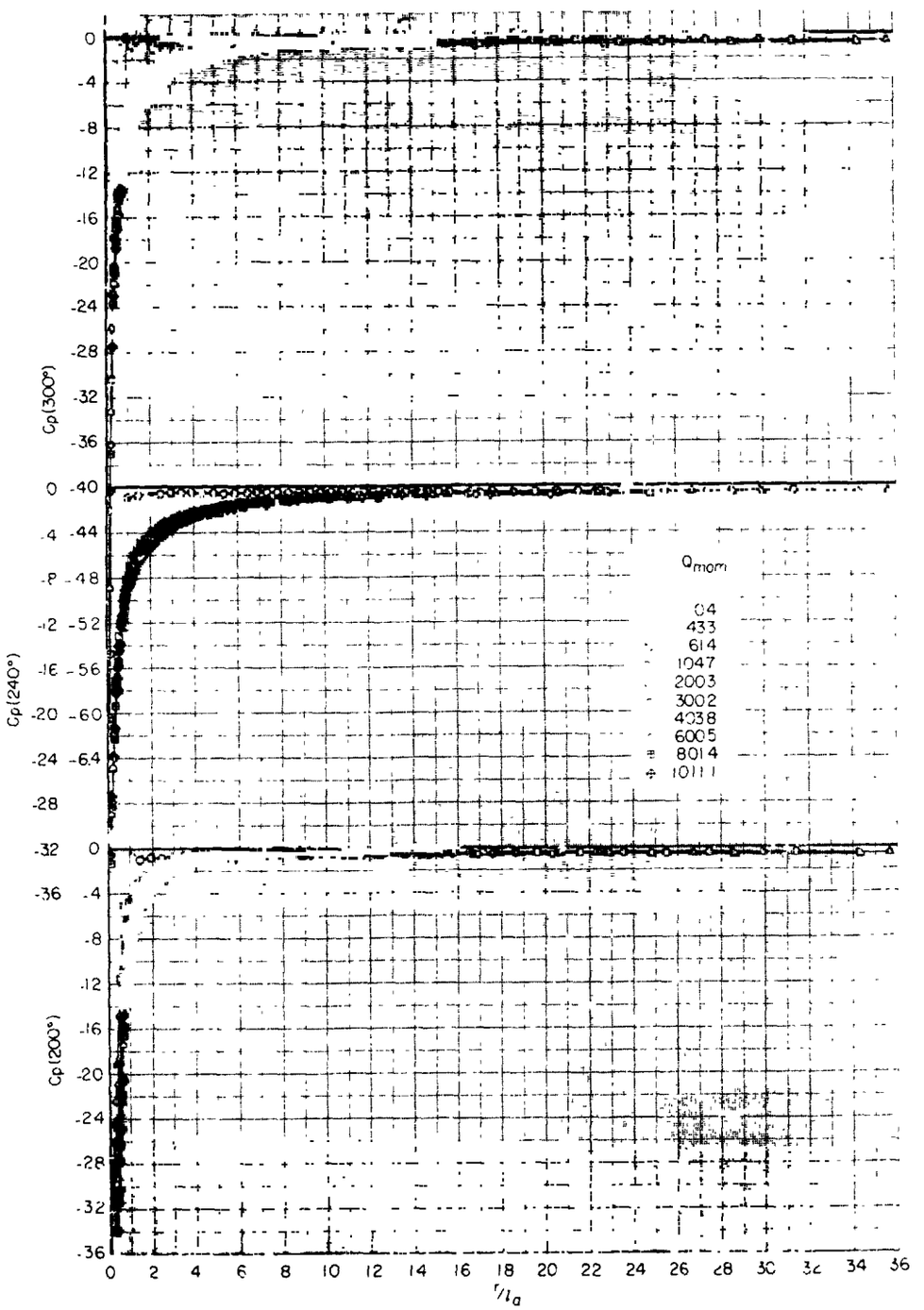

Figure 28. - Concluded.

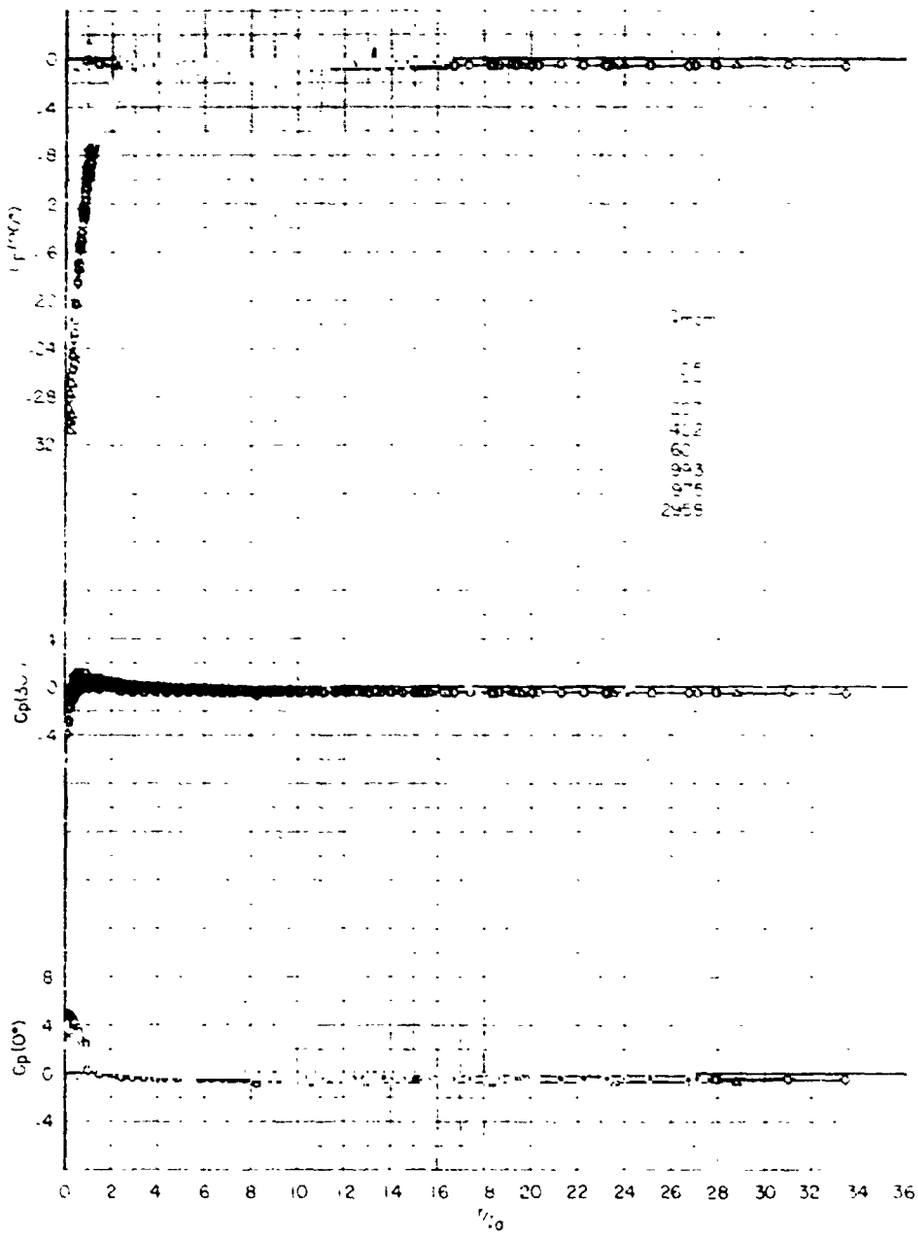

Figure 29.- Correlation of pressure data using the analytical relationship for plume length with $M_\infty = 0.4$.

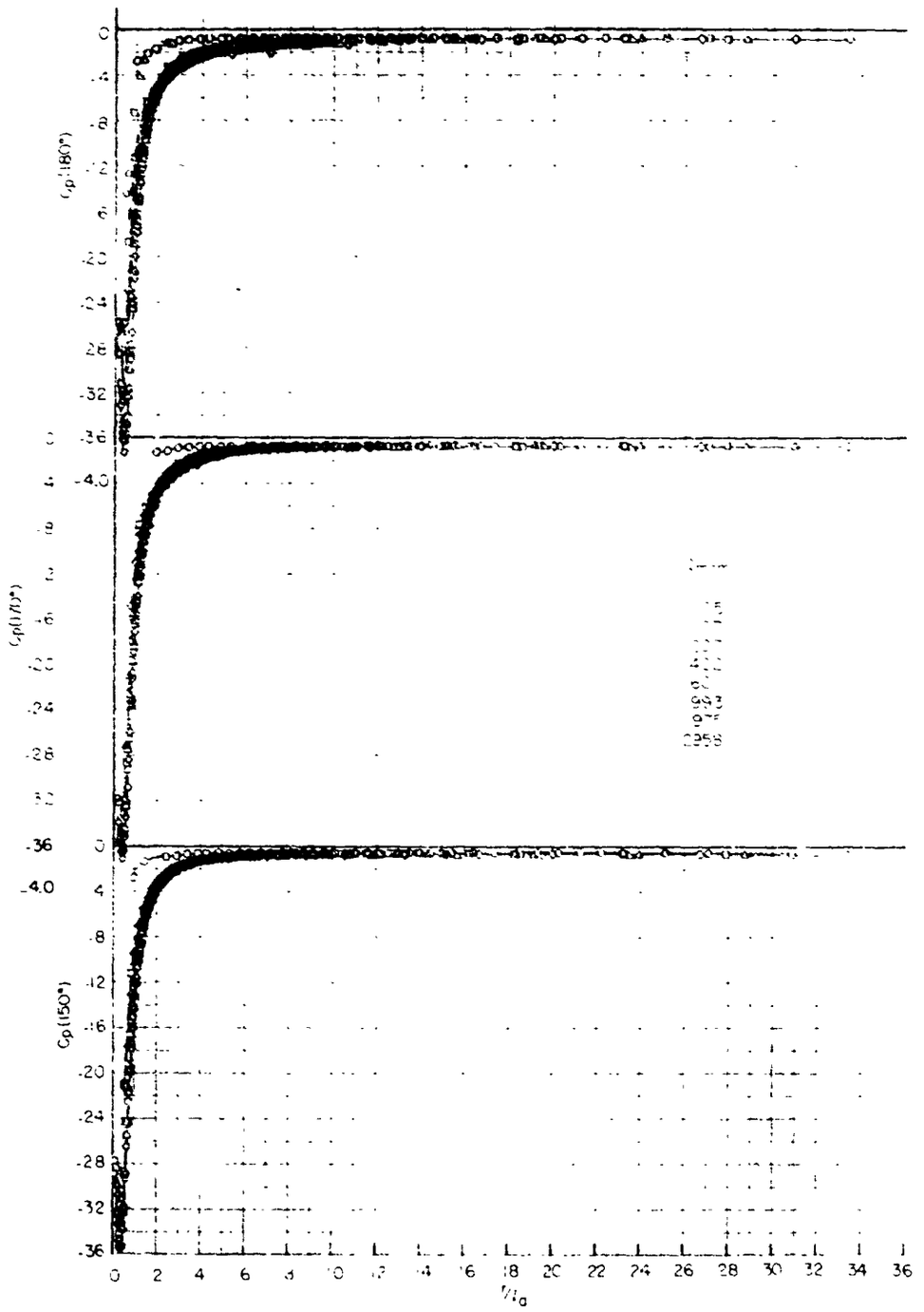

Figure 29.- Continued.

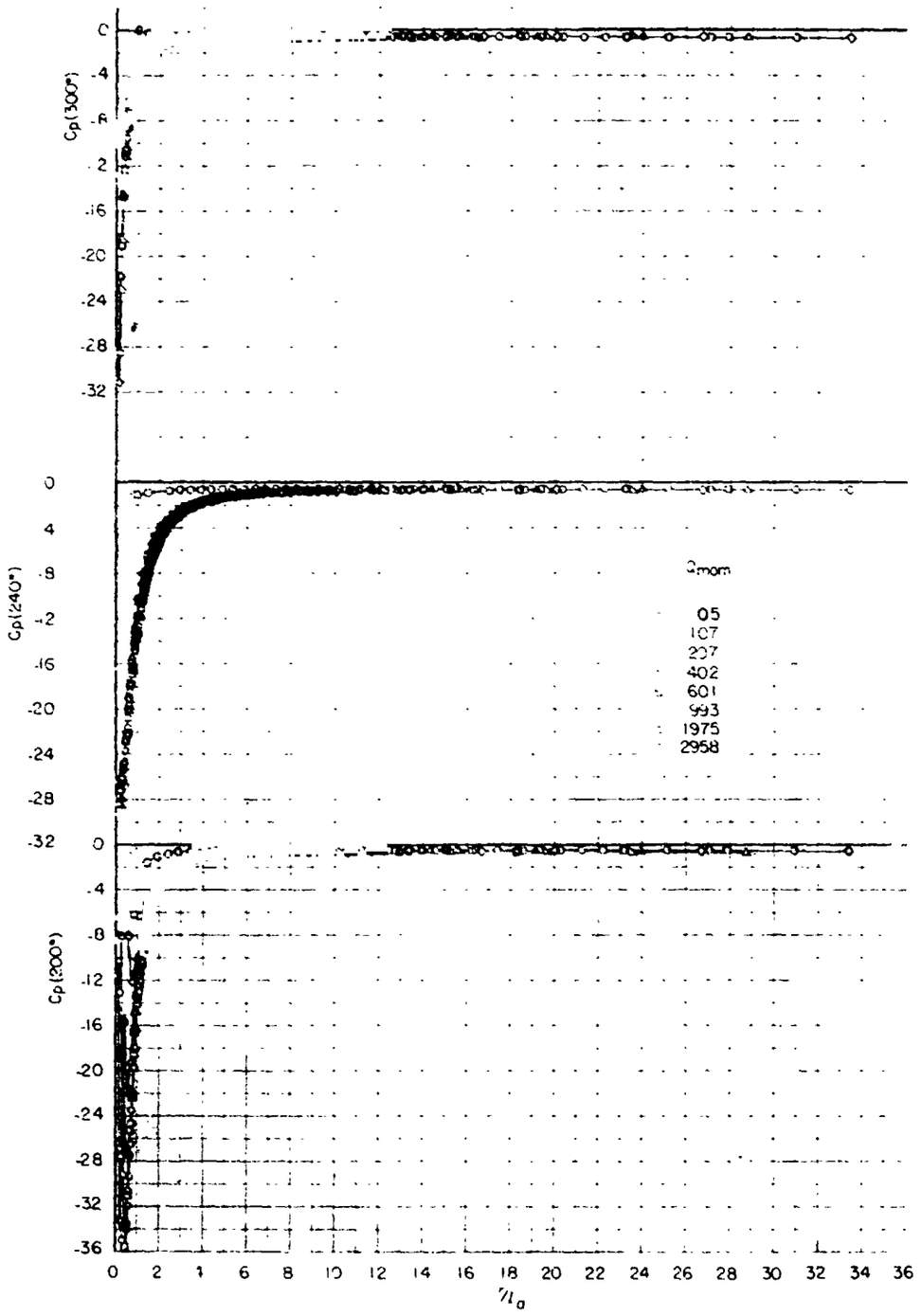

Figure 29.- Concluded.

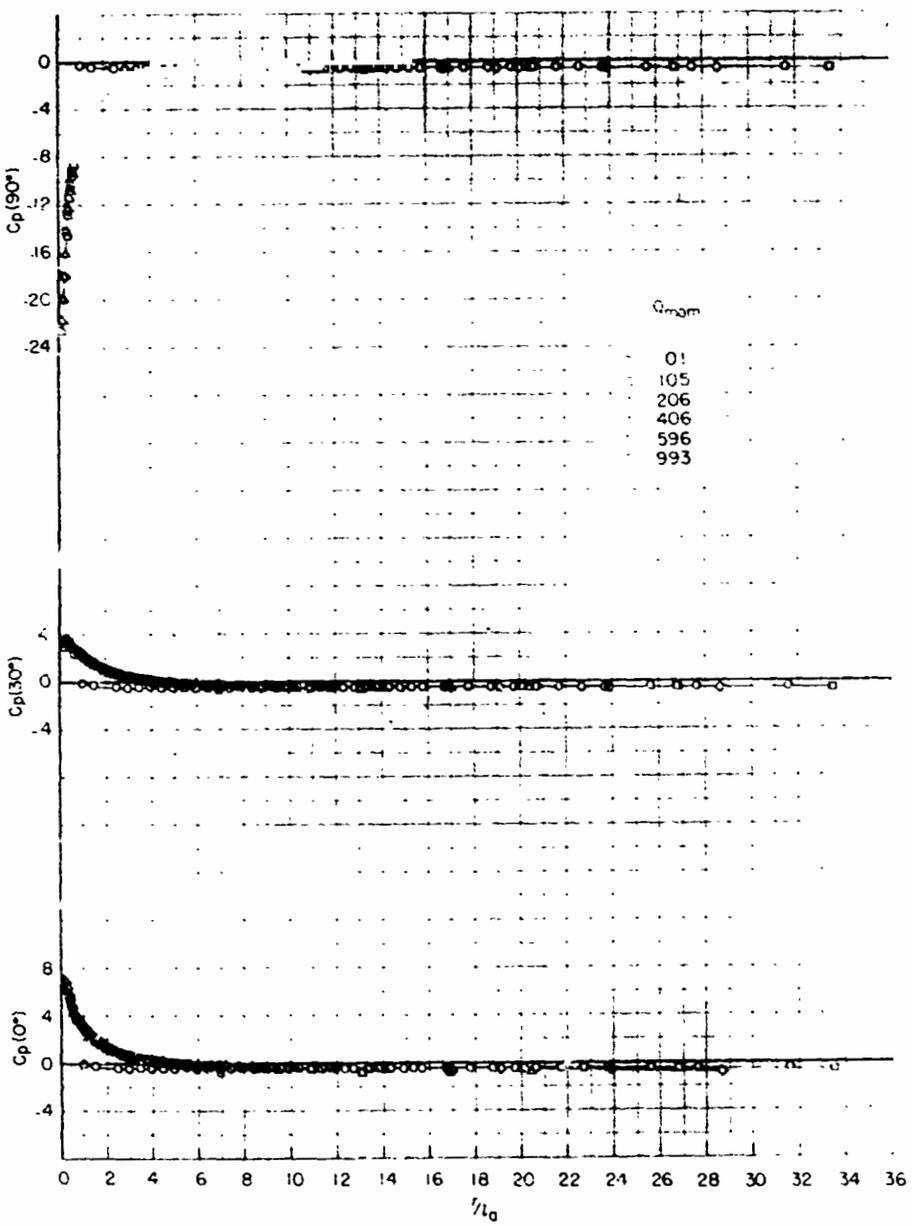

Figure 30.- Correlation of pressure data using the analytical relationship for plume length with $M_\infty = 0.6$.

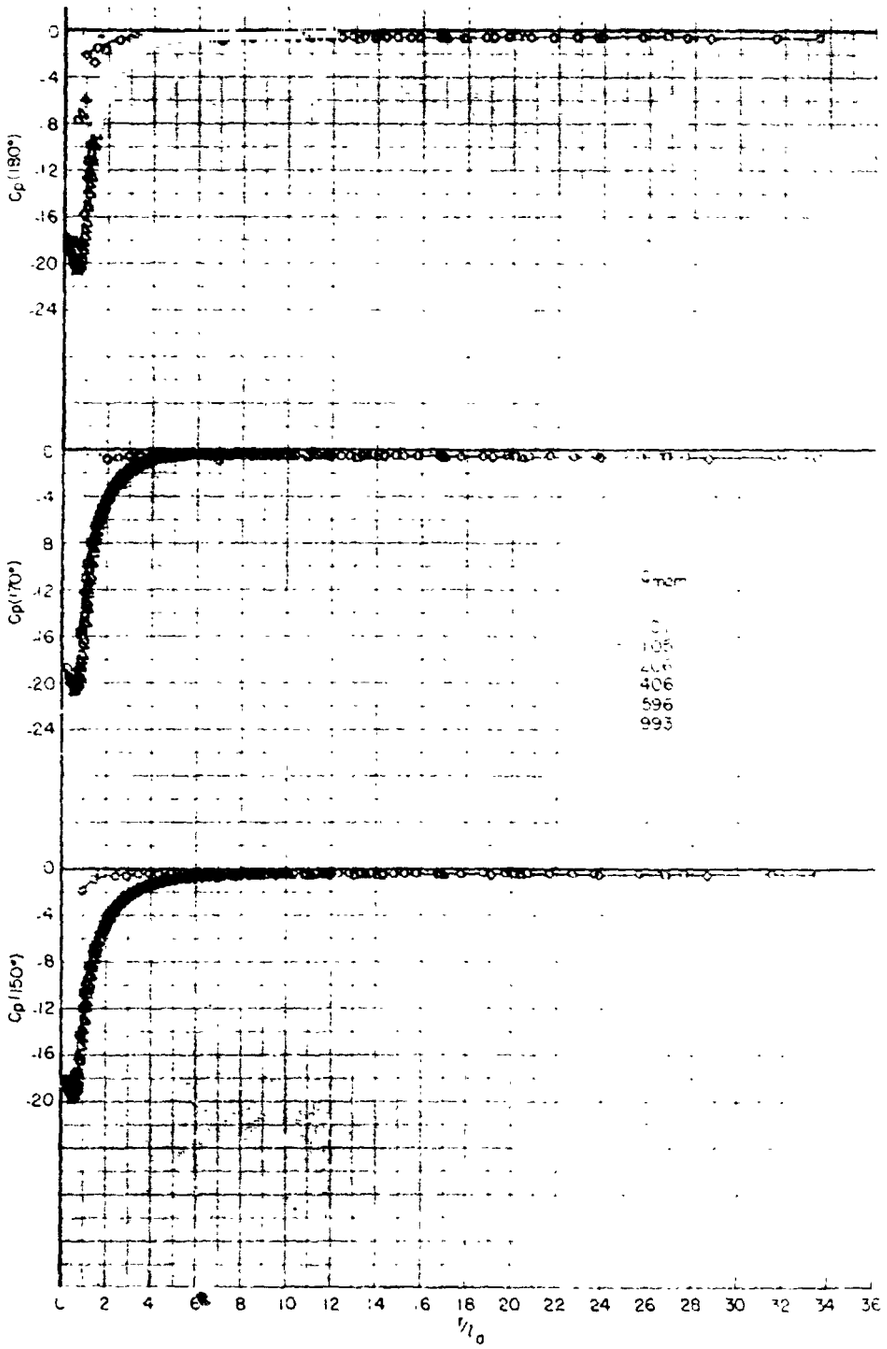

Figure 30.- Continued.

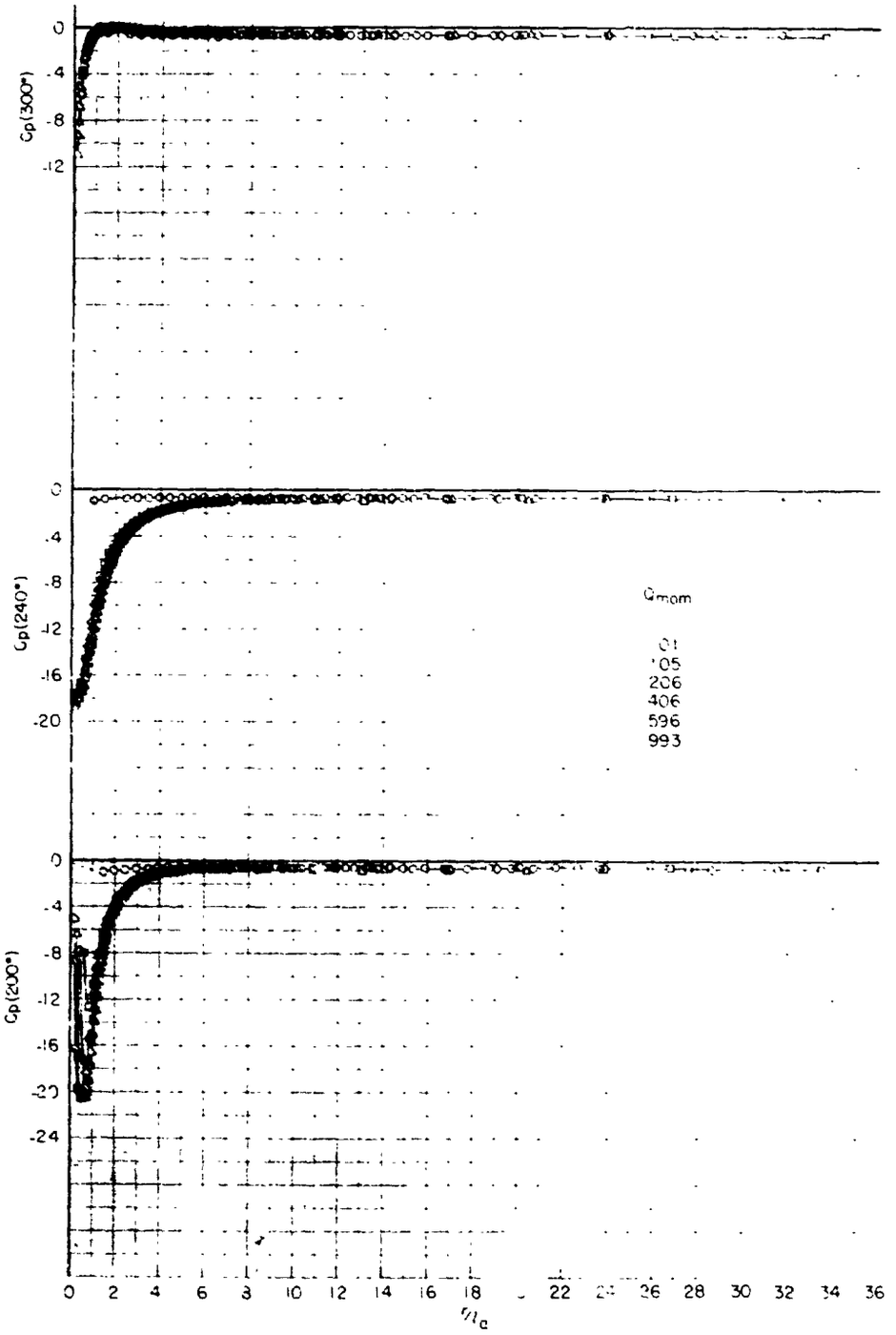

Figure 30.- Concluded.

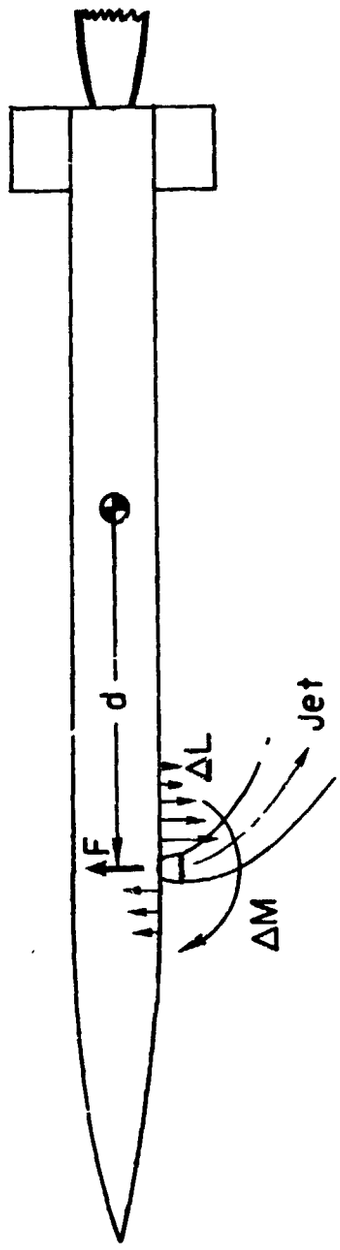

Figure 31.- Representation of aerodynamic interference on a missile equipped with a reaction-control jet.

NASA-Langley, 1973 — 1 L-8863